

GULF OF MEXICO HYDROGRAPHIC CLIMATOLOGY
AND METHOD OF SYNTHESIZING SUBSURFACE PROFILES
FROM THE SATELLITE SEA SURFACE HEIGHT ANOMALY

H. James Herring

Prepared for the

United States Department of Commerce
National Oceanographic and Atmospheric Administration
National Ocean Services
Coast Survey Development Laboratory

March 2010

Dynalysis of Princeton
18 Winfield Road
Princeton, New Jersey 08540
www.dynalysis.com

ABSTRACT

The hydrographic conditions in the Gulf are expressed in terms of two climatological water mass distributions, the background Gulf Common Water and the Loop and Eddy Water. The climatology consists of monthly climatological fields for both water masses and the probability of finding Loop and Eddy Water at a given location in the Gulf, which in combination yield the conventional atlas of mean monthly water properties. The distribution of sea surface height for each water mass is calculated and the mean climatological sea surface height distribution is determined. The satellite sea surface height anomaly is then used to determine the proportion of Loop and Eddy water present and, therefore, the temperature and salinity profiles. Climatological comparisons are made with the National Ocean Data Center (Levitus) climatology and the NAVOCEANO Global Data Environmental Model (GDEM) climatology. Finally, the synthesized profiles from this study and those from the Naval Research Laboratory Modular Ocean Data Assimilation System (MODAS) system are compared with *in situ* temperature data from NAVOCEANO along TOPEX/Poseidon satellite tracks.

1. INTRODUCTION

In the ongoing effort to forecast ocean conditions, the solution of the equations of motion will inevitably play the leading role. However, for the solutions to be meaningful, accurate and timely observational data must be employed in solving the equations in order to achieve realistic predictions. Of course, accurate initial conditions and boundary conditions must be prescribed. Even then, using present and even foreseeable computer capacity, numerical solutions of the equations necessarily involve physical and numerical approximations imposed by limitations on grid resolution. The result is that the solutions diverge from reality, limiting the duration of meaningful forecasts. Data assimilation methods have been developed to assure that the solutions do not diverge from reality; for example Ghil and Malanotte-Rizzoli (1991), Mellor and Ezer (1991) and Bennett, *et al.* (2008), but here again accurate and timely observational data must be available to assimilate. The primary focus of the present effort is to assist in developing more accurate methods of providing the assimilation data.

Examination of the comparison between numerical model forecasts of Gulf of Mexico circulation and observations from drifters and satellite imagery indicates that a large part of the forecast error is due to inaccurate model initial conditions. Forecast errors occur despite the use of a number of different data assimilation methods to spin-up the initial model fields. The conclusion is that the initial temperature and salinity fields, from correlations of climatological hydrographic profiles with the local satellite derived sea surface elevation anomaly, are not sufficiently accurate. The climatological analysis and profile synthesis method described below is proposed to improve accuracy.

To actually obtain *in situ* measurements of the temperature and salinity distribution in a body of water such as the Gulf of Mexico with sufficient resolution to initialize a model will be unlikely in the foreseeable future. This will remain true even with the considerable strides being made in deploying profiling drifters and gliders, Pazan and Niiler (2004). Use of satellite altimetry to infer subsurface conditions is essential, but again the spatial and temporal resolution is insufficient. The most realistic method of determining the existing conditions is to assimilate all available data in a continuously running model and then use the model to interpolate the sparsely distributed data in a dynamically consistent nowcast. In this system, the model is constantly running and each new data set is used to assess the skill of yesterday's forecast and then is assimilated in today's nowcast. The issue addressed here is how to develop the most accurate temperature and salinity fields to assimilate from the observational data that are available.

Since the ultimate test of the accuracy of the model forecasts will be against observed conditions, the assimilation data should be firmly grounded in observed data. Much of the work on data assimilation has been with model derived hydrographic data. While model hydrographic data are conveniently available, and ideal for identical twin model comparisons, they have only a tenuous connection with the actual observed conditions. Therefore the approach used here is to establish a relatively high resolution climatology based on the comparatively large amount of hydrographic data available in the Gulf of Mexico and then, based purely on observational data,

develop a method of inferring the subsurface temperature and salinity profiles from the satellite sea surface height anomaly.

2. HYDROGRAPHIC CLIMATOLOGY

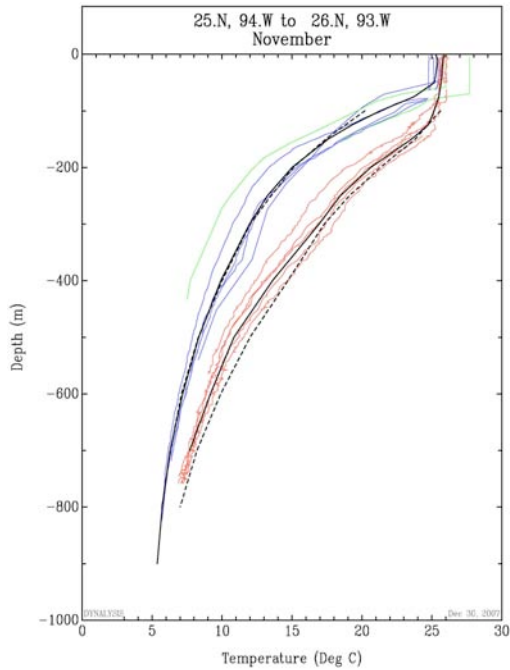
Previous hydrographic climatologies have been prepared by calculating the mean value of all of the available data in a given geographical area in the vicinity of a grid point, during a period during the year, such as a season or month. The result is a series of fields representing the geographical distribution of the mean temperature and salinity during that time period. While this is a useful product, the characteristics of the Gulf of Mexico lend themselves to a more refined and physically revealing analysis.

The distribution of temperature and salinity at any time in the Gulf is actually the result of the interplay between two separate and distinct water masses, the Loop and Eddy Water (LEW) from the Caribbean and the background long-term distribution of Gulf Water, sometimes referred to as Gulf Common Water (GCW). As the Loop Current passes through the Gulf it naturally mixes with the surrounding GCW to some extent, but most LEW passes through with little change. At irregular intervals, between 6 and 17 months, Vukovich, (1995), the Loop pinches off, shedding a large Eddy consisting of water with LEW properties which migrates slowly southwestward and gradually mixes with the GCW until it is dissipated in the western Gulf. This process provides an infusion of Loop Water properties to the GCW which presumably maintains the Gulf in its present climatological equilibrium.

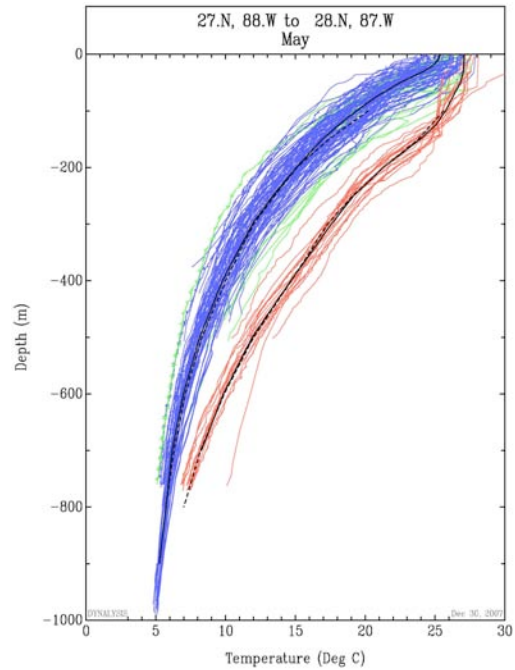
The objective here is to develop separate descriptions of the properties of the GCW mass distribution and of the LEW and then construct a climatology of the statistical likelihood of finding one or the other water mass at any given location in the Gulf. In addition to providing a more detailed and physically meaningful analysis of the prevailing conditions, this description will be shown to be more useful for the later phases of this study.

2.1 Water Mass Description

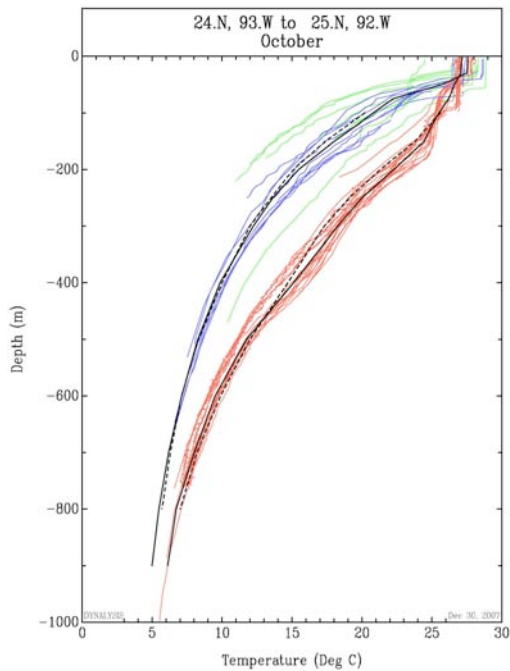
The Yucatan Current enters the Gulf through the Yucatan Straits, becomes the Loop Current as it forms a loop of varying northward extent in the Eastern Gulf and then leaves the Gulf through the Florida Straits. In the pycnocline, from depths of 200m to 600m, the Loop Current is 5 to 7 C° warmer and 1 part per thousand (ppt) more saline than the GCW. In regions where both water masses occur frequently and the presence of the LEW is intermittent, bimodality of the profiles is clearly evident as shown for four locations around the Gulf in Figure 2.1. Equally evident is that the mean of the two profiles in each case is not a good representation of the prevailing conditions, since, while the two obviously mix at their interface, the fully mixed condition is less common than the presence of one or the other water mass. When the GCW and the LEW coexist continuously, profiles exhibiting mixing of the LEW with the GCW are apparent. Along the boundary of the Loop, even though the presence of pure GCW and LEW are dominant, profiles illustrating extensive mixing are shown at four locations around the boundary of the Loop in Figure 2.2. Finally, in regions where the Loop and Eddies do not penetrate, such as the North Eastern Gulf and the Gulf of Campeche, only GCW is found to exist.



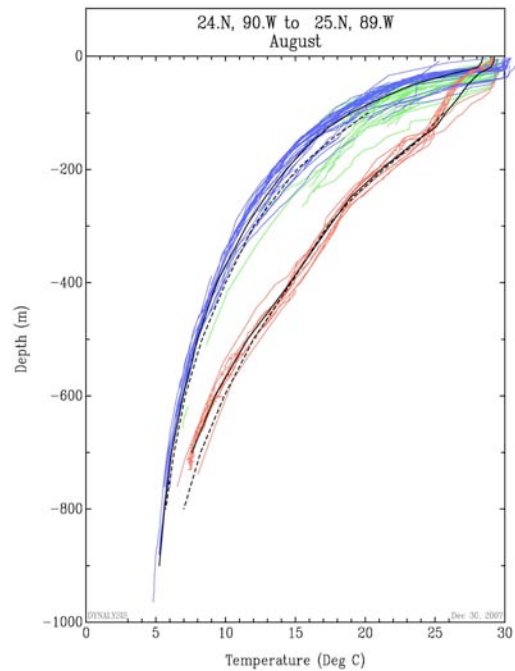
(a) Central Western Gulf



(b) Northeastern Gulf

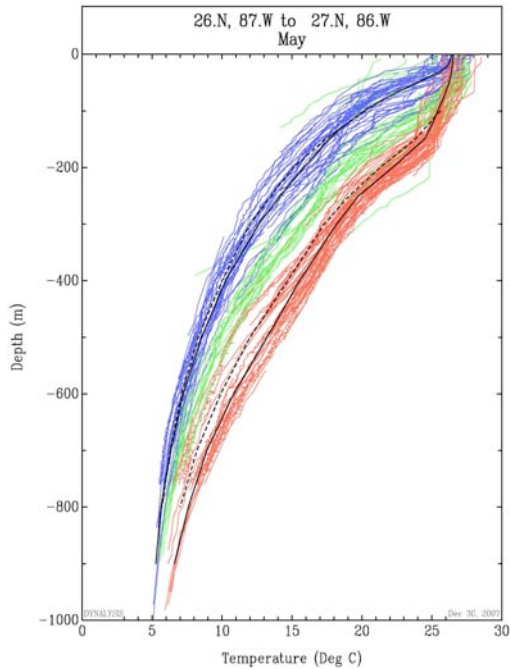


(c) Southwestern Gulf

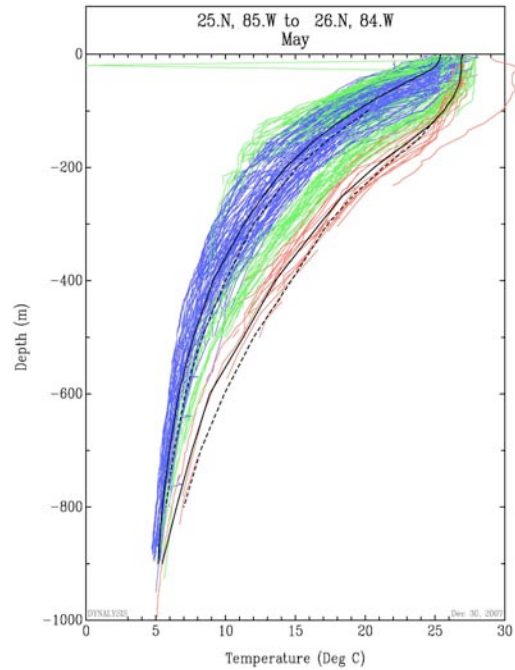


(d) Central Gulf

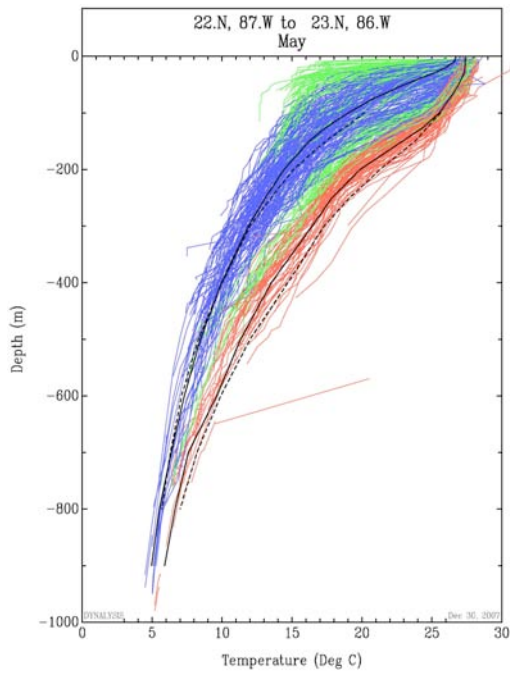
Figure 2.1 Examples of bimodality at four locations around the Gulf, where the profiles colored blue are identified as GCW, the red as LEW and the green not clearly either or some mixture of the two. The solid line profiles are the local averages of the GCW and LEW profiles shown and the dashed lines are the Gulf-wide mean profiles of each.



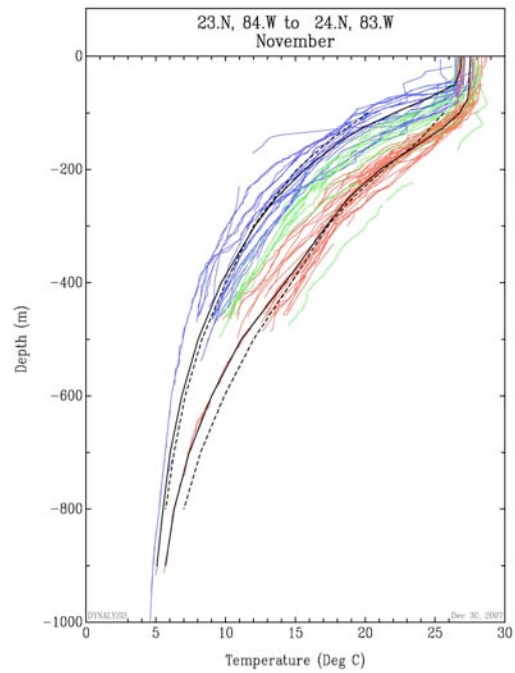
(a) Northern Loop Boundary



(b) Eastern Loop Boundary



(c) Southwestern Loop Boundary



(d) Southeastern Loop Boundary

Figure 2.2 Examples of bimodality but including profiles showing evidence of mixing at four locations around the Gulf, where the profiles colored blue are identified as GCW, the red as LEW and the green some mixture of the two or neither. The solid line profiles are the local averages of the GCW and LEW profiles shown and the dashed lines are the Gulf-wide mean profiles of each.

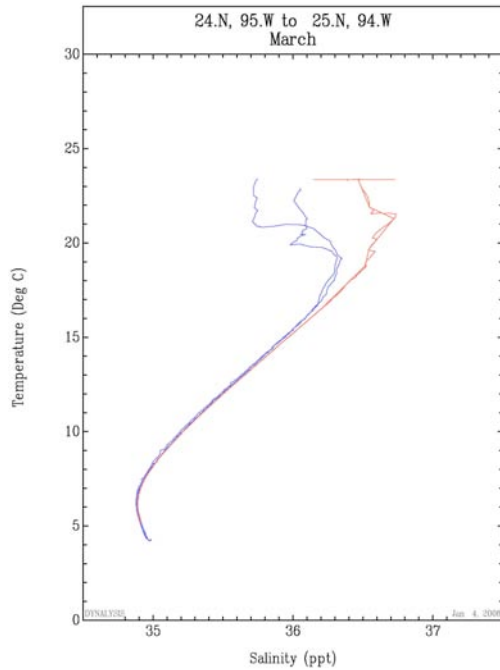
The temperature and salinity profiles are influenced by the mixed layer near the surface where turbulence generated by the prevailing wind stress mixes the surface conditions down as far as 50 m with perceptible effects down as far as 100 m. This layer is a function of the surface conditions and consequently varies with Latitude and season. There is a transition layer between 100 m and 200 m to the pycnocline, which extends down from 200 m to 1000 m. Between 200 m and 600 m the difference between the GCW and the LEW is well defined, as is evident from Figure 2.1. Below 1000 m the temperature and salinity profiles are effectively uniform throughout the Gulf and, since they are below the sill depth of both the Yucatan Straits and the Florida Straits, the water properties are not measurably influenced by the Loop Current.

Fortunately the temperature-salinity correlation below the mixed layer appears to be very robust and, as observed by Thacker (2006), is the same for the GCW and the LEW masses as shown in Figure 2.3. This implies that the information necessary to discriminate between water masses is contained in the temperature profiles alone, and therefore the large preponderance of temperature-only profiles in the dataset is not a liability for the purpose of this study.

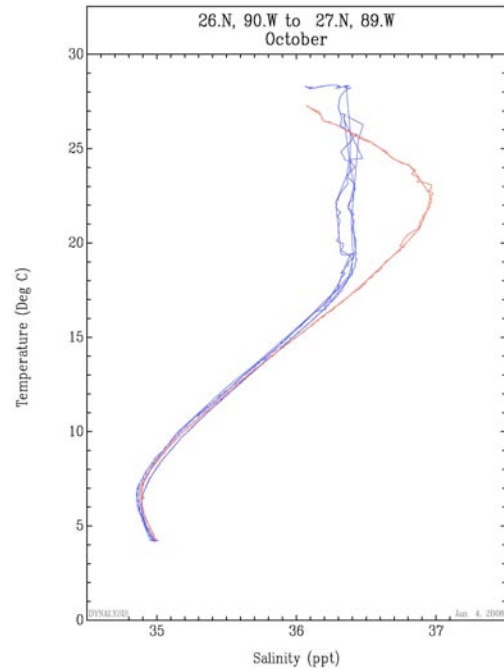
The hydrographic dataset used here for the Gulf of Mexico, bounded by the Yucatan Straits and the Florida Straits, consists of 182,378 profiles; 27,039 report both temperature and salinity and the remainder are temperature only. These data have been assembled from many sources. Most are from National Oceanographic Data Center (NODC), Levitus (1994), with updates through 2008, with important contributions from the Navy MOODS4 dataset, Bauer (1985) and the TAMU/MMS Deepwater dataset, DiMarco, *et al.* (2001). A number of Principal Investigators, also, have generously provided data from their individual studies (for example Donohue, *et al.* (2006)). The distribution of the profiles throughout the Gulf and surrounding waters is shown in Figure 2.4. The data that is conspicuously absent in this data set is a large quantity of proprietary hydrographic data acquired on behalf of the petroleum companies operating in the Gulf. These data include AXBT casts deployed by Horizon Marine as a component of the Eddy Watch program and also hydrocasts performed by Texas A&M and others during a series of Eddy tracking studies over the past several decades, DiMarco, *et al.* (2001). The omission of these data may actually be desirable, since they favor Eddies and are likely to cause an Eddy bias.

Working with 180 thousand profiles it is impractical to differentiate manually between GCW and LEW profiles on an individual basis. A robust quantitative, numerical method is necessary to differentiate in an efficient, impartial, and objective manner. As is evident from the profiles shown in Figure 2.1, while the distinction between GCW and LEW profiles is always clear, the profiles of each do vary over the Gulf. The GCW is warmer and saltier in the western Gulf and the Eddy profiles do show evidence of mixing as they move to the west. Therefore it would bias the result to define, for instance, a typical GCW profile and chose only profiles that are similar to it.

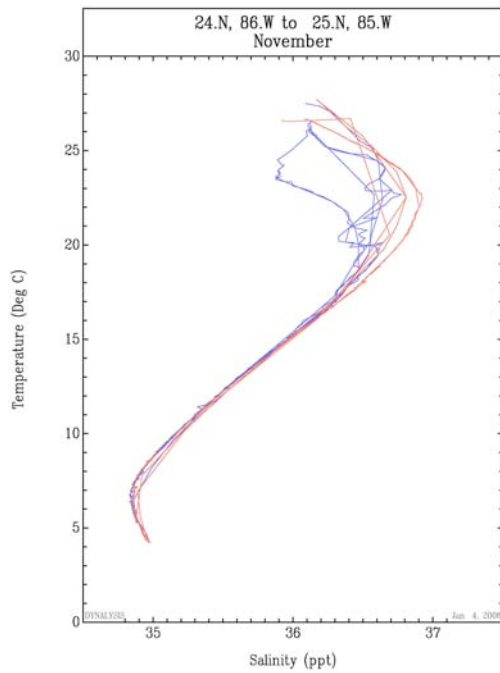
Recognizing the inherent bimodality of the water masses, histograms of water properties are calculated for local regions to aid in their classification. Examples of such histograms are shown in Figure 2.5 for two different 1°x1° Latitude and Longitude areas.



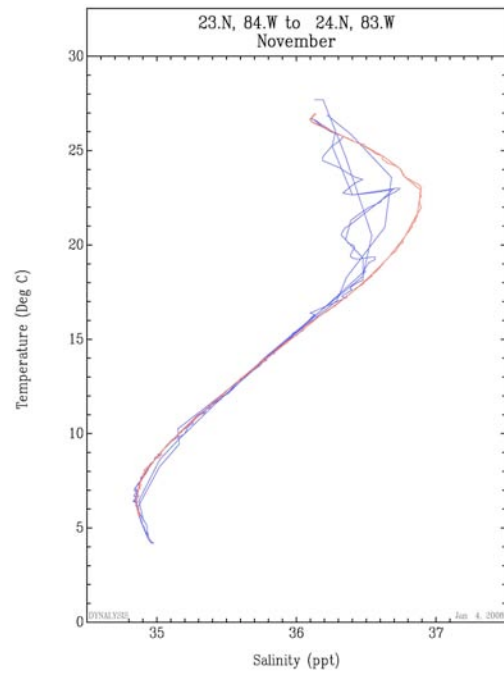
(a) Central Western Gulf



(b) North Central Gulf

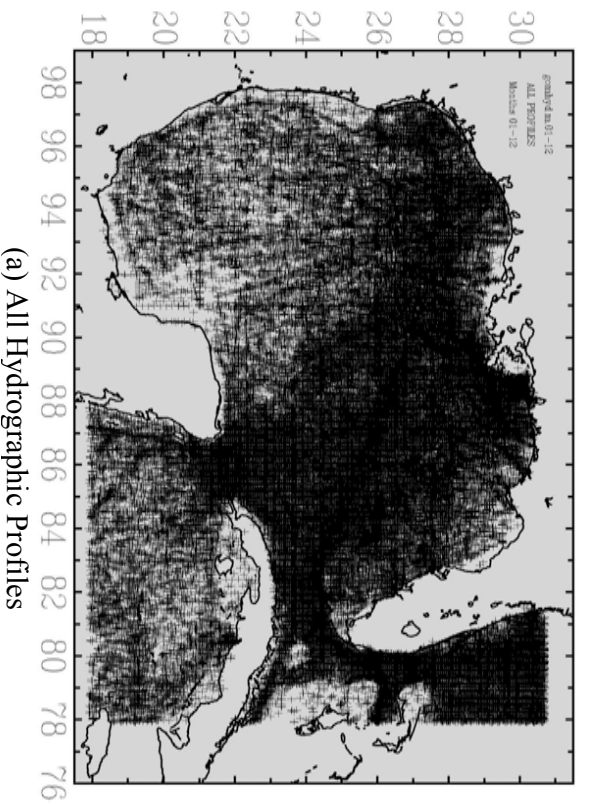


(c) Southwestern Loop Boundary

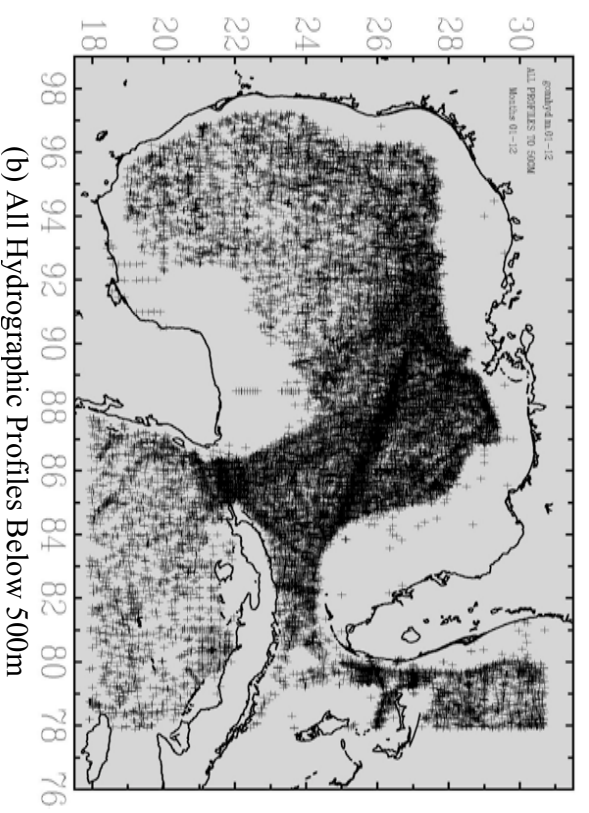


(d) South Eastern Gulf

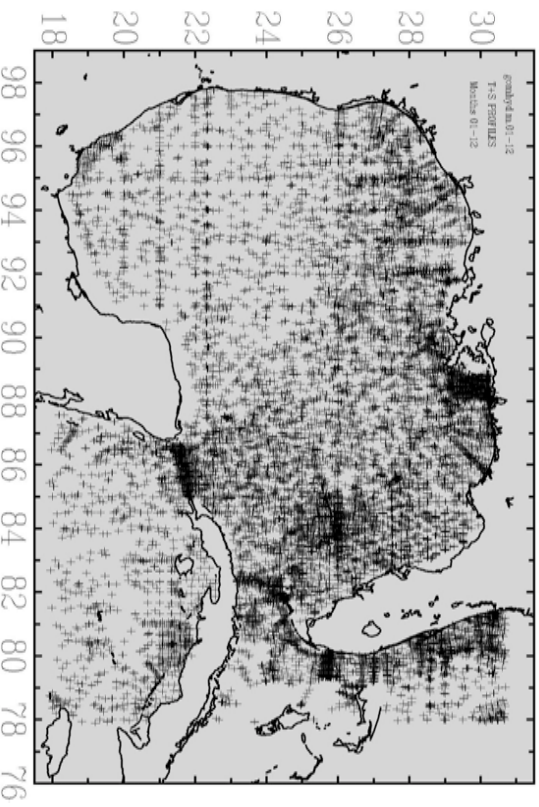
Figure 2.3 Temperature-Salinity diagrams for four locations around the Gulf illustrating the close correlation between the temperature-salinity relation for the GCW, shown in blue, and the LEW, in red, below the mixed layer from a temperature of about 16 C° to the bottom.



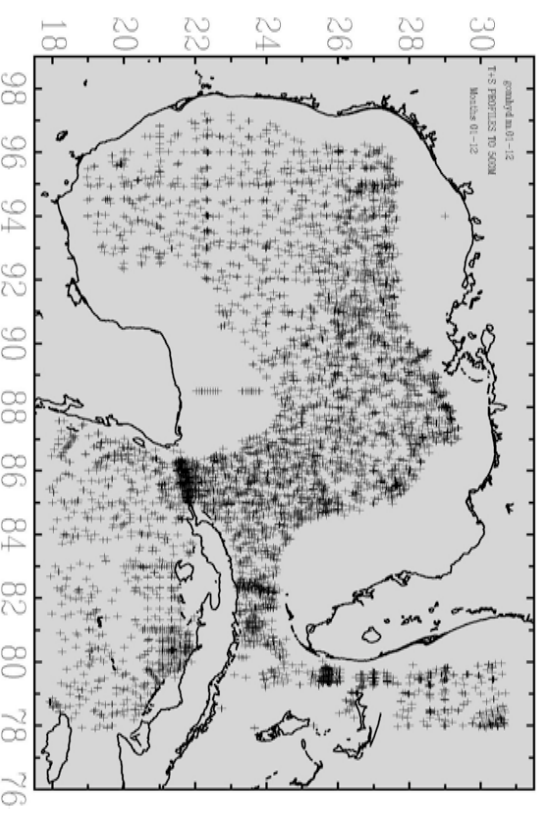
(a) All Hydrographic Profiles



(b) All Hydrographic Profiles Below 500m

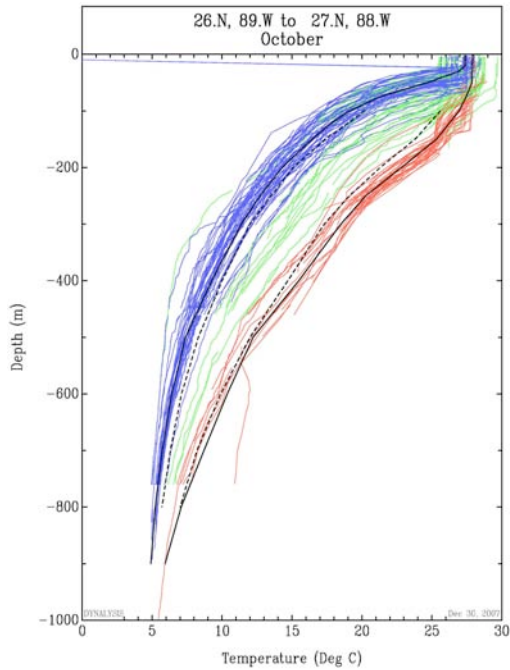


(c) Temperature and Salinity Profiles

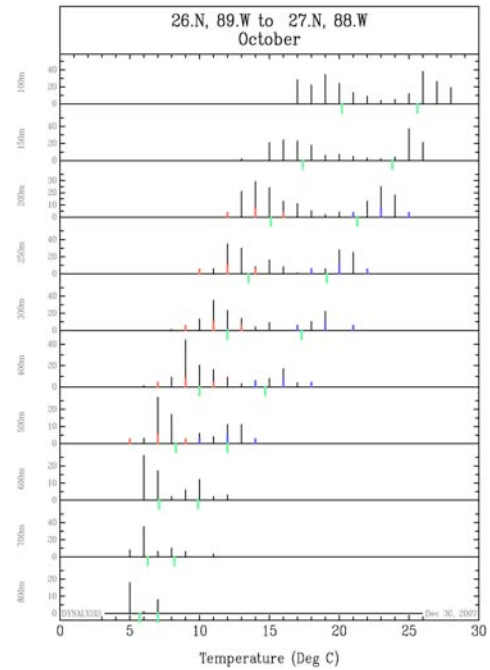


(d) Temperature and Salinity Profiles Below 500m

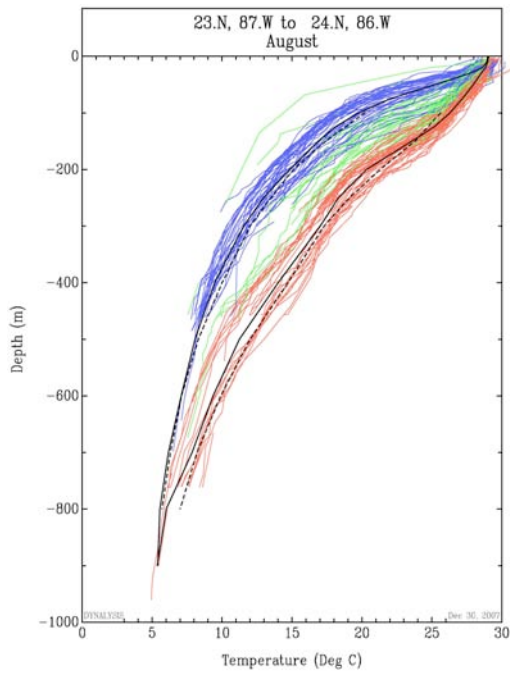
Figure 2.4 Geographical location of all profiles (top) and those including both temperature and salinity data (bottom).



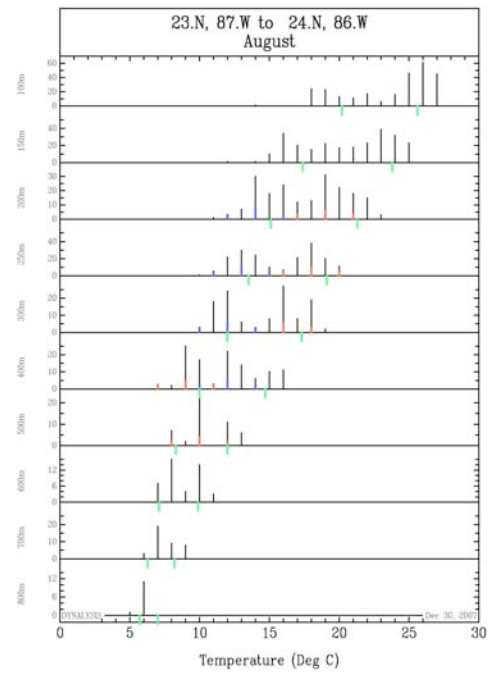
(a) Northern Loop Boundary



(b) Histograms for Profiles (a)



(c) Southwestern Loop Boundary



(d) Histograms for Profiles (c)

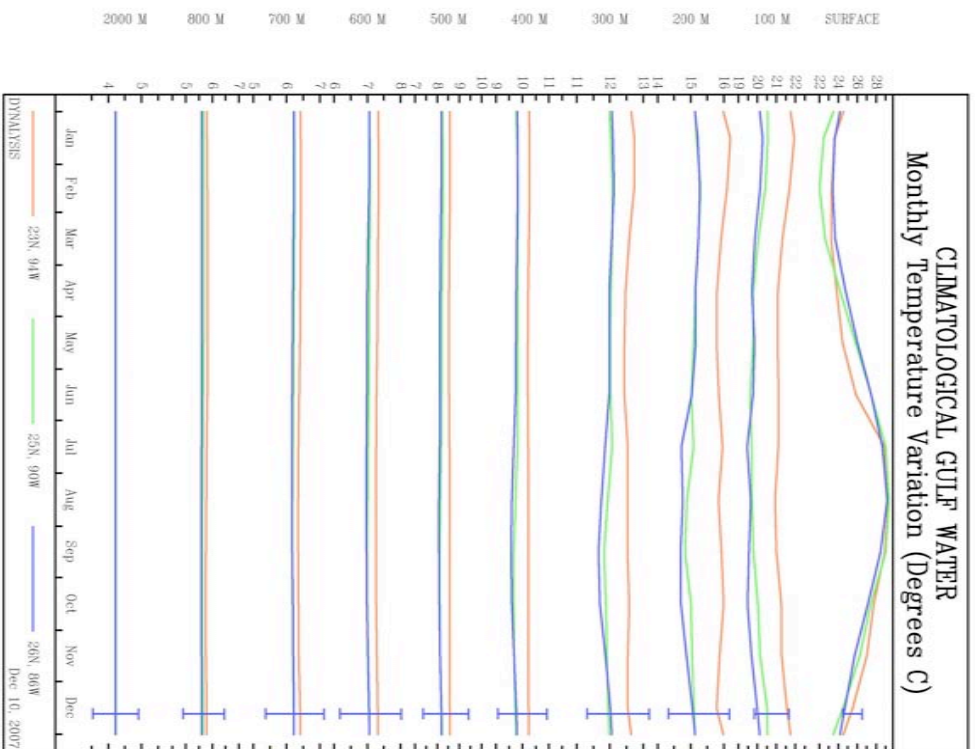
Figure 2.5 Histograms (b) and (d) for two sets of temperature profiles (a) and (c), respectively, at a number of depths in the pycnocline, where the green ticks indicate the Gulf-wide mean temperatures of the GCW and LEW profiles at each depth.

Histograms of the number of profiles for temperatures at depths of 200, 250, 300, 400 and 500 m were used to identify groups of profiles that were within 2 C° of the two peak values of the histogram nearest, respectively, the GCW and LEW mean profile temperatures at that depth. Using this technique the actual temperature level of the water mass is not constrained; the only purpose of comparing with the mean profiles is to identify and distinguish between the GCW and LEW peaks. Profiles within 2 C° of the two peak values of the histogram were then classified as local GCW and LEW profiles, respectively. All other profiles were then classified as neither, meaning that they were a mixture of GCW and LEW, or are shelf water, and therefore were not use in calculating the characteristics of the pure water masses.

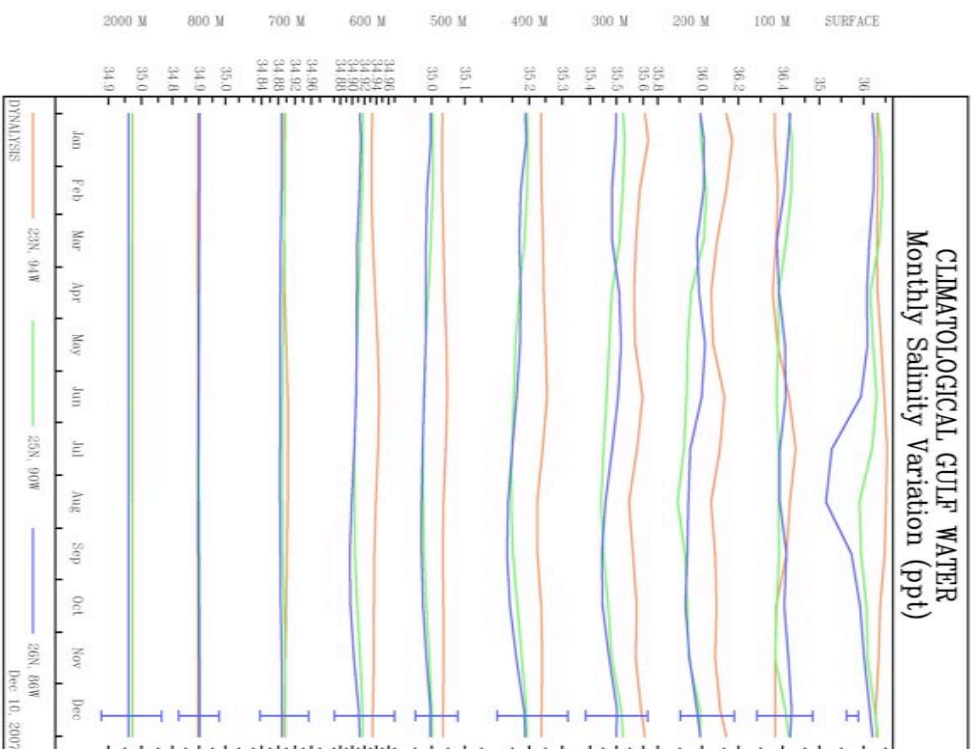
Using only the profiles for GCW selected in this fashion, a climatological distribution of GCW was constructed for monthly intervals on an eighth degree grid (186x121). As might be anticipated, for depths between 200m and 1000m shown in Figure 2.6, the properties of GCW are statistically constant in time, varying only with location in the Gulf. Figure 2.6 shows the monthly variation of temperature and salinity for a variety of depths through the pycnocline at three locations, the Western Gulf, the Central Gulf and the Eastern Gulf. The vertical intervals plotted at the right of each depth time series represent the standard deviation at that depth and it is clear that the monthly variation has no statistical significance below 200 m. Evidently the variability in the Gulf below 200m is entirely due to the presence or absence of the Loop and Eddies.

Therefore in the pycnocline it is appropriate to employ annual mean temperature and salinity fields to represent the GCW distribution. Examples of the mean temperature and salinity fields for several depths are shown in Figures 2.7 and 2.9, and the corresponding standard deviation distributions in Figures 2.8 and 2.10, respectively. The absence of the Loop Current signature is noteworthy, but of course, these fields represent the conditions that exist at times when the Loop Current and Eddies are not present at any specified location. Given the parallel set of LEW profiles, it would be possible to construct a companion set of fields for the distribution of LEW throughout the region where LEW exists. These distributions would show the gradual mixing as the Eddies moved toward the Western Gulf and the apparent cooling of the LEW. However, since the purpose of this study is to estimate the likelihood of encountering LEW at a given point, this would require a two-step process – to determine the local characteristics of an Eddy and then the likelihood of finding an Eddy. It is more direct to simply determine the proportion of original LEW at a given point, where the LEW profile is defined as the mean conditions at the Yucatan Strait, shown as the higher temperature dashed line in Figures 2.1 and 2.2.

This conclusion is strengthened by the observation that original LEW is present even fairly far west, presumably from the interior of Eddies that have not, as yet, fully mixed. The Yucatan Current flowing in through the Yucatan Strait has well defined temperature and salinity profiles in the pycnocline that are uniform throughout the year.



(a) Monthly temperature variation



(b) Monthly salinity variation

Figure 2.6 Monthly variation of the climatological GCW temperature and salinity at the surface and at a number of depths through the pycnocline for typical locations in the Western (red), Central (green) and Eastern (blue) Gulf, illustrating that, except at the surface, the seasonal variation is negligible compared with the standard deviation, shown with bars at the right ends of each plot.

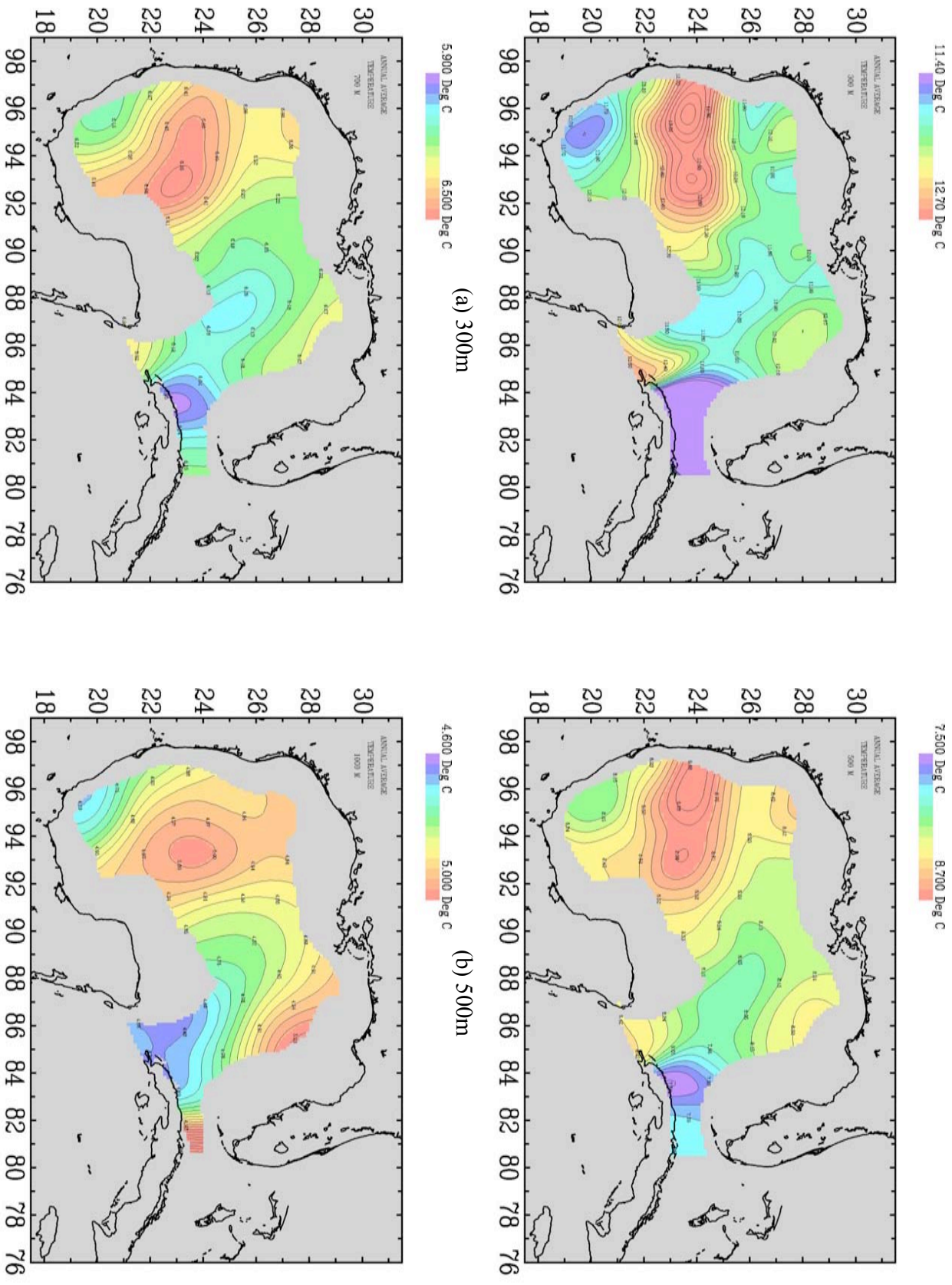


Figure 2.7 Annual average distribution of climatological GCW temperature at several depths on an eighth degree grid (186x121).

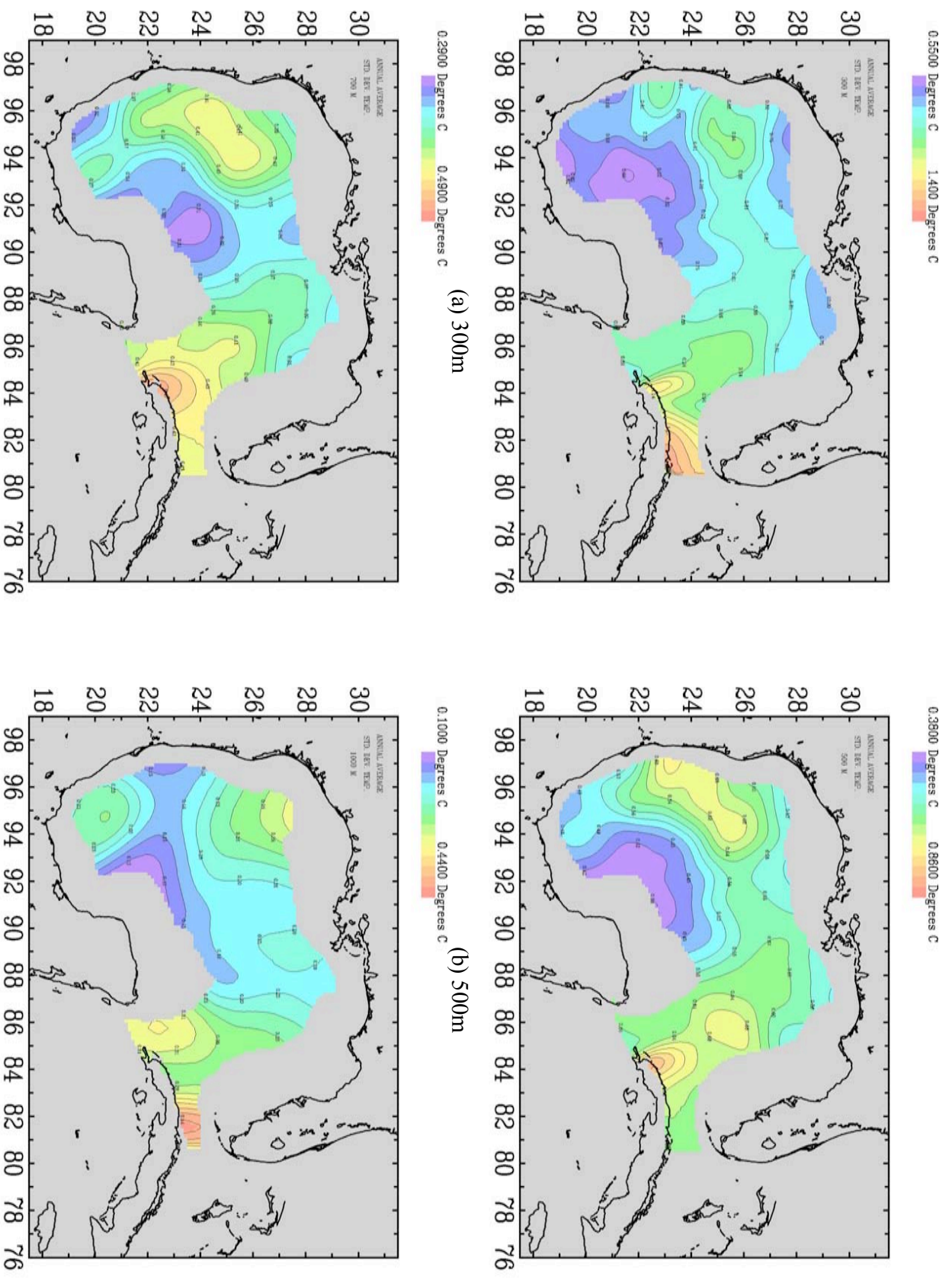


Figure 2.8 Annual average distribution of standard deviation of GCW temperature at several depths on an eighth degree grid.

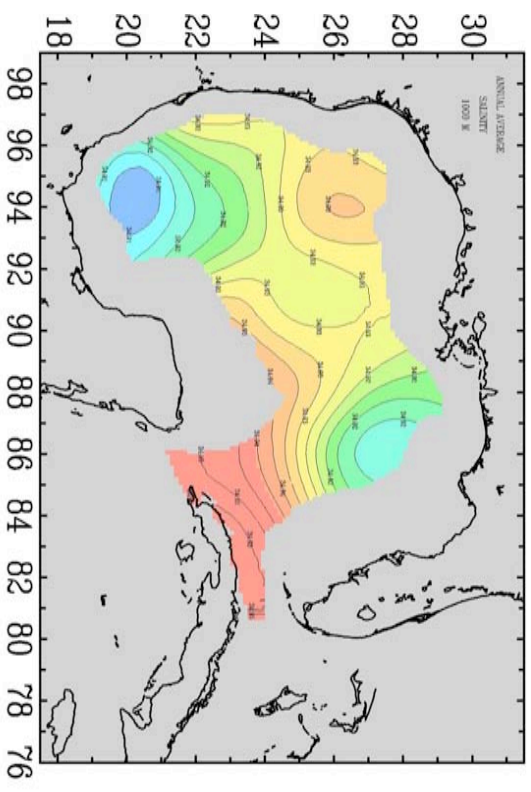
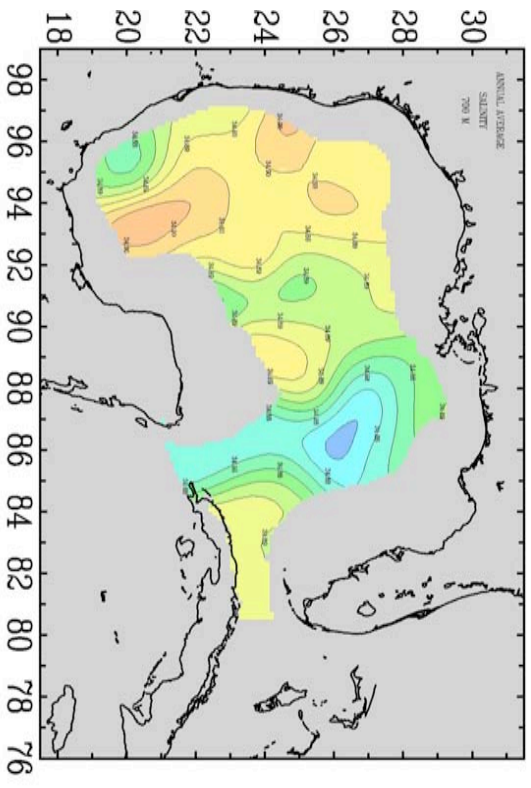
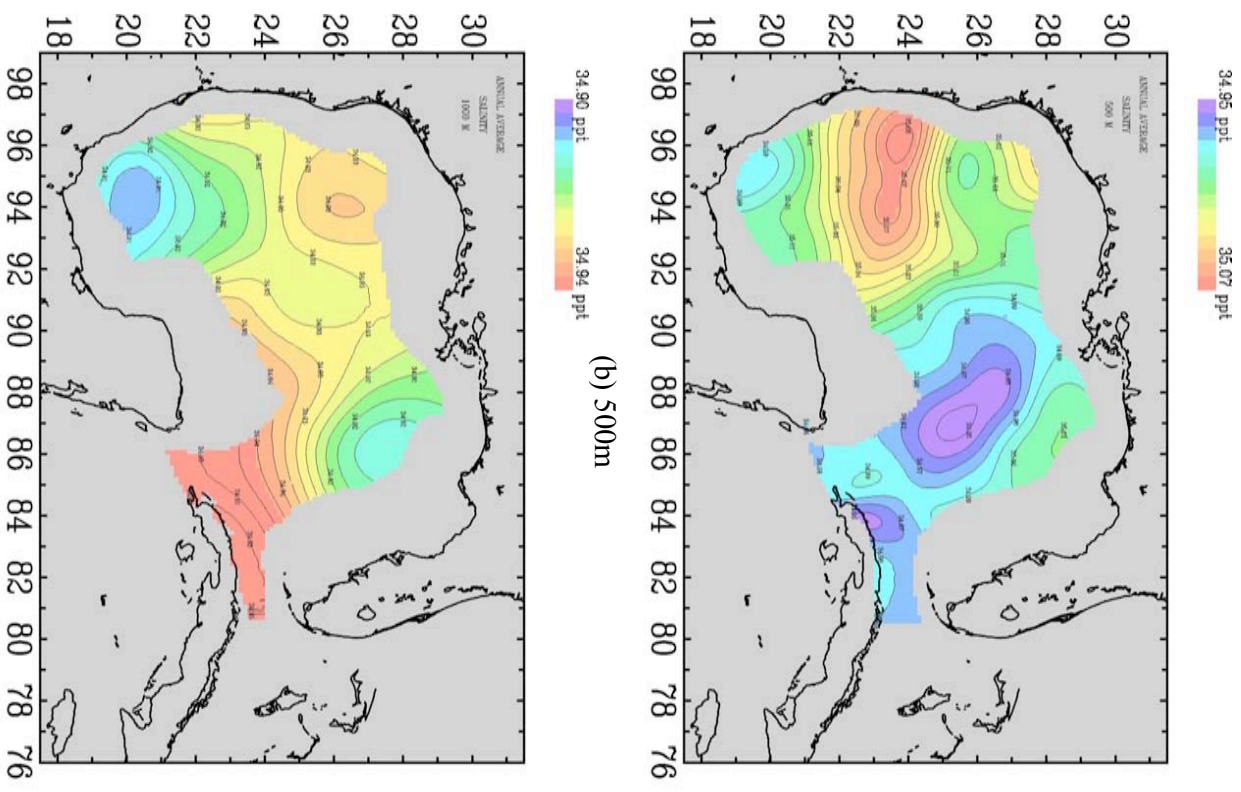
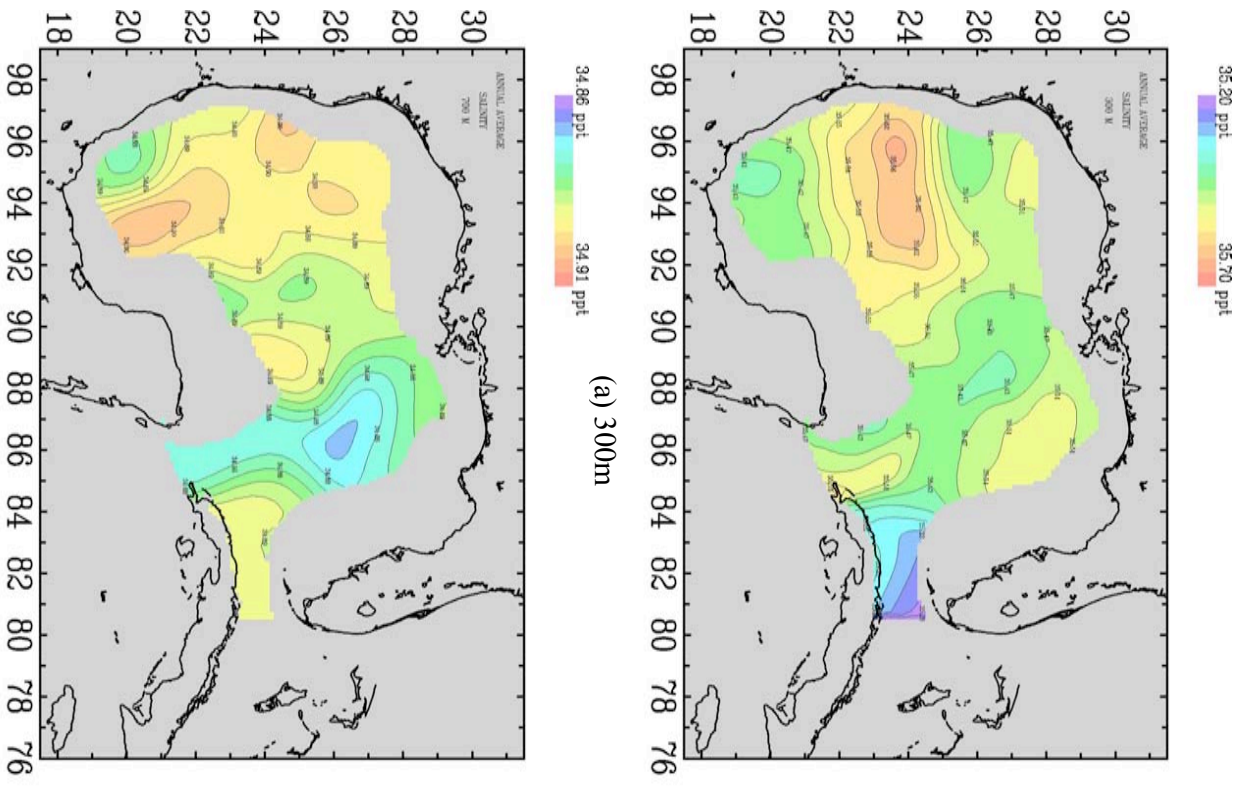


Figure 2.9 Annual average distribution of climatological GCW salinity at several depths on an eighth degree grid (186x121).

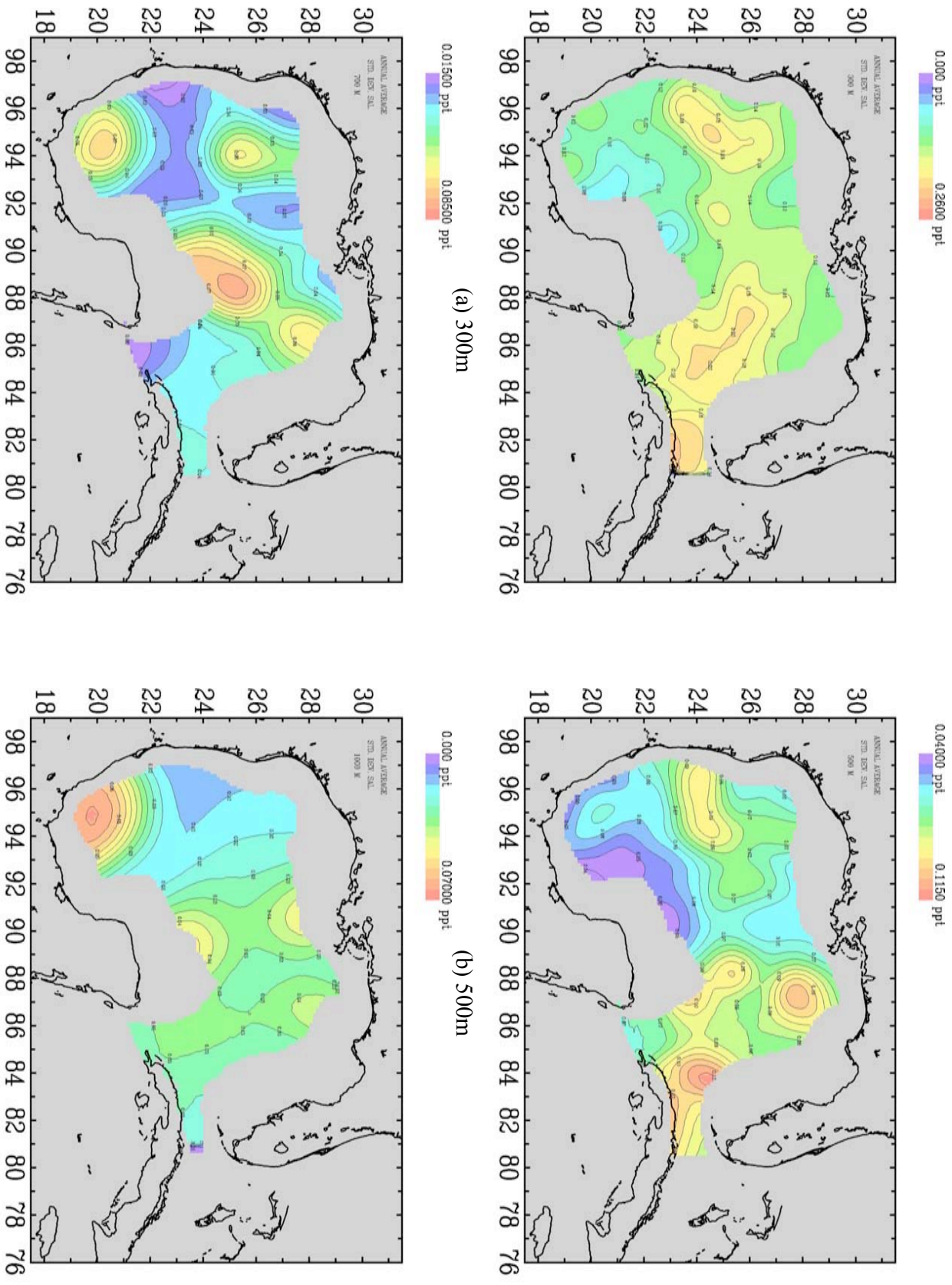


Figure 2.10 Annual average distribution of standard deviation of GCW salinity at several depths on an eighth degree grid.

These profiles persist as the current moves up into the Gulf, around the Loop and flows out through the Florida Strait, being modified only along the boundaries as the Loop Current mixes with the surrounding GCW. The Eddies, also, contain a core of LEW which remains intact until the mixing finally extends to the Eddy center. Therefore, as shown for example at the four locations in Figure 2.1, pure unmixed LEW is found at locations in the Gulf where the Loop and Eddies are still robust. Therefore, as described in the previous paragraph, it is simplest to define LEW properties as those which enter through the Yucatan Strait and the probability of finding LEW at any location as the proportion of LEW properties compared to the local GCW properties.

2.2 LEW Probability

Having established the characteristics of the GCW and of the LEW, it now remains to determine the combination of the two, which produces the climatological conditions in the Gulf. Defining the climatological GCW as $T_g(x, y, z)$ and the LEW profile as $T_l(z)$, then the likelihood of finding LEW at a given location based on a statistically representative set of N observed profiles, $T_n(z)$, is

$$P(x, y) = \frac{1}{N} \sum_{n=1}^N \frac{1}{(z_2 - z_1)} \int_{z_1}^{z_2} \left[\frac{T_n(z) - T_g(x, y, z)}{T_l(z) - T_g(x, y, z)} \right] dz, \quad (2.1)$$

where T could be either temperature or salinity; however, due to the vast preponderance of temperature profiles in the data set, only temperature was used here. The interval used for comparison was from $z_2 = 200m$ to $z_1 = 500m$, where the separation between profiles was largest. The likelihood, $P(x, y)$, is shown in Figure 2.11.

Of course the question is whether $T_n(z)$ is really a statistically representative set of observations. Clearly the available observations shown in Figure 2.4 are not at regular intervals in time and space, but they may still be representative if they are not biased by some regular inclusion or omission of climatologically significant conditions. For most purposes an uneven distribution of data simply means that the confidence level is greater in some regions and at some times than at others. Here, however, more sampling when Eddies are present results in the conclusion that the statistical likelihood of finding an Eddy is greater than the actual climatological probability.

A large portion of the data is from Navy sampling for anti-submarine warfare and from ship-of-opportunity data, while the coverage in time and space may not be optimal; the sample is at least unlikely to favor Eddies, *per se*. However, with the advent of satellite remote sensing and the concurrent preoccupation with Loop and Eddy behavior, hydrographic surveys of the Loop and Eddies have become very common. Even with the omission of the petroleum industry casts, it is possible that the data sets included Eddy surveys. In order to examine this bias and estimate its effect on the results, several tests were performed, as shown in Figure 2.11. Figure 2.11(a) is the likelihood distribution based on all available data. Assuming that widespread use of satellite data

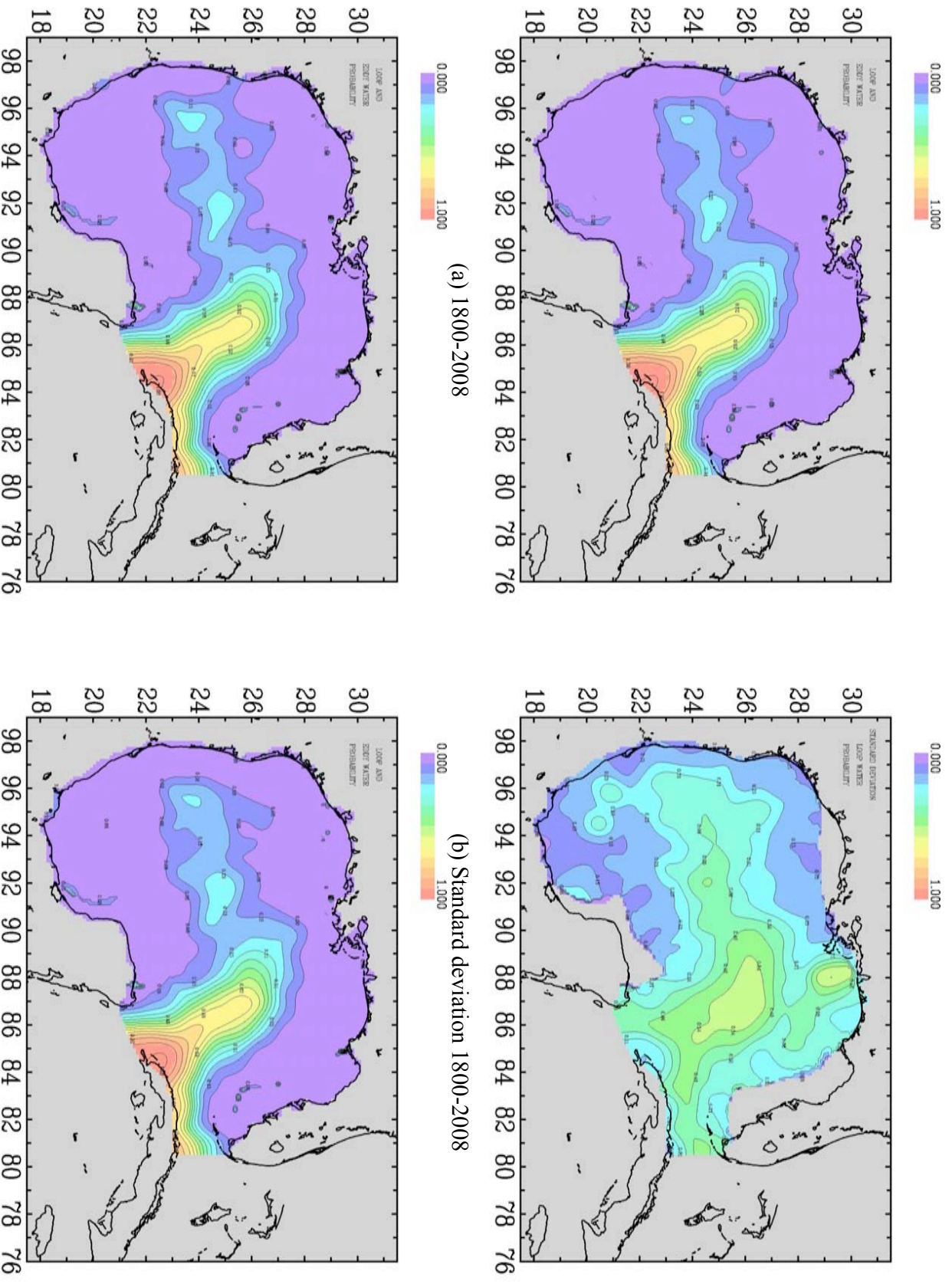


Figure 2.11 Likelihood of finding LEW from all data (a,b) and several subsets of the complete data-set (c) and (d).

began with TOPEX/Poseidon in 1993, the likelihood distribution, shown in Figure 2.11(c), was calculated with only pre-1993 data. Assuming that the Navy anti-submarine data and ship-of-opportunity data was largely in the form of XBT, temperature-only data, and Loop and Eddy survey data was largely CTD data, another likelihood function, shown in Figure 2.11(d), was produced from temperature-only casts. Compared with Figure 2.11(a), Figures 2.11(c) and 2.11(d) are remarkably similar. Figure 2.11(c) indicates that including data after 1992 has no significant effect and Figure 2.11(d) shows that the use of pre-planned hydrographic survey data does not bias the likelihood. Given these results, the likelihood calculated from the entire data-set, Figure 2.11(a), is judged to be the most representative candidate from the data available. The standard deviation for this likelihood distribution is shown in Figure 2.11(b).

2.3 Complete Climatological Distribution

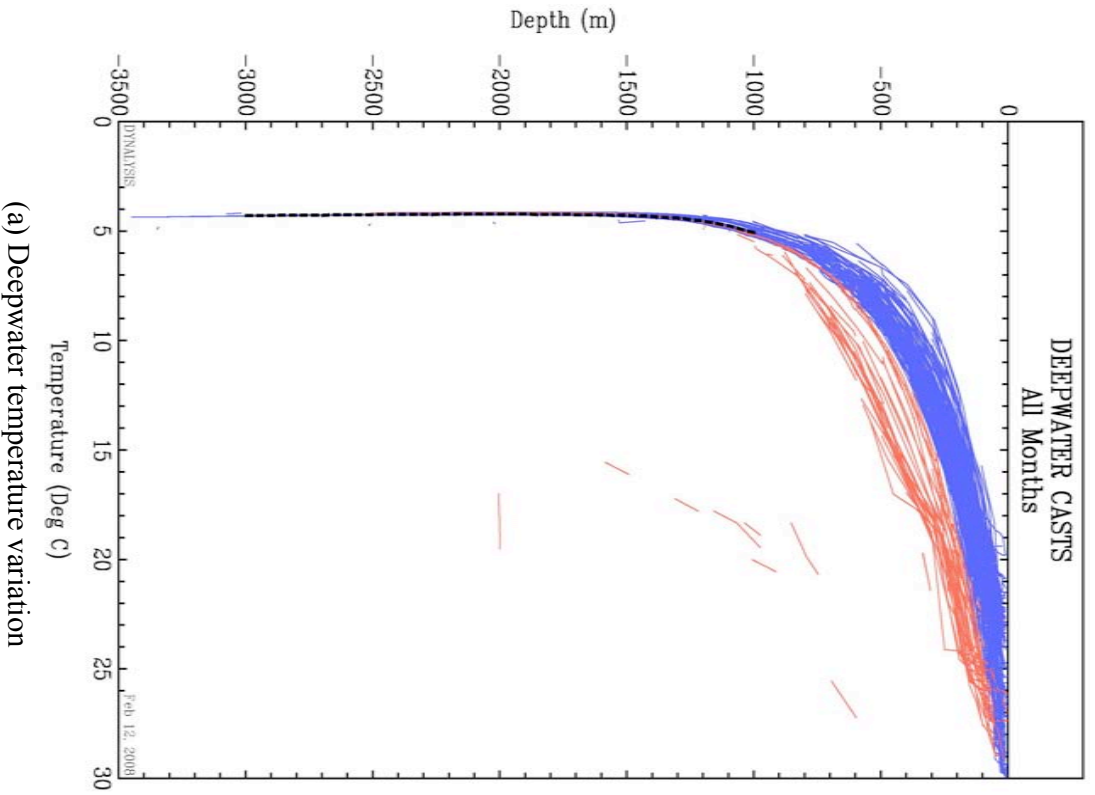
Through examination of the portion of the temperature profiles in the region of the pycnocline, between 200m and 1000m, it has been demonstrated that the hydrographic conditions in the Gulf can be expressed as a combination of the GCW and the LEW determined as a function of the likelihood of finding LEW at any given location in the Gulf. However, it is necessary to determine the distribution of the properties above and below the pycnocline, in order to complete the representation of the Gulf hydrography.

Below 1000m the in situ temperature and salinity are nearly constant in space and time. The number of casts that extend to or near the bottom of the central Gulf is much smaller and are almost entirely research quality temperature and salinity casts. Both GCW and LEW casts are used, since they are indistinguishable below 1000m. The results for both temperature and salinity are shown in Figure 2.12.

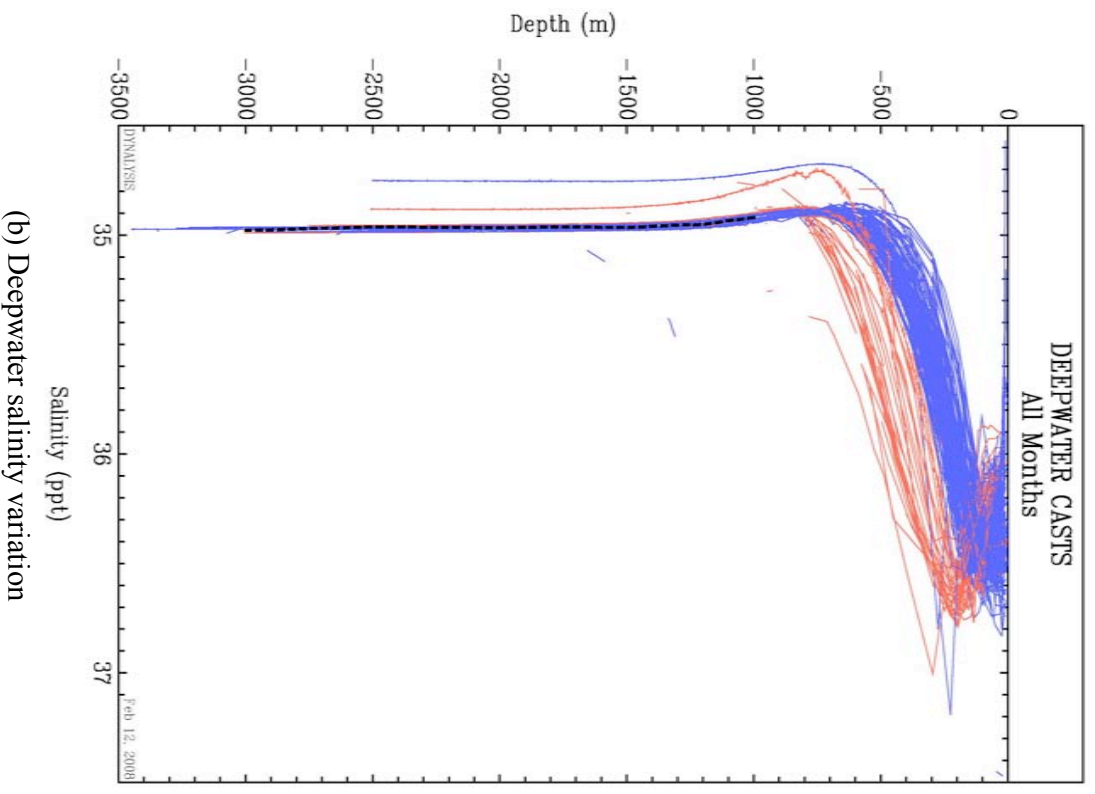
Between 200m and the surface the picture is more complex. In the region above 200m the properties vary strongly with season. The temperature and salinity profiles consist of surface conditions which are mixed down by turbulence, which is related to the strength and duration of the surface winds. This mixed layer consisting of vertically uniform conditions can be of the order of centimeters for long term calm conditions to as much as 50m for sustained, strong winds. Below the uniform portion of the mixed layer, the profiles relax smoothly to the conditions at the upper end of the pycnocline at roughly 200m.

Considering first the GCW climatology, the surface temperature conditions are a strong function of short and long wave radiation, which is a function of season and to a lesser extent surface heat flux, which is proportional to the surface wind stress. The surface salinity is affected by fresh water from seasonal river runoff and to a lesser extent by evaporation and precipitation. The seasonal variation of these conditions is well represented by a monthly climatology of the surface layer calculated from the GCW data. However, since the criteria used to select the GCW effectively excludes shallow water data, these shallow water data are included in the climatological background calculation in order to correctly represent the surface water on the shelves. Seasonal samples of these temperature and salinity surface distributions are shown in Figures 2.13 and 2.14, respectively.

The influence of surface forcing on LEW is similar to that of GCW. In addition to mixing laterally, as the Eddies move across the Gulf, they also age as their surface conditions respond to the surface forcing. The LEW surface layer, however, is warmer and less saline than the GCW and the



(a) Deepwater temperature variation



(b) Deepwater salinity variation

Figure 2.12 Mean variation of the deepwater temperature and salinity shown with black dashed lines over-plotted with both GCW (blue) and LEW (red) profiles that extend into the deepwater illustrating that, with the exception of several obviously errant salinity profiles, the deepwater conditions, below 1000 m, are remarkably uniform in space and time.

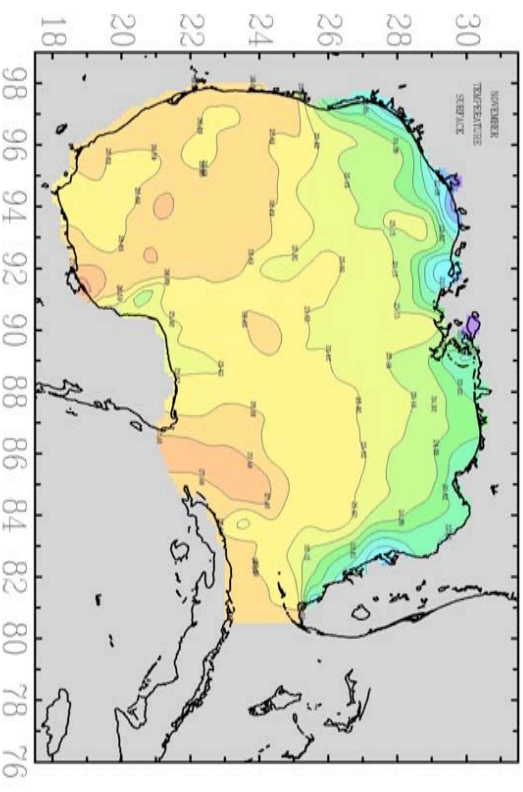
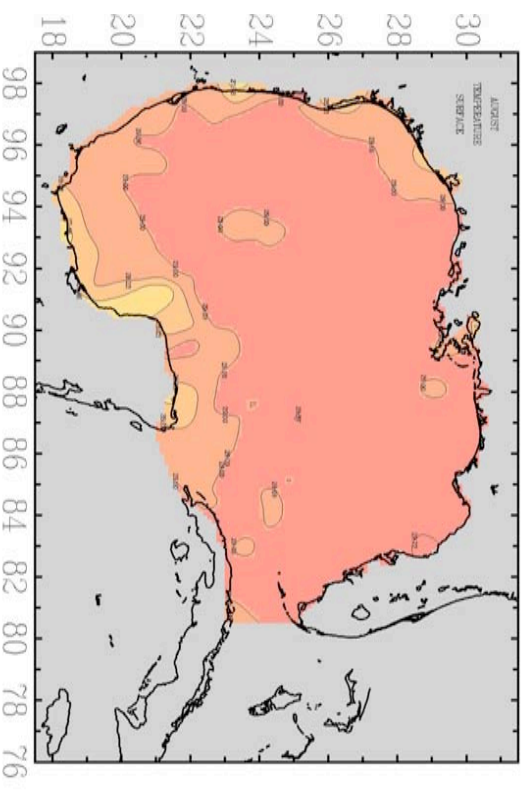
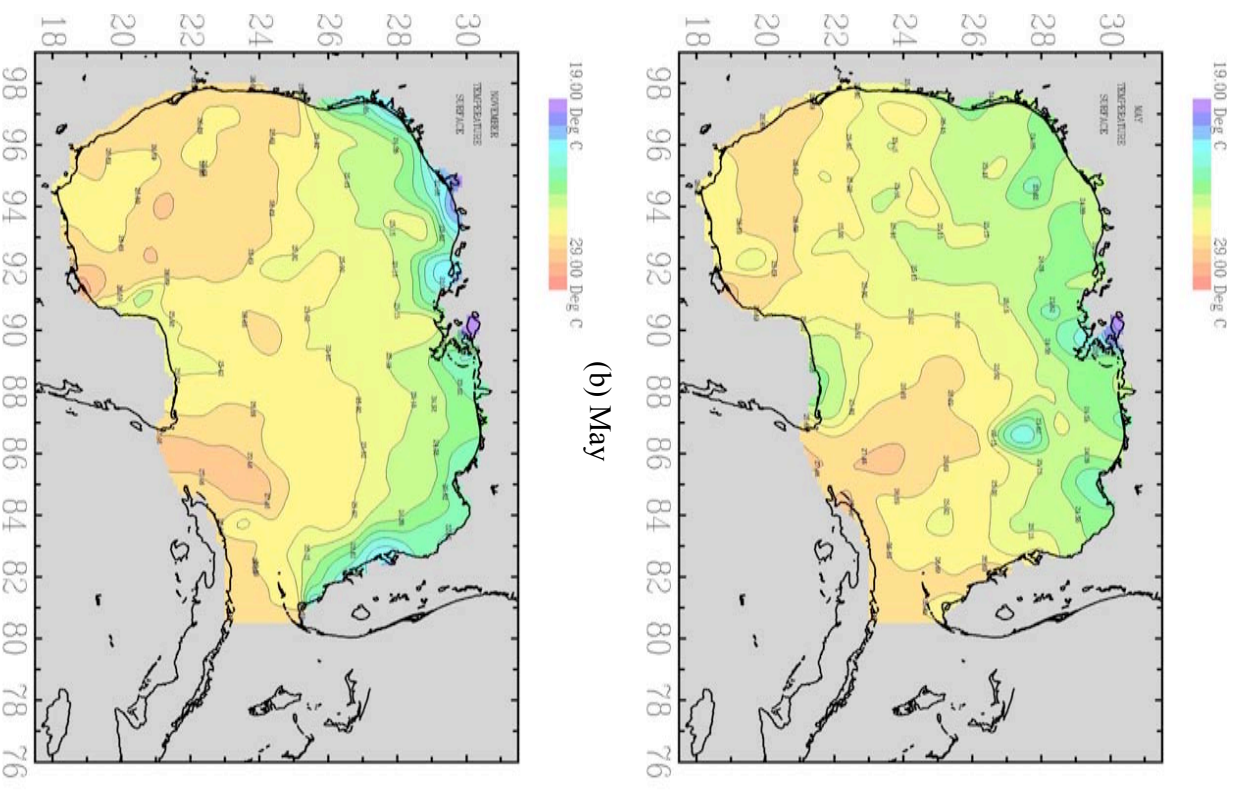
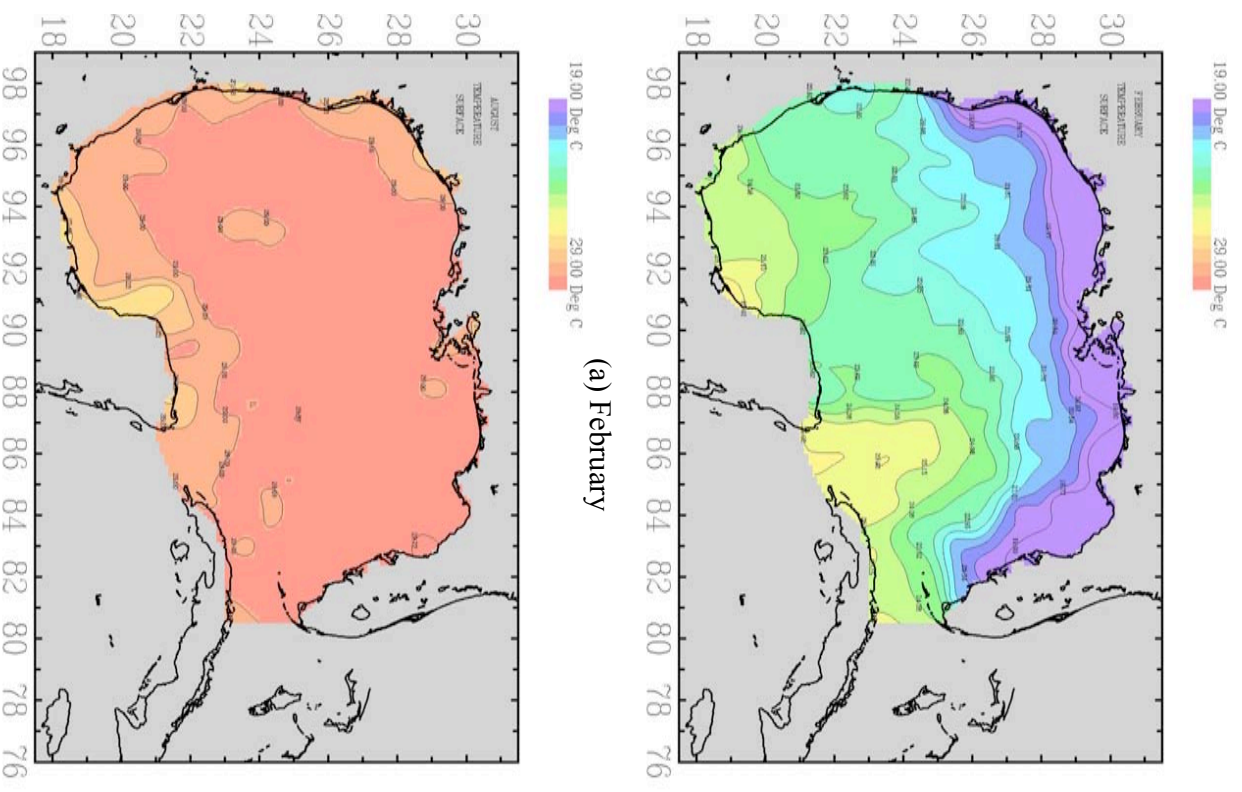


Figure 2.13 Climatological surface temperature distributions of GCW for representative months during each season.

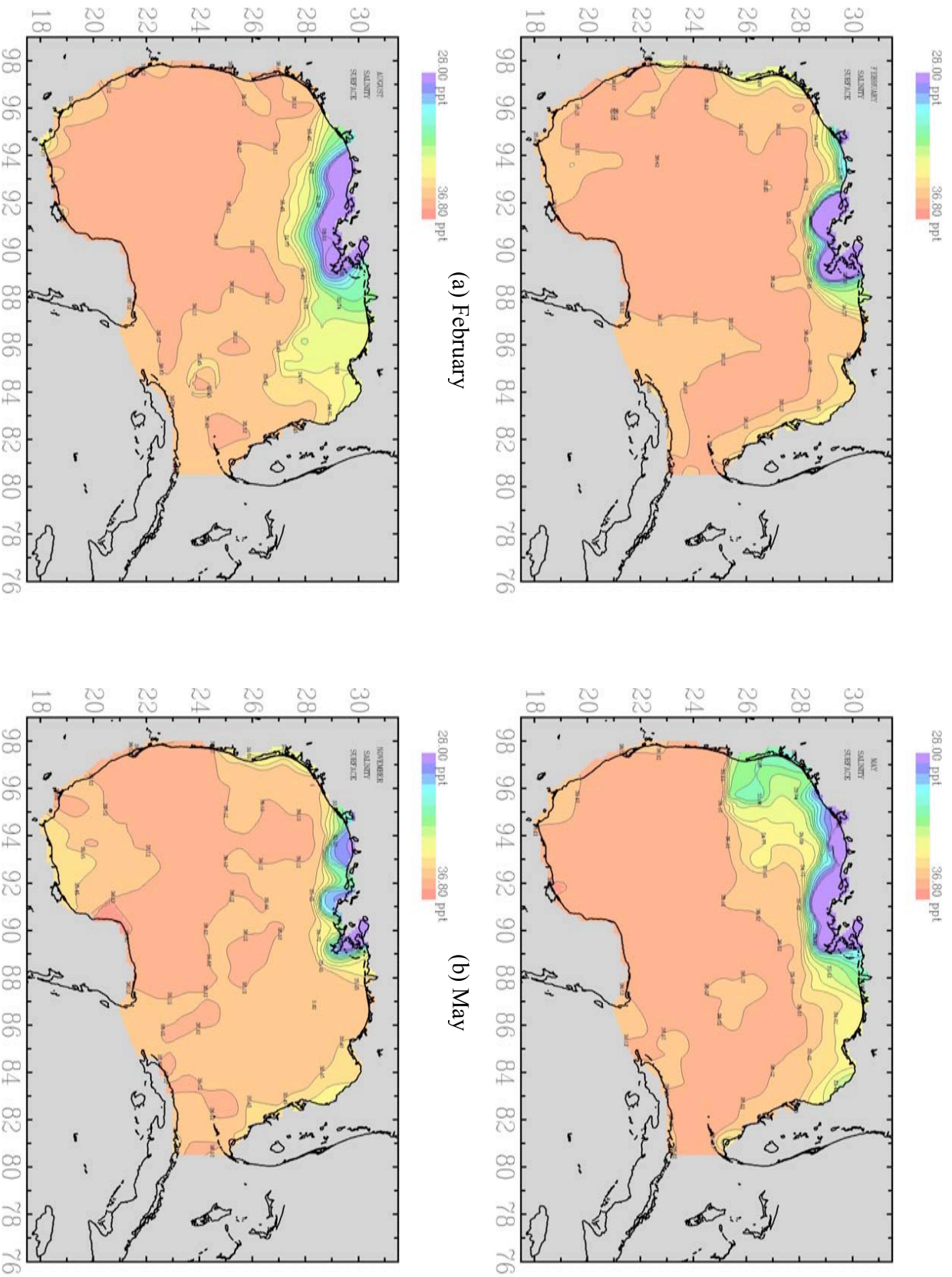


Figure 2.14 Climatological surface salinity distributions of GCW for representative months during each season.

salinity profile of the LEW has a pronounced subsurface maximum at 200m depth. The result is that at times and locations that the LEW is present, the surface layer profiles differ from those of the GCW. Samples of the seasonal surface values of LEW temperature and salinity are shown in Figures 2.15 and 2.16, respectively.

Using these components it is possible to construct a complete hydrographic climatology for the Gulf. The climatological profile of temperature can be expressed as,

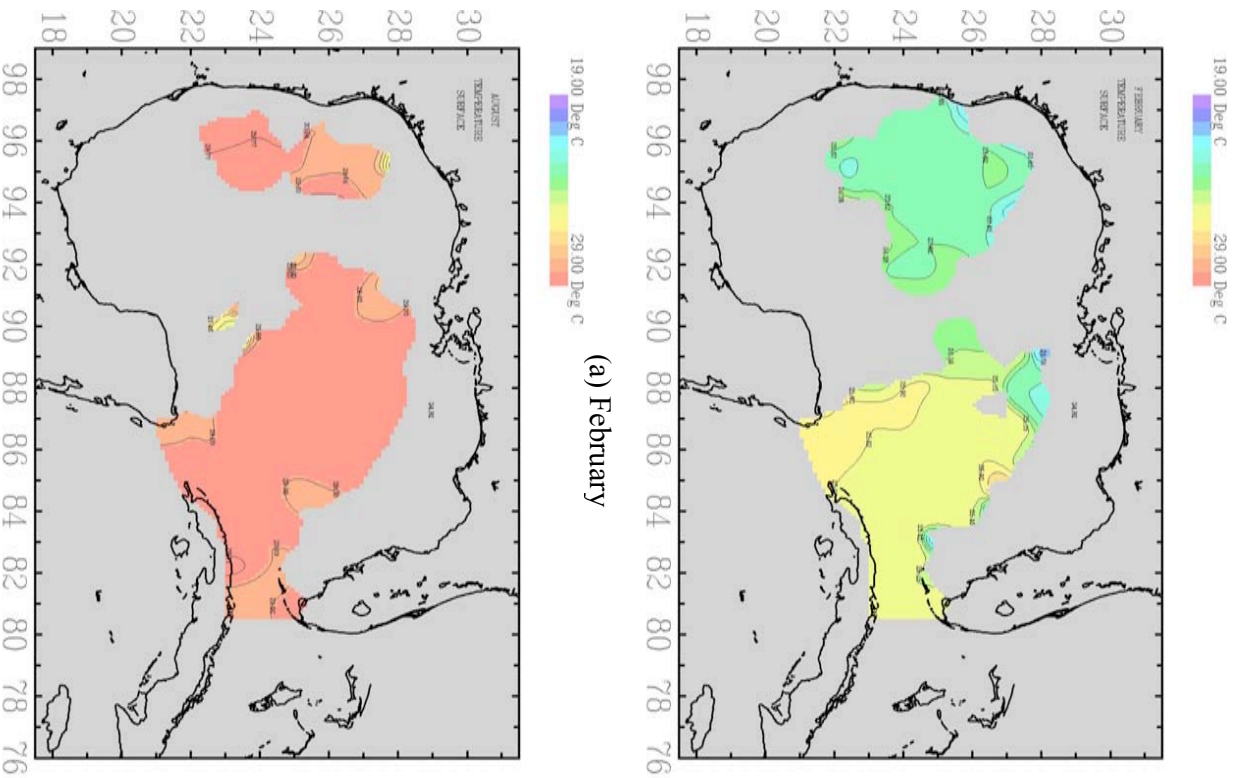
$$T(x, y, z, m) = [T_g^s(x, y, z, m) + T_g^p(x, y, z)] [1 - P(x, y)] + [T_l^s(x, y, z, m) + T_l^p(z)] P(x, y) + T^d(z) \quad (2.2)$$

where $T_g^s(x, y, m)$ are the monthly climatological surface fields of GCW shown in Figure 2.11, $T_g^p(x, y, z)$ is the GCW distribution in the pycnocline, shown in Figure 2.7, $T_l^s(x, y, m)$ are the monthly climatological surface fields of LEW shown in Figure 2.15, $T_l^p(z)$ is the dashed profile in Figure 2.5 representing the LEW profile in the pycnocline, $T^d(z)$ is the deepwater temperature profile below 1000m shown in Figure 2.12(a) and, finally, $P(x, y)$ is the likelihood of finding LEW at a particular location shown in Figure 2.11(a). The climatological salinity profile was constructed in the same manner using the data in the accompanying Figures 2.14 and 2.16.

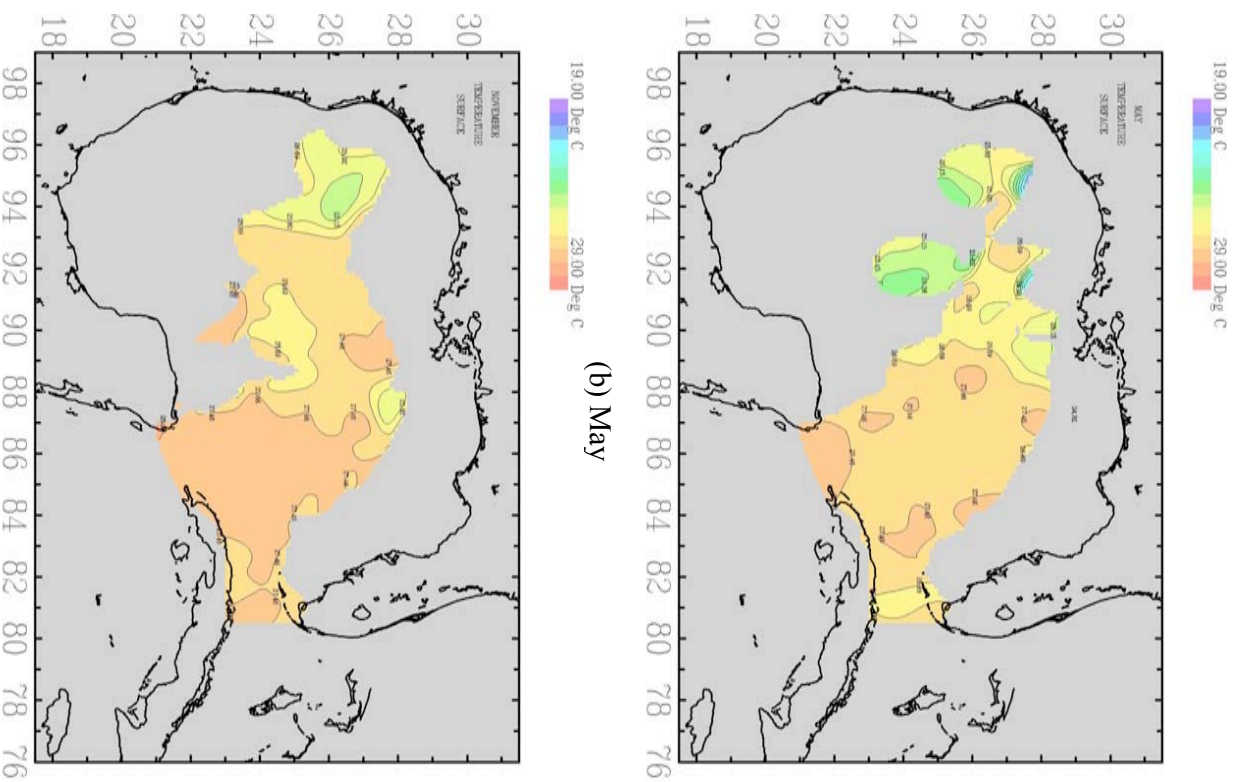
The resulting hydrographic climatology for the Gulf is shown in Figures 2.17 through 2.20. The distribution of climatological surface temperature and salinity are shown as four months representing the four seasons in Figures 2.17 and 2.18, respectively. The small but perceptible difference between the full climatological surface distributions and that of the GCW alone, in Figures 2.13 and 2.14, indicates that the influence of the surface fluxes on the surface layer is greater than that of the mixing of the subsurface conditions up to the surface.

In the pycnocline, the temperature and salinity profiles, for both GCW and LEW, are not a function of season, so that the distributions are described by the annual averages, shown in Figures 2.19 and 2.20. Here, with reference to the annual average climatological GCW fields shown in Figures 2.7 and 2.8, the presence of the LEW is pronounced and well defined. Ultimately, this sharper definition of the fields in the pycnocline is the result of two improvements in the climatological averaging methodology; first, the recognition that the profiles in the pycnocline are independent of season, results in the availability of more than an order of magnitude of additional profiles to define a single, statistically more robust, annual average profile; and second, the method of selecting the GCW profiles and the LEW profiles automatically eliminates outlying profiles that blur the basic structure. The resulting climatology is both more representative and more succinct than a conventional climatology based on a simple monthly average of all available data.

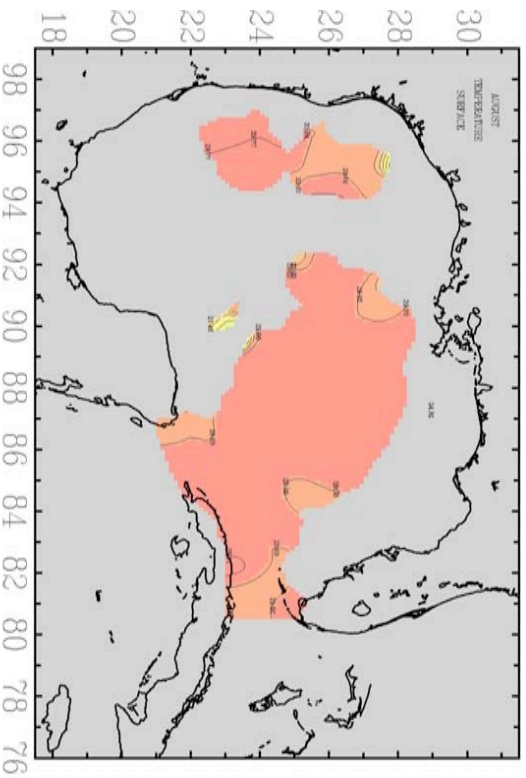
The final form of the atlas, then, consists of three dimensional monthly distributions of the GCW temperature and salinity and of the LEW temperature and salinity and the annual average probability distribution of LEW at any location in the Gulf. While both the GCW and LEW fields vary monthly in the surface layer, from 200 m depth to the bottom, the GCW



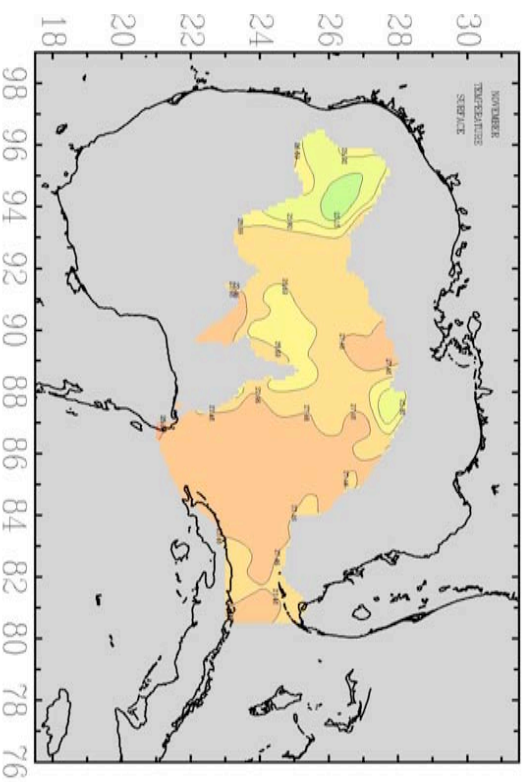
(a) February



(b) May

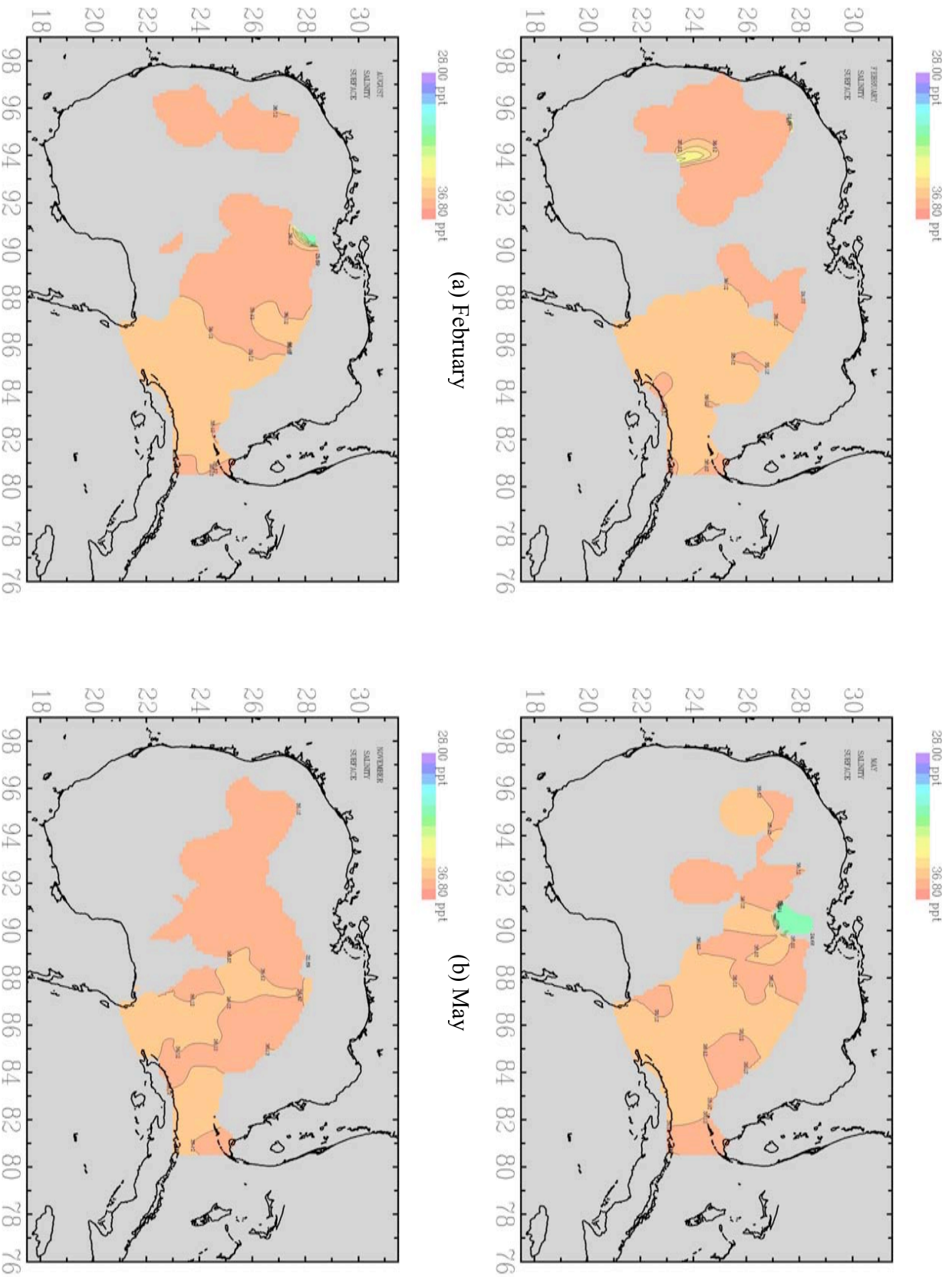


(c) August



(d) November

Figure 2.15 Climatological surface temperature distributions of LEW for representative months during each season.



(a) February
 (b) May
 (c) August
 (d) November
 Figure 2.16 Climatological surface salinity distributions of LEW for representative months during each season.

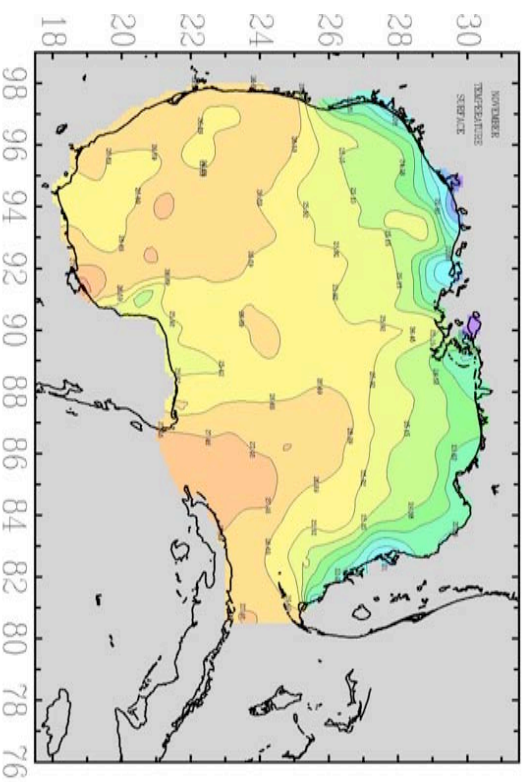
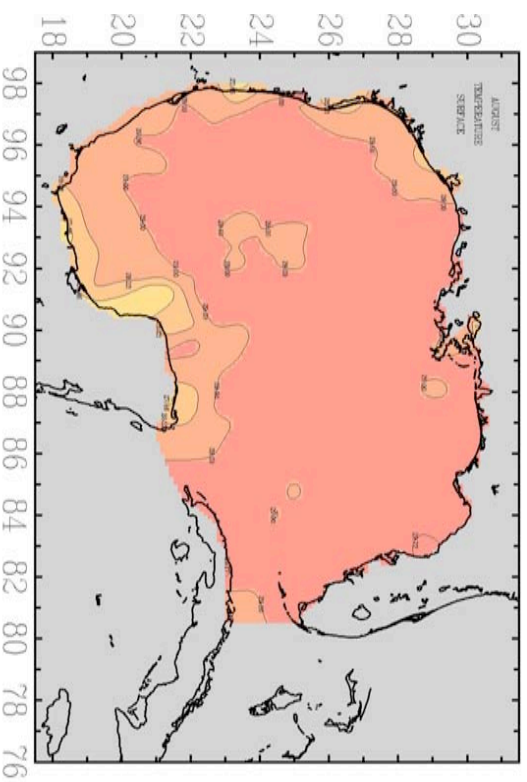
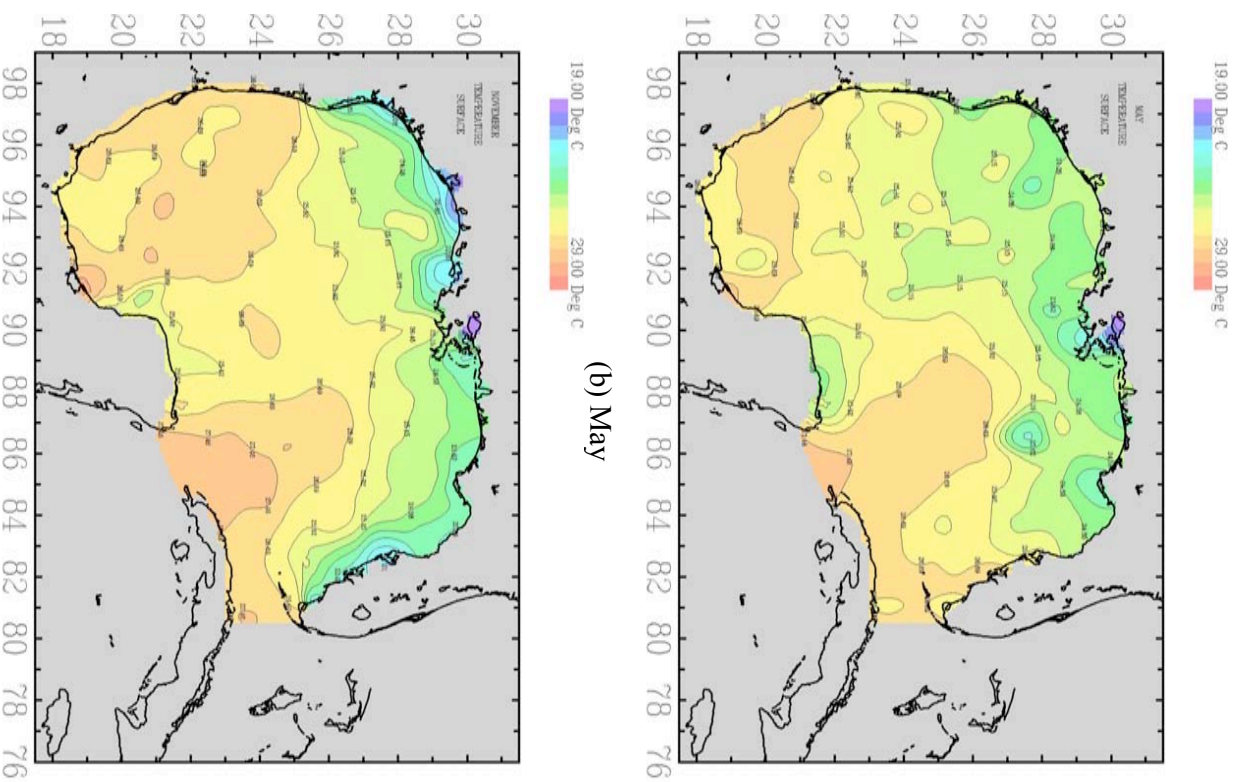
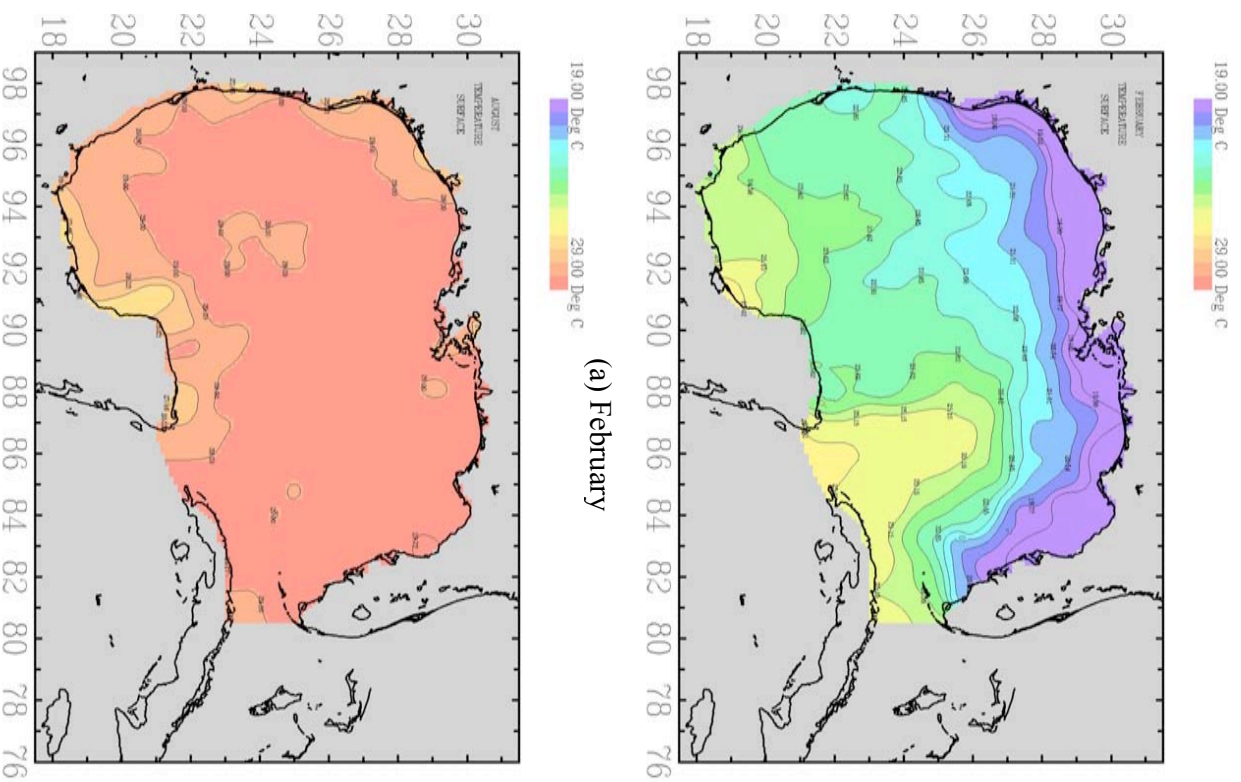


Figure 2.17 Complete climatological surface temperature distributions for representative months during each season.

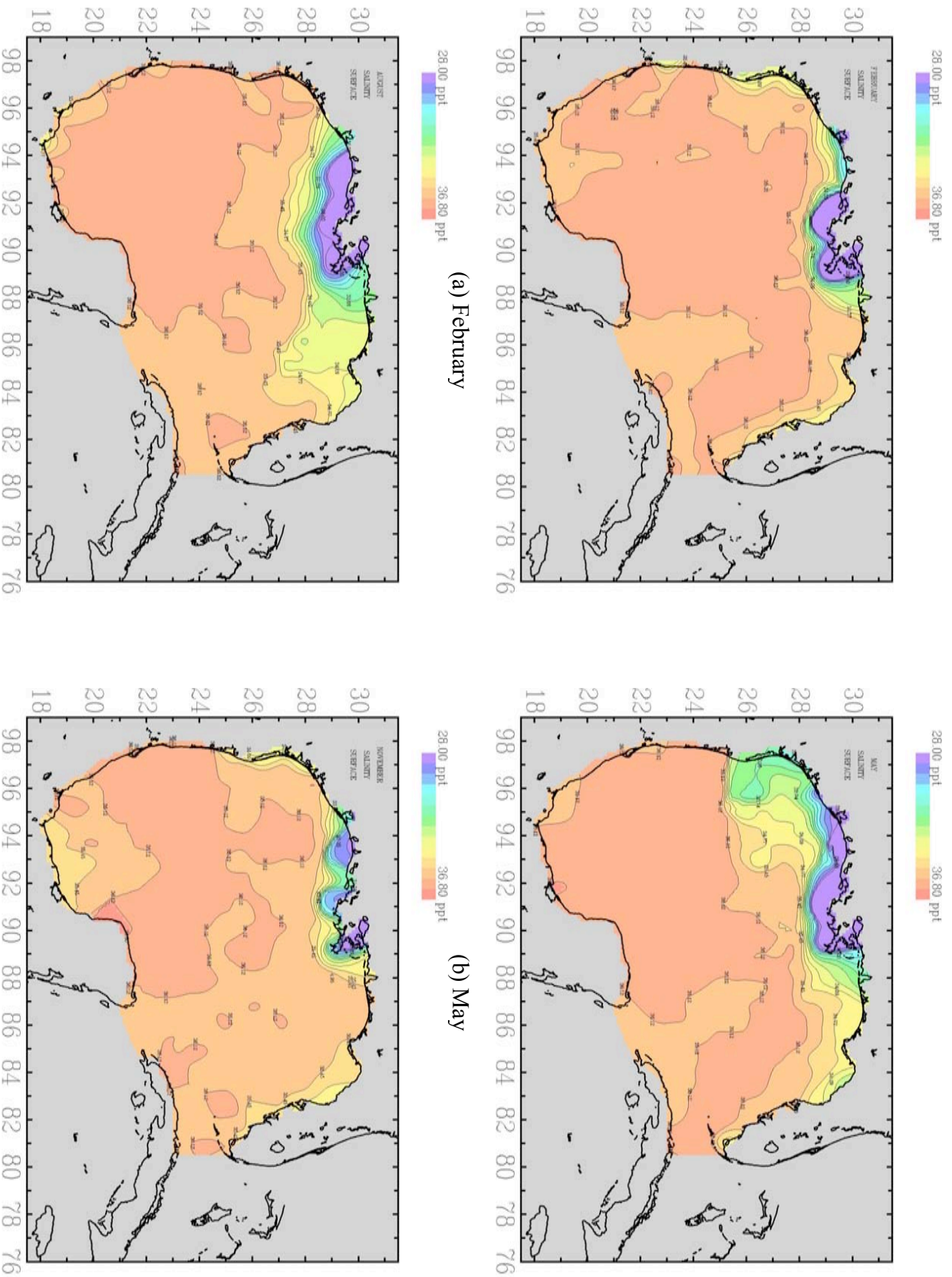


Figure 2.18 Complete climatological surface salinity distributions for representative months during each season.

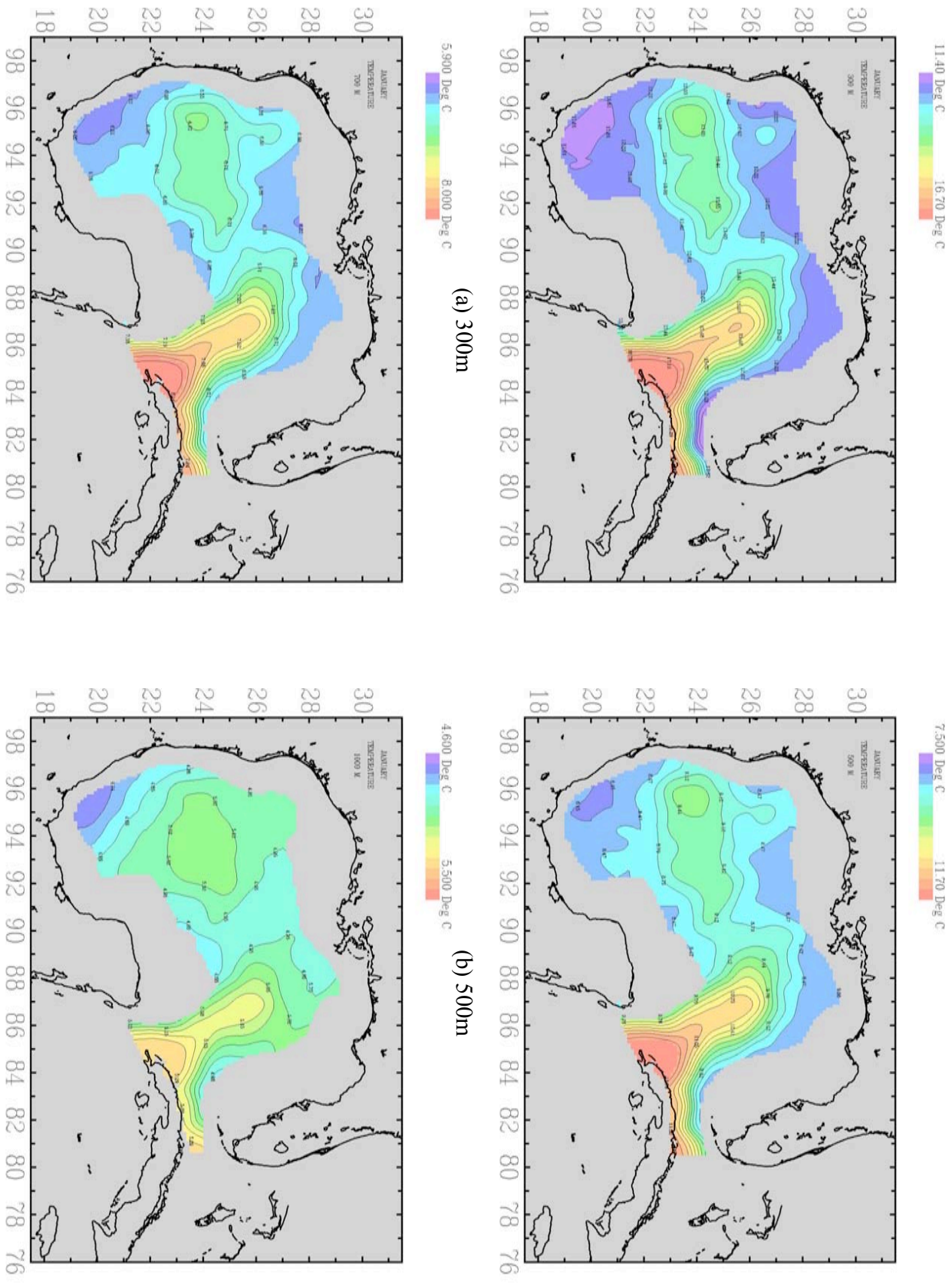


Figure 2.19 Complete climatological annual average temperature distributions for several depths in the pycnocline.

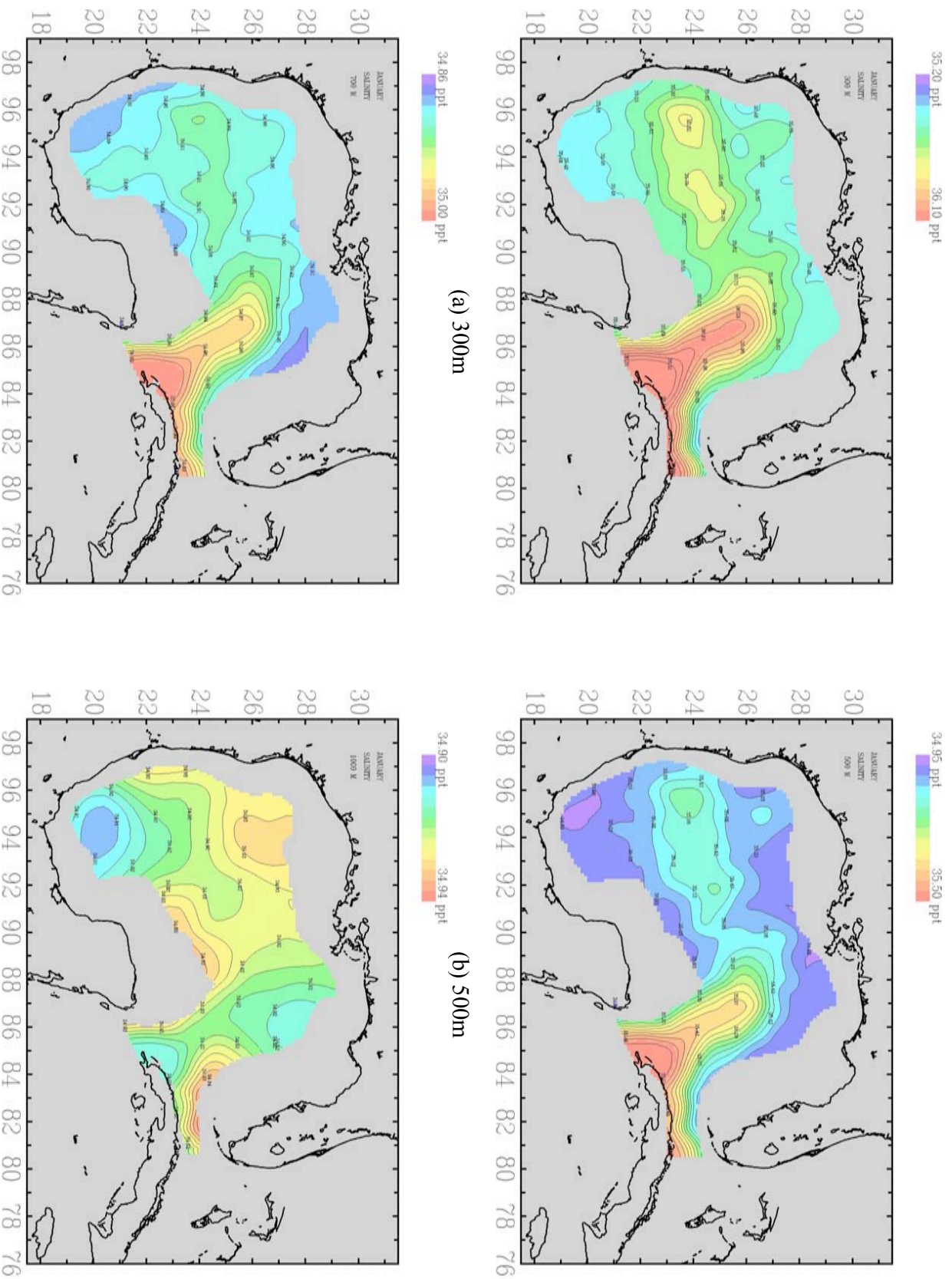


Figure 2.20 Complete climatological annual average salinity distributions for several depths in the pycnocline.

fields do not change and the LEW profile is fixed at the Yucatan Strait condition. This comparatively high resolution eighth-degree grid is practical since the annual average profiles in the pycnocline are well populated compared to what they would be for monthly means and there is adequate data in the surface layer to define monthly averages. The climatological interpolation to the grid for all fields is performed using a Gaussian influence function with a radius of influence of 30km.

Not only does this description produce the conventional atlas of mean properties, it also facilitates two important additional lines of inquiry. Given a hydrocast at any location, the cast properties can be compared with the local GCW and LEW profiles to determine the presence or absence of the Loop or an Eddy at that location. Conversely, if the presence or absence of the Loop or an Eddy is known from an independent source, such as satellite SST images, the subsurface conditions can be ascertained more accurately than from the conventional mean climatology.

2.4 Temporal Changes

Finally, considering the popular preoccupation with global warming, it is tempting to examine what the present data can shed some light on this issue. While a small amount of data extends back to the beginning of the twentieth century, statistically meaningful records begin with the antisubmarine data from World War II. Furthermore, up until the early 1970's, the vast majority of the data is from XBT's with a depth limit of 400m. Even then, the number of CTD measurements to depths greater than 1000 meters is not sufficient to determine statistically reliable trends. Therefore, as a practical matter, the results are only meaningful within the pycnocline from 1940 to the present.

Figure 2.21 shows the Gulf wide mean variation of the individual observations from the climatological temperature during the period 1940 to the present for a number of depths. The lighter line represents a running annual average of the variation and the heavier line is a running ten year mean. The average standard deviation for each depth is indicated by the bar at the right end of the plot. The gradient of the least squares best fit to a linear function is given below the depth label at the left of each depth plot in degrees/year.

Apparently the surface layer is cooling at the rate of 0.002 degrees/year during this period, which is probably not statistically meaningful. However, at 100m and 200m depths the temperature rise is 0.018 and 0.016 degrees/year, respectively, which may be significant. An increase in temperature of the order of 0.010 degree/year is observed down to 600m, below which it begins to drop rapidly into the noise. On balance, the observational data does appear to support a non-negligible temperature increase at depths between 100m and 800m of the order of 0.010 degrees/year in the Gulf of Mexico during the period 1940 to 2008.

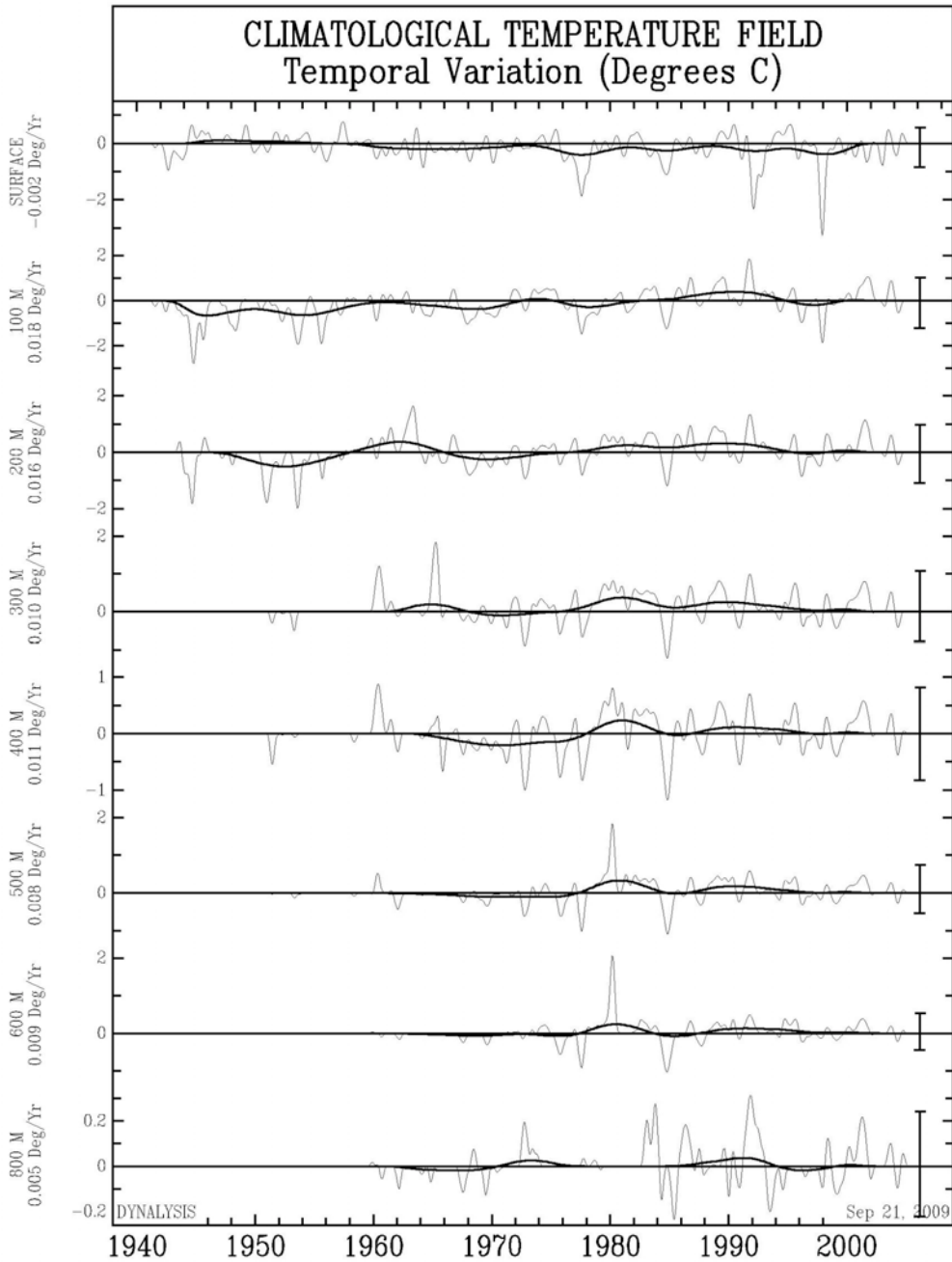


Figure 2.21 Temporal variation of the Gulf wide mean of the difference between individual temperature measurements and the climatological temperature at several depths through the pycnocline for the years 1940 to the present. The lighter and darker traces are the one year and ten year running averages, respectively and the bar at the right indicates the mean standard deviation for each depth.

3. PROFILE SYNTHESIS

The ultimate objective is to develop a method of providing accurate and detailed synoptic three dimensional fields of temperature and salinity fields simulating prevailing conditions to initialize a forecast model. The most comprehensive source of synoptic ocean data available in near-real time is from satellite remote sensing. Prevailing ocean surface conditions are available in the form of satellite altimeter tracks at regular intervals in time and space.

In order to use the altimetry data, the relationship between the SSH anomaly and the underlying hydrographic profiles will be established. This section describes a method of using these synoptic remote sensing data in conjunction with the climatological data developed in the previous section to synthesize complete three dimensional temperature and salinity fields in the ocean below.

3.1 Elevation Calculation

In their treatise on seasonal variability, Gill and Niiler (1973) separate the causes of long-term sea level variation into three parts: the persistent distribution of atmospheric pressure over the basin; the steric contribution; and the influence of long-term dynamic effects on the bottom pressure. The steric term is clearly dominant, since it is both large and persistent, as is evident from the climatology. Since the Gulf is a relatively small basin, the influence of persistent spatial variations in atmospheric pressure will be negligible. However, without actually solving the equations of motion, the influence of the dynamic contribution to the sea level is not clear. In the large ocean basins Gill and Niiler estimate that the dynamic contribution is small for climatological purposes. In the Gulf, however, the presence of strong features such as the Loop and Eddies, the dynamics might become significant, but would not be correlated with the seasons.

Assuming that only the steric height is important for climatological purposes, the relative elevation distribution for various climatological density fields may be calculated. The integral of the density profile, $\rho(x, y, z, t)$, from the surface, s , to a depth, z , determines the pressure at that depth, $p(x, y, z, t)$, relative to the surface, p_s :

$$p(x, y, z, t) - p_s = g \int_s^z \rho(x, y, z', t) dz', \quad (3.1)$$

where x and y are the horizontal coordinates and the variable t indicates that the fields may vary with time as well. Since there is no benchmark reference for the elevation, the long-term time-average, horizontal basin-wide average conditions are used as a reference. Therefore, the local pressure is

$$p(x, y, z, t) - \overline{\langle p(z) \rangle} = g \int_s^z [\rho(x, y, z', t) - \overline{\langle \rho(z') \rangle}] dz', \quad (3.2)$$

where $\langle \rangle$ brackets indicate a horizontal average over the entire Gulf and the over-bar indicates a long-term time average. This pressure difference produces an elevation, η , relative to the long-term temporal and basin-wide spatial mean such that

$$-g \rho_m \eta(x, y, t) = p(x, y, h, t) - \overline{p(z)}, \quad (3.3)$$

or

$$\eta(x, y, t) = -\frac{1}{\rho_m} \int_s^h \left[\rho(x, y, z', t) - \overline{\rho(z')} \right] dz', \quad (3.4)$$

where h is the bottom depth and ρ_m represents the mean density in the water column.

If $\rho(x, y, z', t)$ in Equation 3.4 is taken to be the mean density field over all months, the result is, $\eta_c(x, y)$, the climatological mean elevation distribution throughout the Gulf relative to the Gulf-wide mean elevation. This climatological temporal mean elevation distribution is shown in Figure 3.1. Alternatively, if $\rho(x, y, z', t)$ is taken to be the monthly climatological density field from the temperature and salinity distribution of GCW shown in Figures 2.7, 2.9, 2.12, 2.13 and 2.14, the results, shown in Figure 3.2, are $\eta_g(x, y, m)$, the monthly climatological elevation fields of GCW. Similarly, the monthly climatological LEW elevation fields, $\eta_l(x, y, m)$, maybe calculated, recalling that, even though the profile in the pycnocline has been fixed, the contribution of the seasonal variation in the surface layer can not be neglected.

3.2 LEW Proportion

For a given profile, the proportion of LEW present is the difference between the actual density profile and the GCW normalized by the difference between entirely LEW and GCW:

$$P(x, y, t) = \frac{\int_s^h \left[\rho(x, y, z, t) - \rho_g(x, y, z, m) \right] dz}{\int_s^h \left[\rho_l(x, y, z, m) - \rho_g(x, y, z, m) \right] dz}, \quad (3.5)$$

where the argument, m , indicates that the density profiles are interpolated from the monthly climatological profiles and the subscripts g and l designate the GCW and the LEW profiles, respectively. This formulation is functionally similar to that of Equation 2.1 for the probability of the presence of LEW in the previous Section.

Making use of Equation (3.4) with the density profiles $\rho_g(x, y, z', m)$ and $\rho_l(x, y, z', m)$, it is possible to express the LEW probability in terms of the elevation ratio

$$P(x, y, t) = \frac{\eta(x, y, t) - \eta_g(x, y, m)}{\eta_l(x, y, m) - \eta_g(x, y, m)}, \quad (3.6)$$

where $\eta(x, y, t)$, is the actual elevation at any time, t , and the climatological GCW and LEW elevations are interpolated from the monthly values to that time.

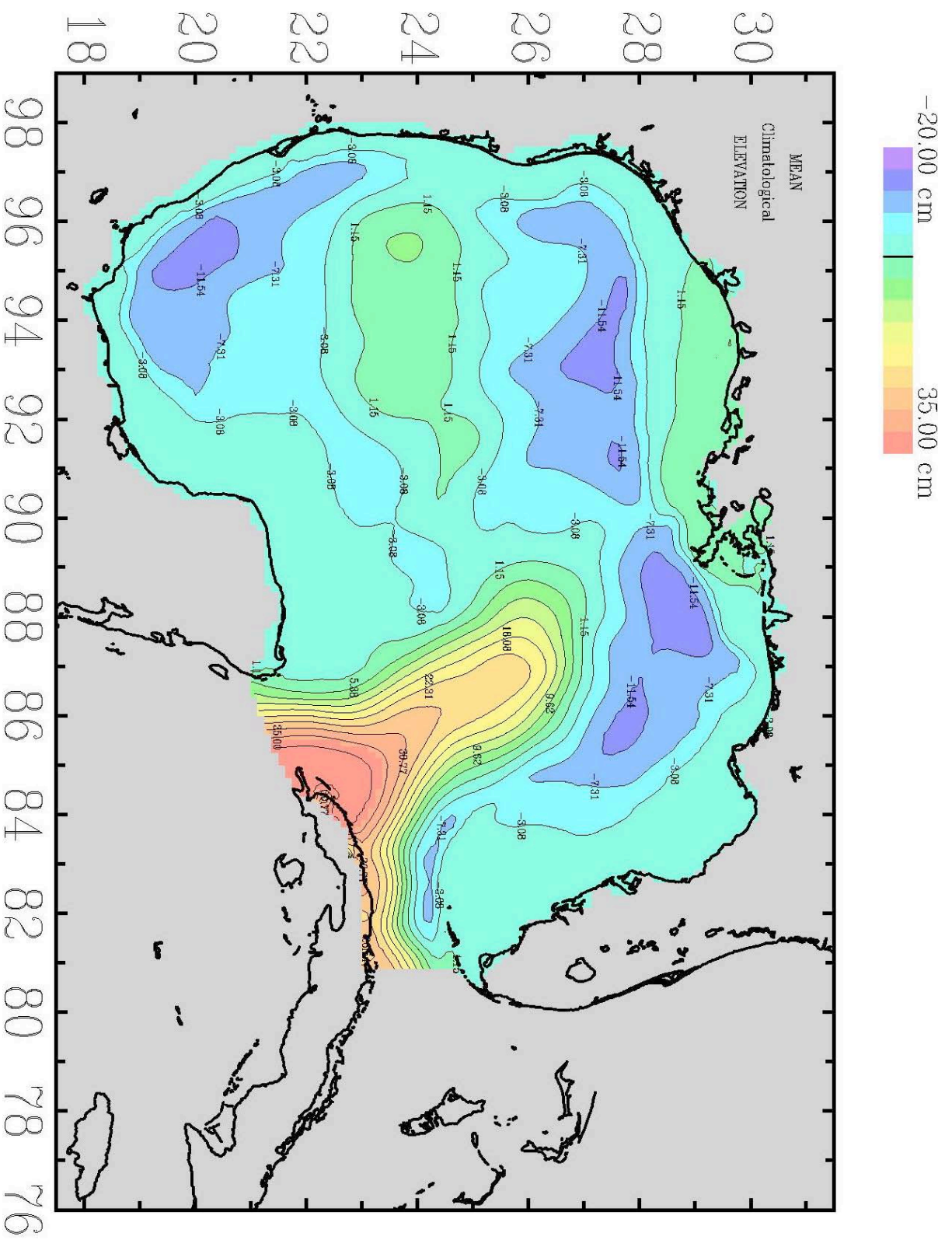


Figure 3.1 The mean surface elevation distribution measured relative to the Gulf-wide spatial and temporal mean elevation.

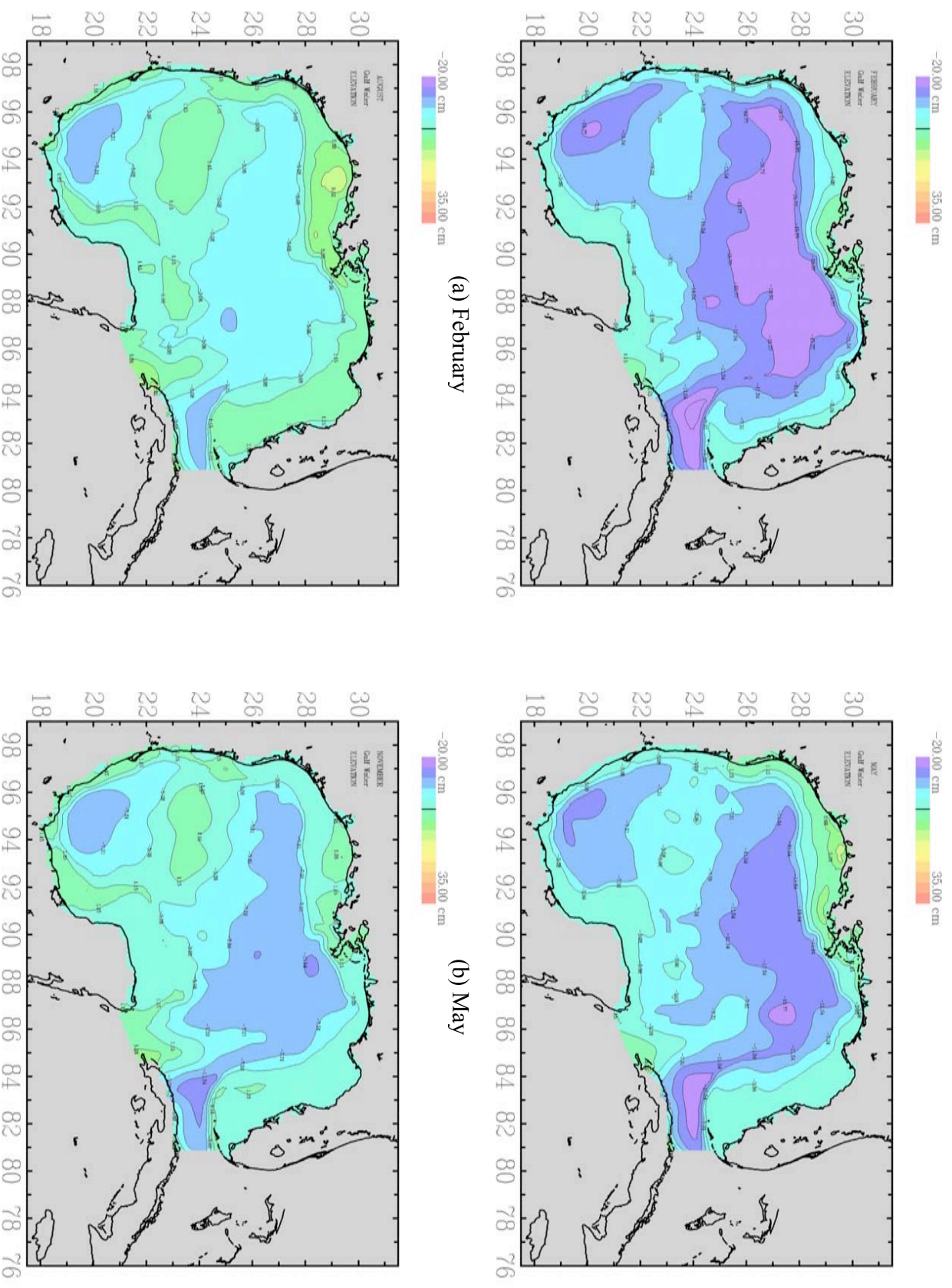


Figure 3.2 Seasonal variation of the climatological GCW surface elevation field relative to the Gulf-wide mean.

The SSH data from the satellite altimeter consist of measurements of the distance from the satellite to the sea surface that are accurate to several centimeters along the satellite track. Since there is no absolute datum, the measurements are referred to the mean elevation at that location obtained from the average of all measurements at that location, yielding a sea surface height anomaly. The sea surface height anomaly, $\Delta\eta_s(x, y, n)$, is defined as the measured height relative to the mean of all measurements at the location (x, y) ,

$$\Delta\eta_s(x, y, n) = \eta_s(x, y, n) - \frac{1}{N} \sum_{i=1}^N \eta_s(x, y, i), \quad (3.7)$$

where N is the total number of satellite over-flight measurements, $\eta_s(x, y, n)$. As the number of measurements, N , at a given location becomes large, the average closely approximates the climatological long-term mean height at that location, $\overline{\eta_c(x, y)}$, as shown in Figure 3.1.

During the early years of TOPEX/Poseidon one over flight every 10 days did not offer a large N or provide a robust average. Now after 14 years, the satellite has produced over 500 measurements at each location. These data now represent not only a statistically meaningful sample with an uncertainty of about 3%, but more importantly they span over nearly 20 eddy-shedding cycles and 14 seasonal cycles to represent an unbiased mean elevation. Therefore, for large N :

$$\eta(x, y, t) = \Delta\eta_s(x, y, t) + \overline{\eta_c(x, y)}, \quad (3.8)$$

where $\eta(x, y, t)$ is the sea surface elevation referred to the climatological basin-wide mean height.

This is an important result because, while the sea surface height anomaly from satellite altimetry provides the temporal variation at a given location, the spatial distribution of the height can only be established with reference to the elevation field from climatological hydrography.

Equation 3.6, for the proportion of LEW, $P(x, y, t)$, may now be expressed in terms of the sea surface height anomaly:

$$P(x, y, t) = \frac{\Delta\eta_s(x, y, t) + \overline{\eta_c(x, y)} - \eta_g(x, y, m)}{\eta_l(x, y, m) - \eta_g(x, y, m)}, \quad (3.9)$$

using Equation 3.8, where, again, the argument m indicates that the monthly elevation fields resulting from the GCW and the LEW will be interpolated to the time t .

3.3 Profile Construction

Based on the temperature and salinity profile descriptions from Equation 2.2 in the previous section and the time dependent proportion from Equation 3.9, it is possible to specify the local, time-dependent temperature and salinity profiles:

$$T(x, y, z, t) = \left[T_g^s(x, y, z, m) + T_g^p(x, y, z) \right] \left[1 - P(x, y, t) \right] + \left[T_l^s(x, y, z, m) + T_l^p(z) \right] P(x, y, t) + T^d(z) \quad (3.11)$$

where T is either temperature or salinity, the superscripts (s,p,d) refer to properties in the surface layer, the pycnocline and the deep Gulf, respectively and the subscripts (g,l) refer to GCW properties and the LEW properties, respectively.

The result is a method of specifying the vertical structure of the temperature and salinity using information from satellite altimetry that is simple to apply and empirical content is derived from a century of hydrographic data archives.

However, the satellite repeat tracks are several hundred kilometers apart and are traversed at approximately 10 day intervals. Therefore, the data is sparse in both space and time. Features of interest such as the Eddies, may be 100 to 300 kilometers in size and move at a speed of 3 to 5 kilometers per day are not well resolved with this sampling. Larger Eddies will register on one track at a time and smaller Eddies may not even be observed.

In order to provide entire fields of temperature and salinity throughout the Gulf on, say, a daily basis, the elevation anomaly available at the discrete locations and times must be interpolated in time and space over the entire Gulf. There are various methods of accomplishing this interpolation. The daily surface anomaly fields produced by Robert Leben at UCAR, Leben (2004), are available in near real time. Also, as a component of MODAS, Fox *et al.* (2002), the Naval Research Laboratory produces a global daily sea surface height anomaly field. These are impressive efforts and produce a remarkably accurate result, particularly in the large oceans where the features of interest are large and slow moving. These methods are, however, essentially kinematic, in that they depend on moving the features around to match the satellite elevation measurements and the sea surface temperature distribution without recourse to the dynamics that control the ocean currents.

The most satisfactory method is to assimilate the available data in a numerical model in the vicinity of the times and locations where it is available and allow the model to perform the dynamic interpolation in the course of its calculations. This insures that the Loop and Eddies are convected in a manner which satisfies the dynamical constraints of the equations of motion and that the resulting fields are always in dynamic balance.

4. EVALUATION OF RESULTS

The method of inferring the density structure throughout the water column as a function of a near real time satellite derived sea surface height anomaly described above will require substantial testing and evaluation. While the underlying assumptions appear robust, there are arbitrary choices made in calculating the climatology that have significant effects on the results, which further parametric studies could refine.

The climatological grid is $0.125^\circ \times 0.125^\circ$, or about 14 km. While this grid is too coarse to represent smaller Eddies in a numerical simulation, it is reasonable for a climatology since for the most part fronts are not present. The one place where the resolution is inadequate is in the near coastal regions in the vicinity of a river outflow, where, for instance, the Mississippi plume is not well resolved. In the deep Gulf the data density does not yet support a finer grid and a higher resolution is not beneficial. Needless to say, regardless of the climatological grid resolution, the results of the analysis could be interpolated to a finer grid for purposes of numerical simulation.

Also related to the grid scale is the radius of influence used to analyze the data. The radius of influence used here is about 30 km, again dictated by the data density. A smaller radius of influence is desirable, but in data-sparse regions produces voids and artificial fronts. As more data becomes available a finer grid resolution and radius of influence are possible. These will result in larger local values of LEW probability.

In order to examine the influence of these assumptions and to assess the behavior of the method it is desirable to compare the results with those of other approaches. In this section some initial comparisons will be made.

4.1 Climatological Comparison

By definition, when the sea surface height anomaly is zero everywhere, the resulting fields represent climatological conditions. However, this is not a trivial result since the mean conditions in this analysis, shown in Figures 2.17 through 2.20, are obtained from a combination of GCW and LEW according to the long term mean probability of finding LEW.

An initial comparison can be made with a monthly climatology that was constructed from the 14 years of TOPEX/Poseidon AVHRR sea surface temperature data that is available as a component of MODAS, Kara, *et al.* (2009). Samples of the results are shown in Figure 4.1 for comparison with the climatological surface temperature distribution deduced from the hydrographic data. While these satellite SST data could be used later along with the hydrographic data in constructing synoptic temperature profiles, the SST archive, Barron, *et al.* (2006), represents a source of surface temperature data for comparison which is completely independent of the *in situ* hydrographic climatology. The variation of the temperature distribution of the composite climatology is within 0.1°C of the SST climatology, both spatially and seasonally, but the temperature level of the SST is uniformly about 0.7°C higher. As previously noted, this difference maybe due to the fact that the SST is a true surface temperature, whereas the *in situ* data recording begins at a meter below the surface. Therefore, the comparison is reassuring.

The most direct comparison of the composite climatology results is with a conventional climatology constructed directly from all of the same hydrographic data using the same grid and parameters. Not surprisingly, the surface conditions are virtually identical and are not shown. However the comparison with the conventional climatology in the pycnocline is instructive, since the distributions of the conventional climatology vary throughout the year whereas those of the composite climatology are unchanging. Samples are shown in Figure 4.2, at the depth of 300m and in Figure 4.3 at 700m for comparison with the constant distributions in Figures 2.19 (a) and (c), respectively. The presence of the Loop in the composite climatology is considerably more pronounced where that of the conventional climatology is noticeably diffuse. This difference is evidently due to the use of more clearly defined profiles of GCW and LEW and provides a distinct advantage for later use in specifying Loop and Eddy features.

The gold standard in hydrographic atlases is the Levitus Atlas. The recent incarnation used here is from NODC called the World Ocean Atlas of 2001 (WOA01). As the title suggests, this is a worldwide atlas on a $0.25^\circ \times 0.25^\circ$ grid, from which the Gulf of Mexico region has been abstracted for this comparison. That the Levitus grid is coarser is unfortunate and should be noted in the evaluation, but the comparison is still appropriate. Comparing the WOA01 surface temperature in Figure 4.4 with that of composite climatology in Figure 2.17, it is evident that both the spatial and seasonal distributions are within 0.5°C . However, for the two depths in the pycnocline, shown in Figures 4.5 and 4.6, there are more perceptible differences compared with the composite climatological field in Figures 2.19 (a) and (c). The primary difference is that the WOA01 Atlas indicates a seasonal variation at 300m and 700m consisting of Eddy-like features that change from season to season where, again, those of the composite climatology are fixed throughout the year. Since it is known that Eddy shedding and transport across the Gulf is not correlated with the seasonal cycle, Vukovich, (1995), it is most likely that these structures are the result of bias caused by a few strong Eddies in the data at those locations. The mean of the fields at those depths are, again, within about half a degree C of that of the composite climatology in Figures 2.19 (a) and (c). All of this considered, the results of the two atlases are within the tolerance of the analysis.

Another monumental achievement is the world wide atlas prepared by NAVOCEANO for use by the Navy. It is a component of the Global Data Environmental Model (GDEM), Countryman and Carron, (1995). Again, the comparison here is with an abstract for the Gulf of Mexico. The GDEM Atlas is also on a $0.25^\circ \times 0.25^\circ$ grid and therefore the same comments on resolution apply to the comparison. As was the case with the Levitus Atlas, the GDEM surface fields, shown in Figure 4.7, are within 0.5°C . The fields have more character than Levitus and the composite atlas, probably due to less smoothing.

The temperature distributions at the two depths, 300m and 700m in Figures 4.8 and 4.9, are distinctly different from those of the composite climatology. One might expect that Eddies migrate to the Western Gulf region and dissipate, but it is unlikely that the final resting place is different in all months of August than it is in all Novembers. Therefore, again, it is likely that a smaller data set with fewer Eddies has biased the results. At the same time, less spatial smoothing results in a stronger, albeit temporally variable, Loop Current signature. Making an allowance for the reasonable variability in the pycnocline versus the fixed profiles of the composite climatology, the GDEM results support the composite climatology described in Section 2.

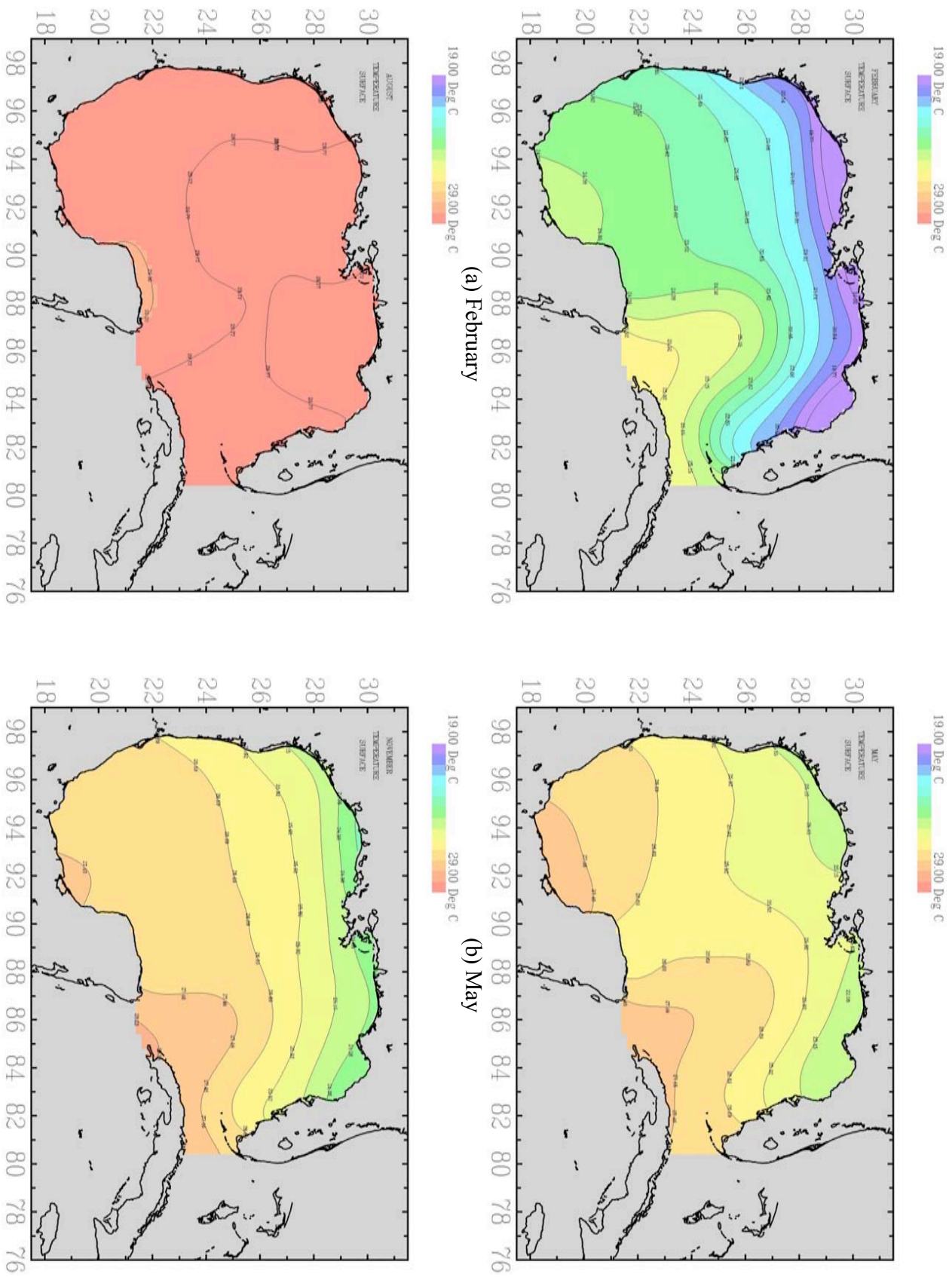


Figure 4. 1 Seasonal variation of the climatological satellite SST fields based in 14 years of TOPEX/POSEIDEN AVHRR data.

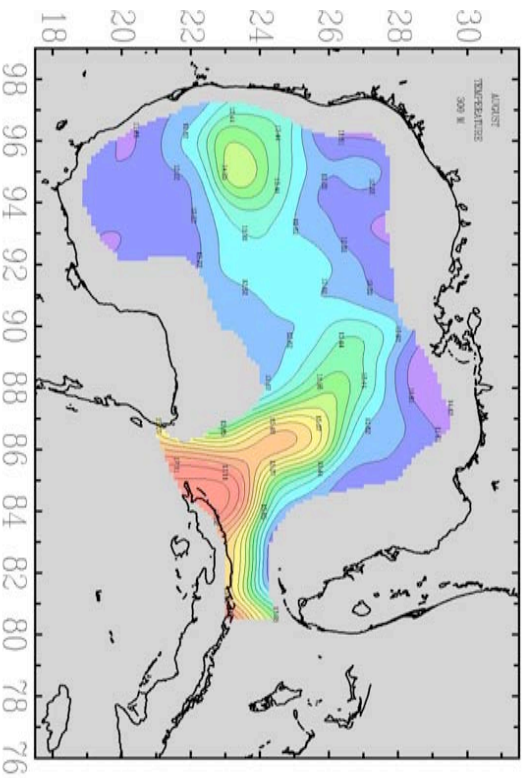
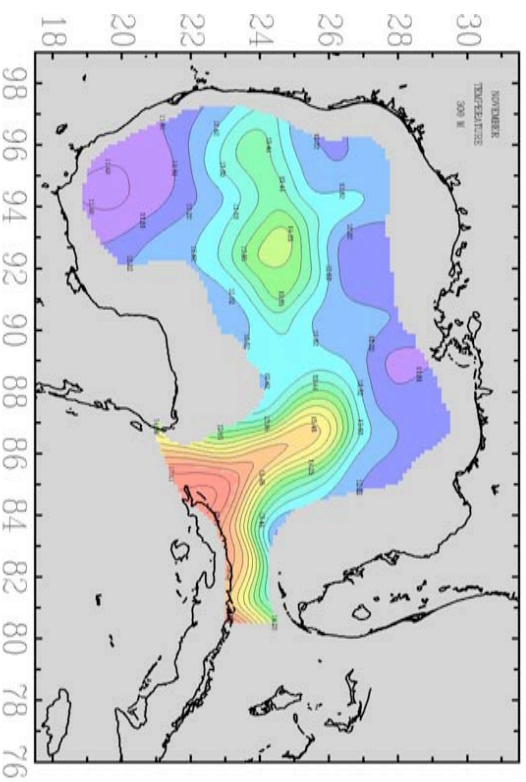
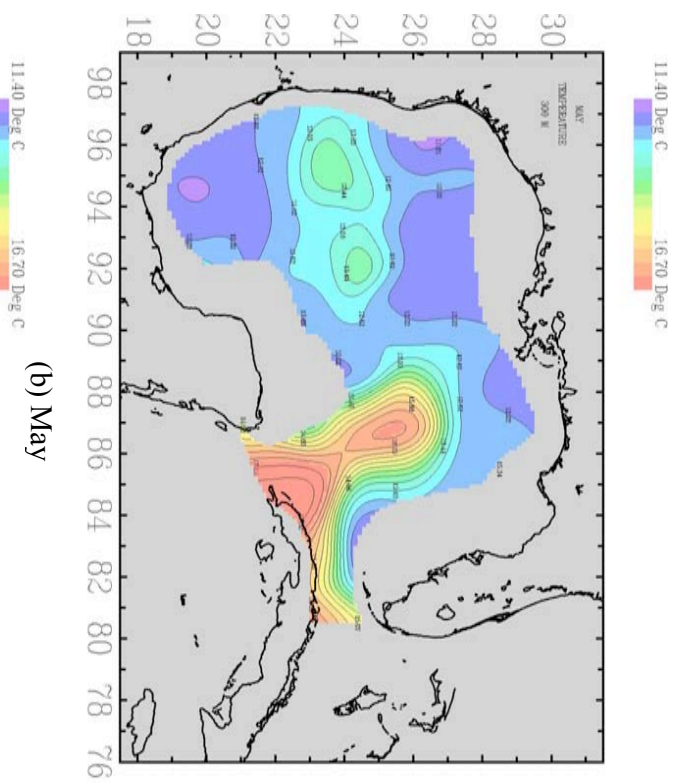
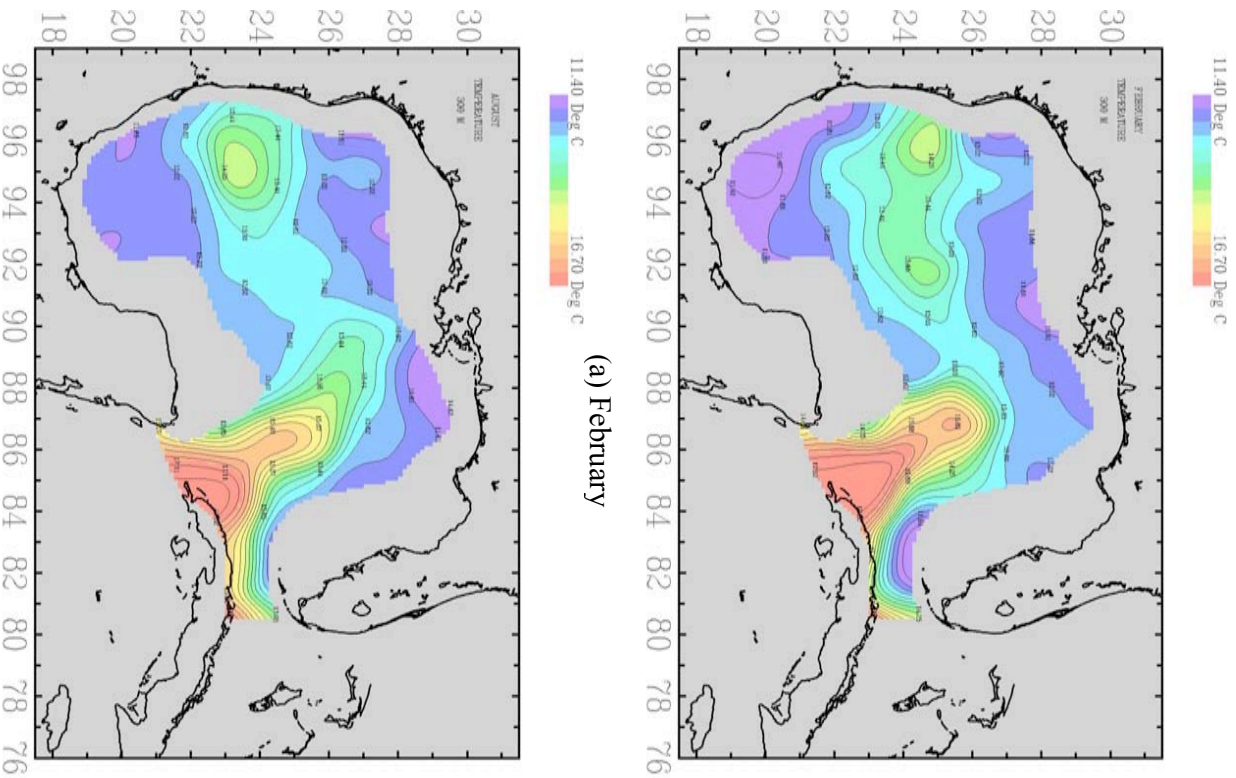


Figure 4.2 Conventional climatological temperature distributions at 300m for representative months during each season.

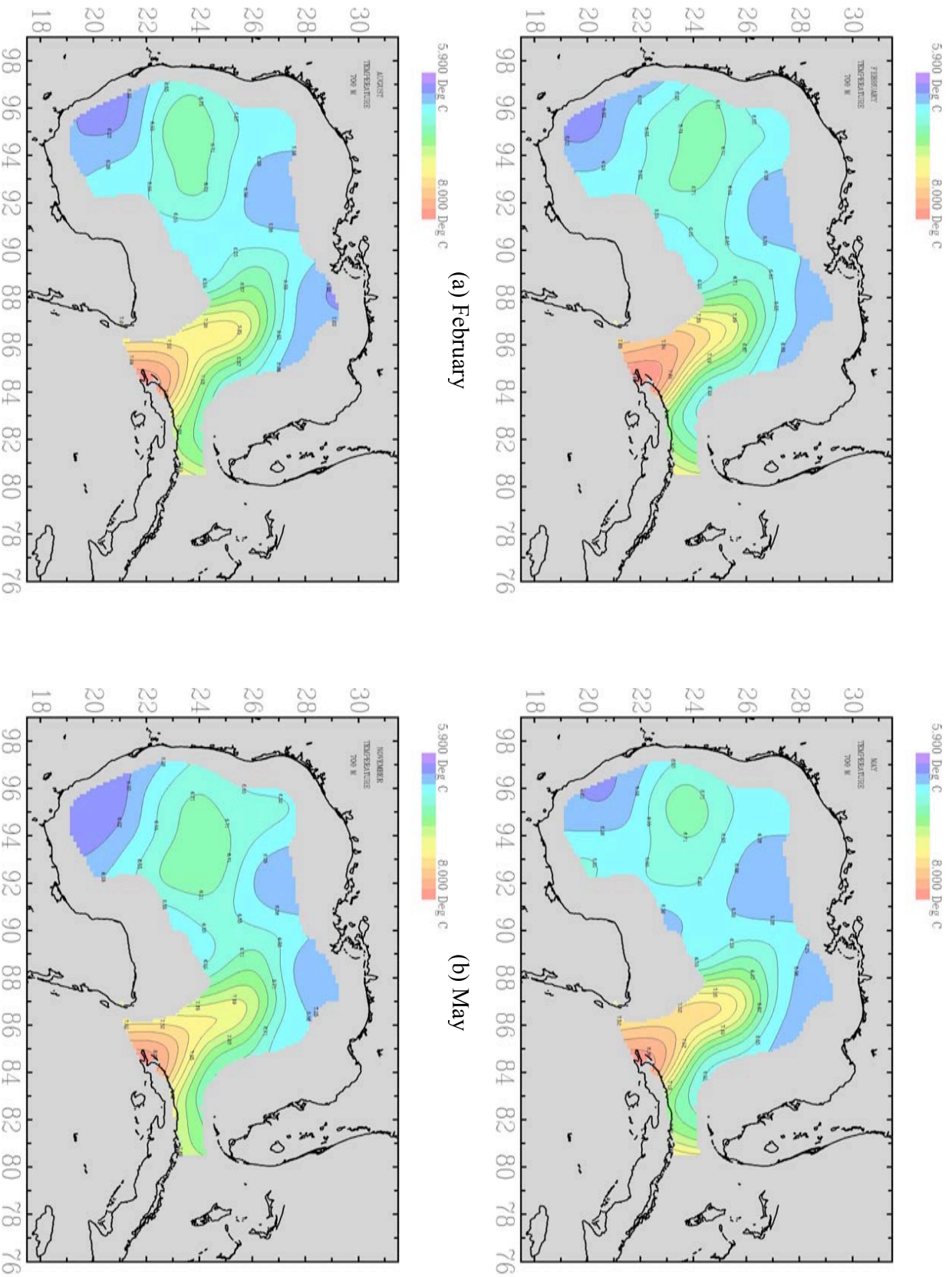


Figure 4.3 Conventional climatological temperature distributions at 700m for representative months during each season.

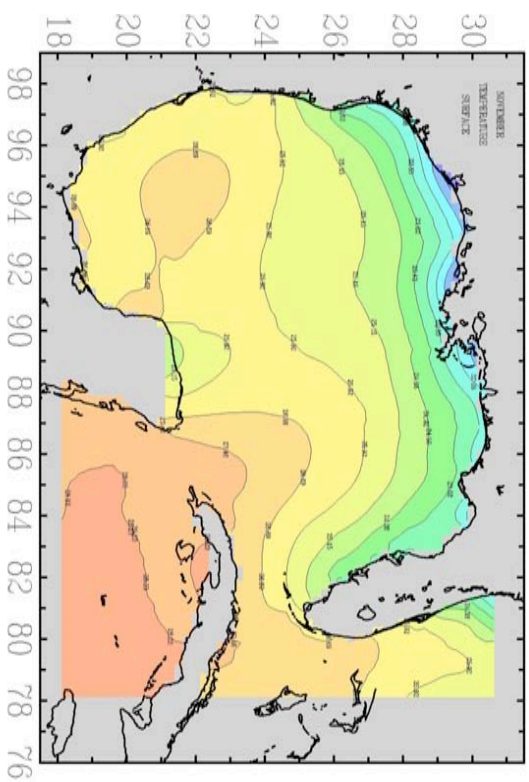
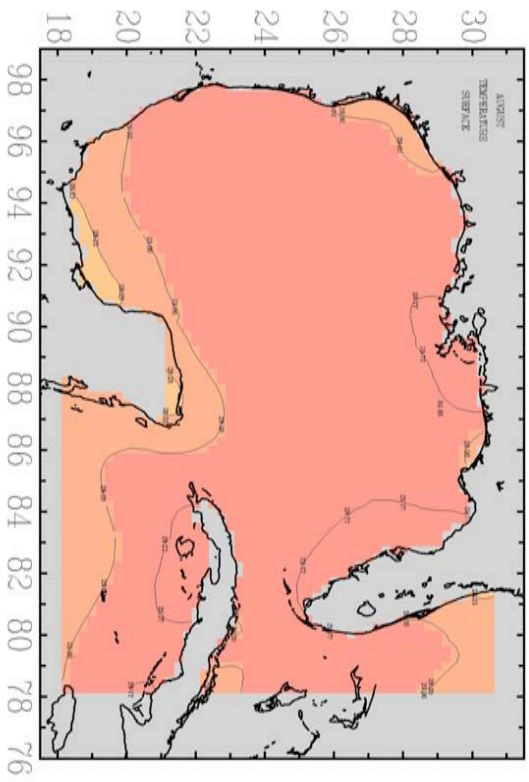
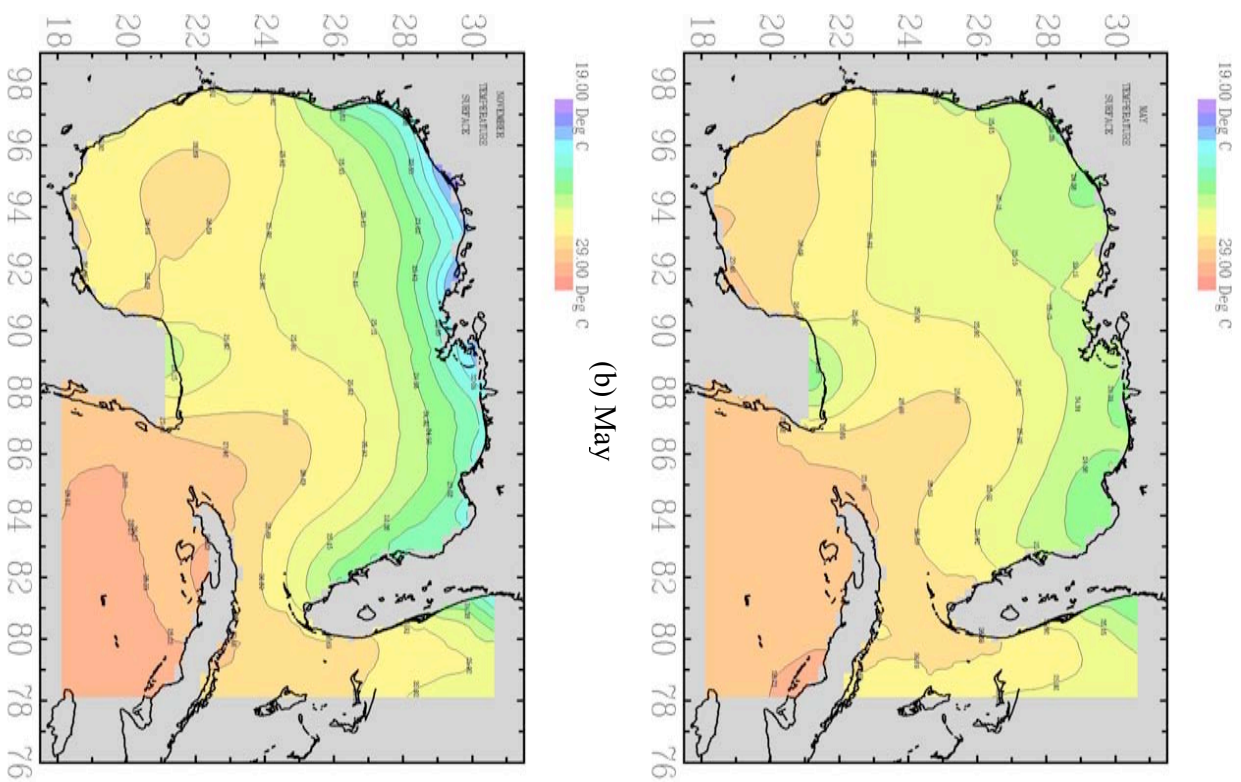
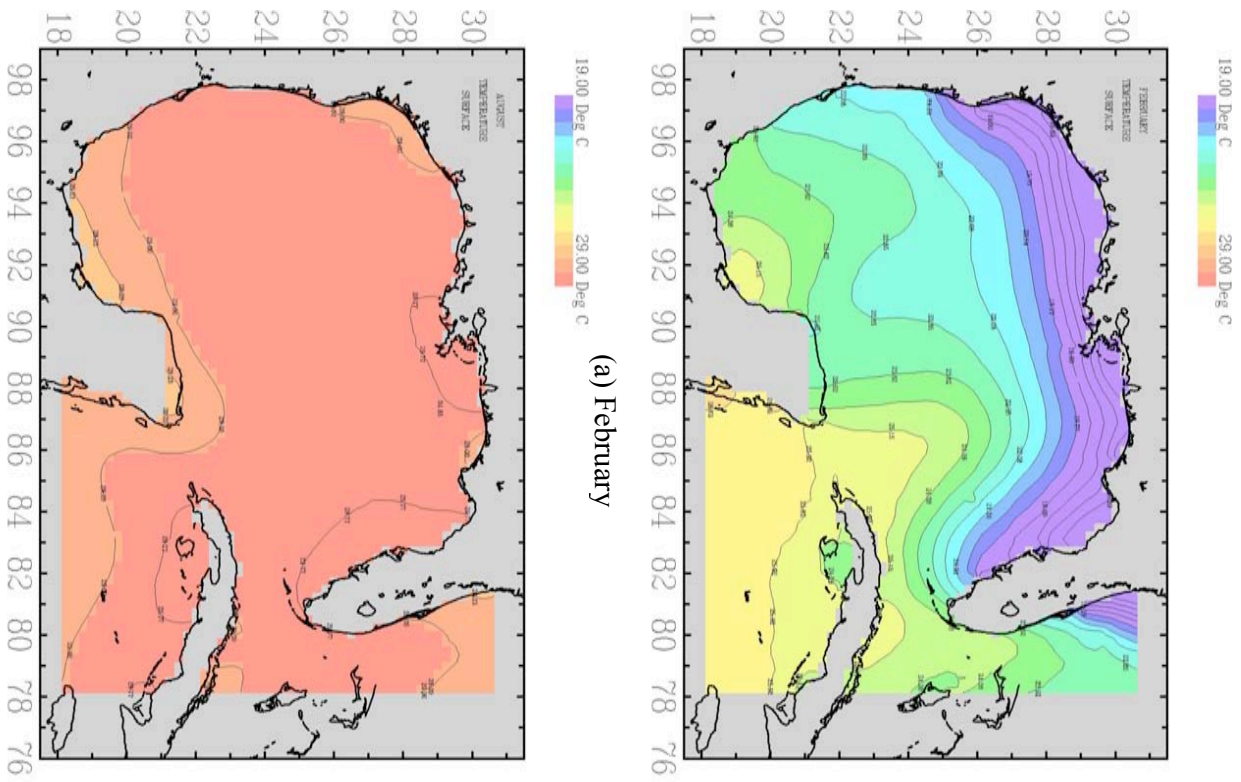


Figure 4.4 Levitus WOA01 climatological surface temperature distributions for representative months during each season.

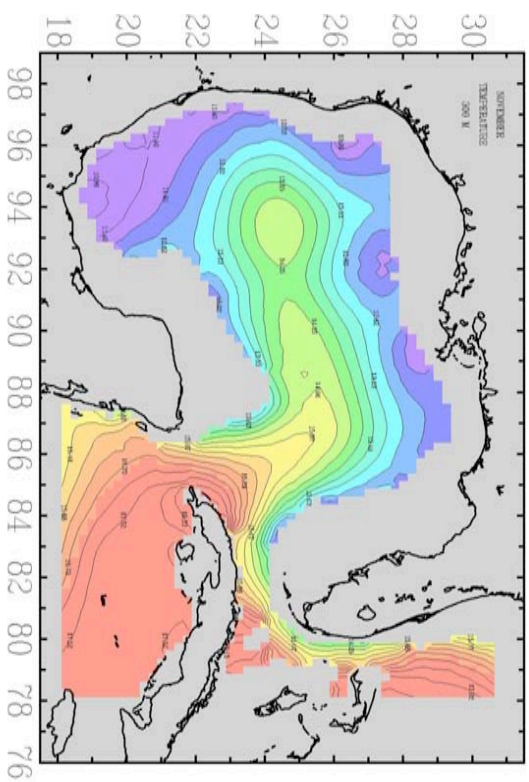
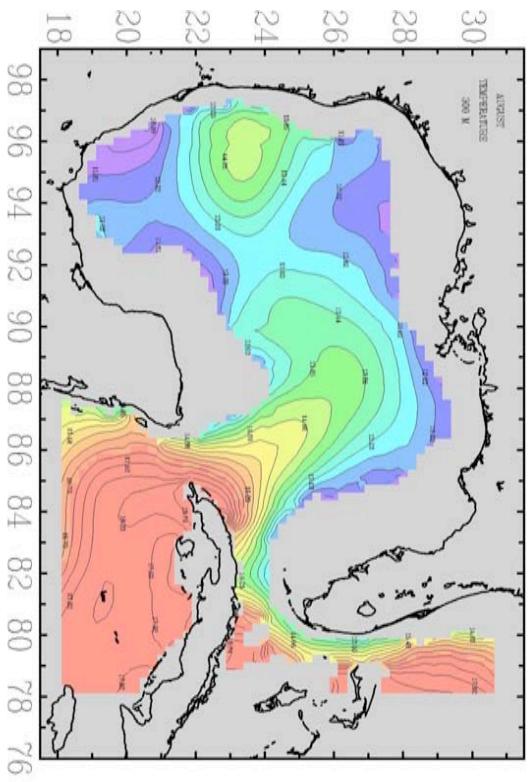
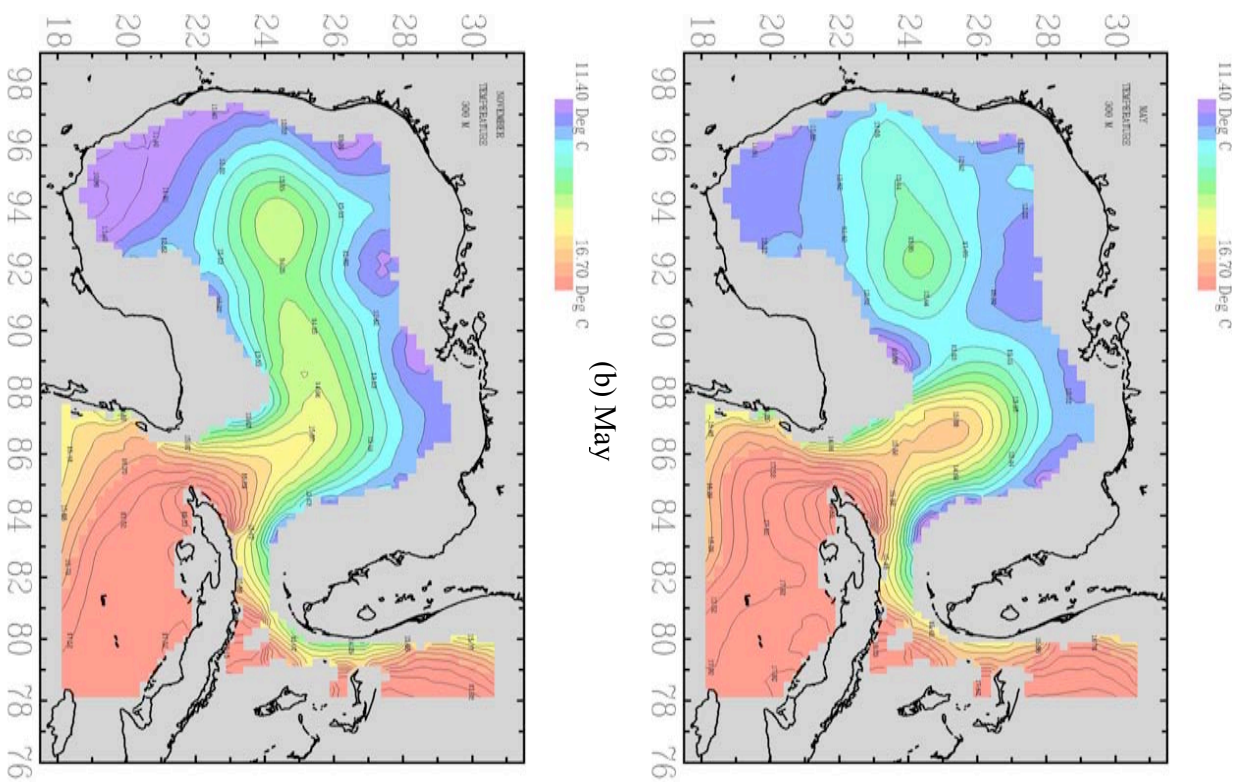
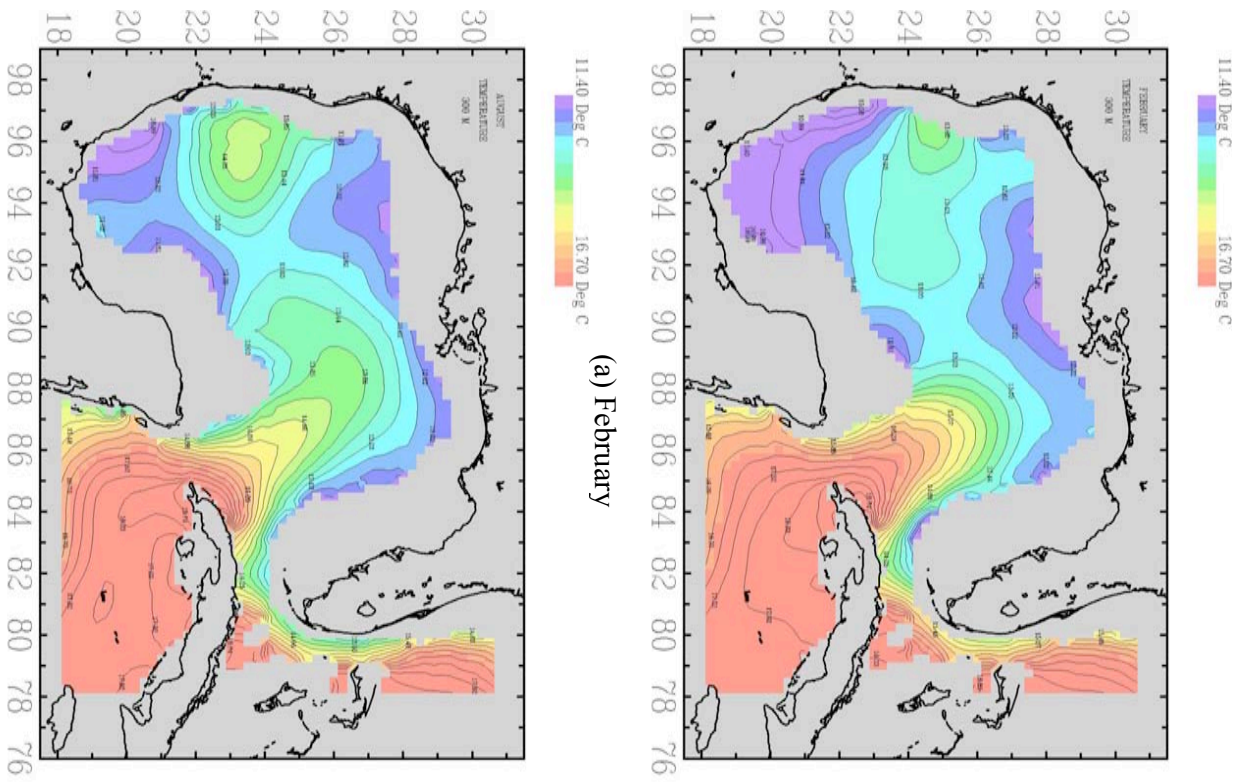


Figure 4.5 Levitus WOA01 climatological temperature distributions at 300m for representative months during each season.

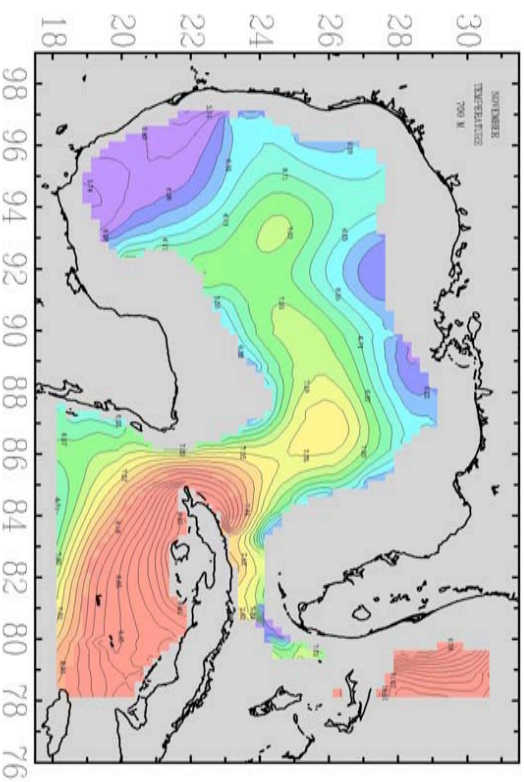
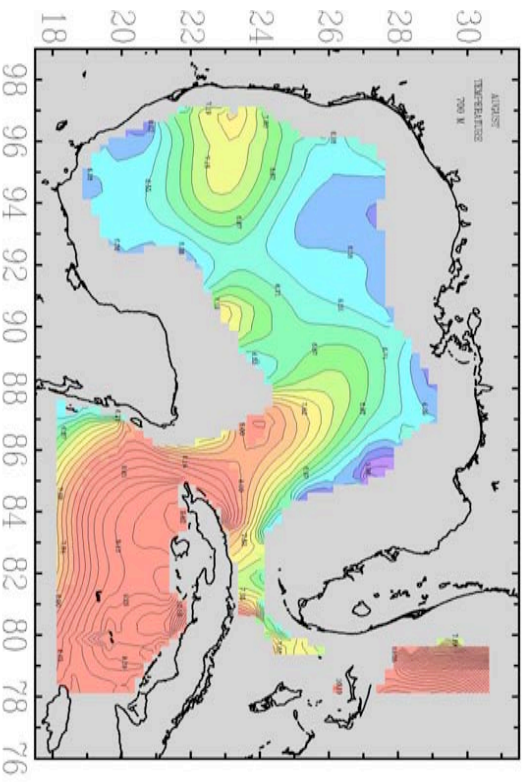
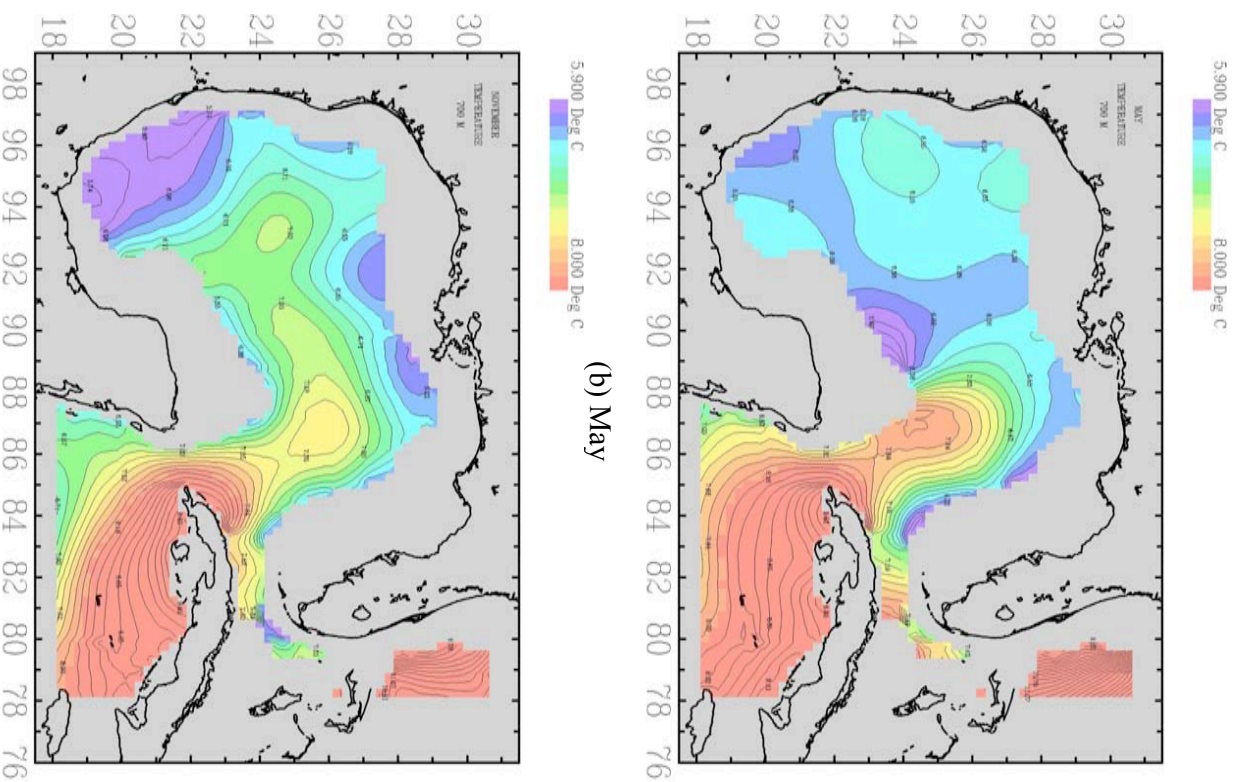
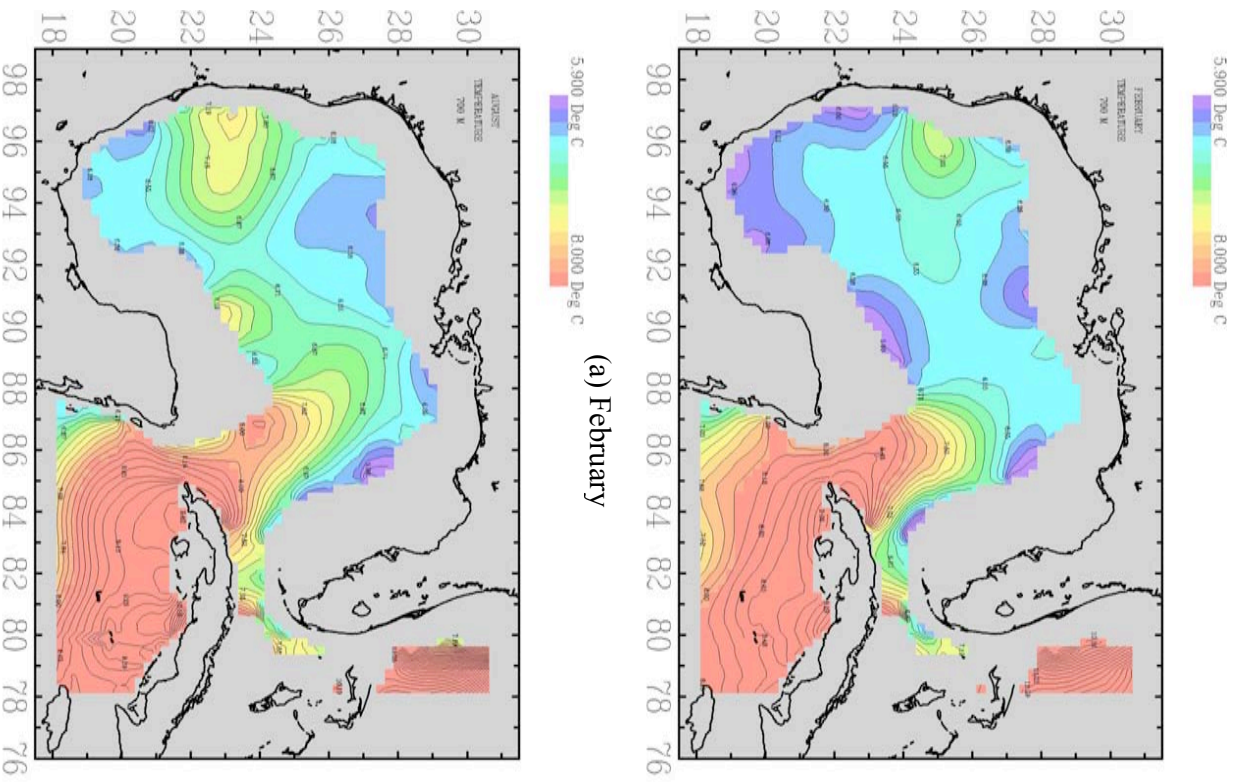


Figure 4.6 Levitus WOA01 climatological temperature distributions at 700m for representative months during each season.

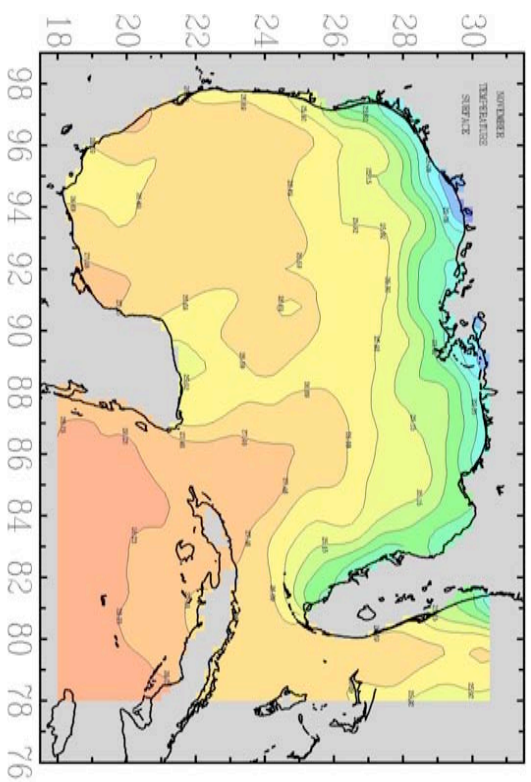
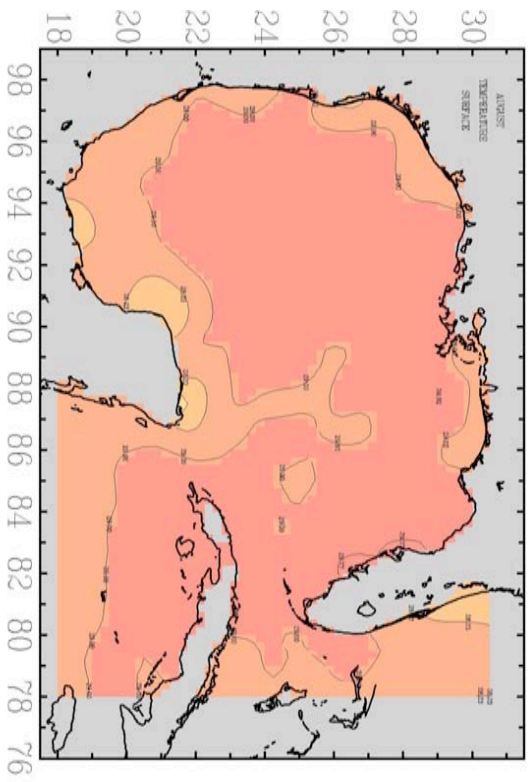
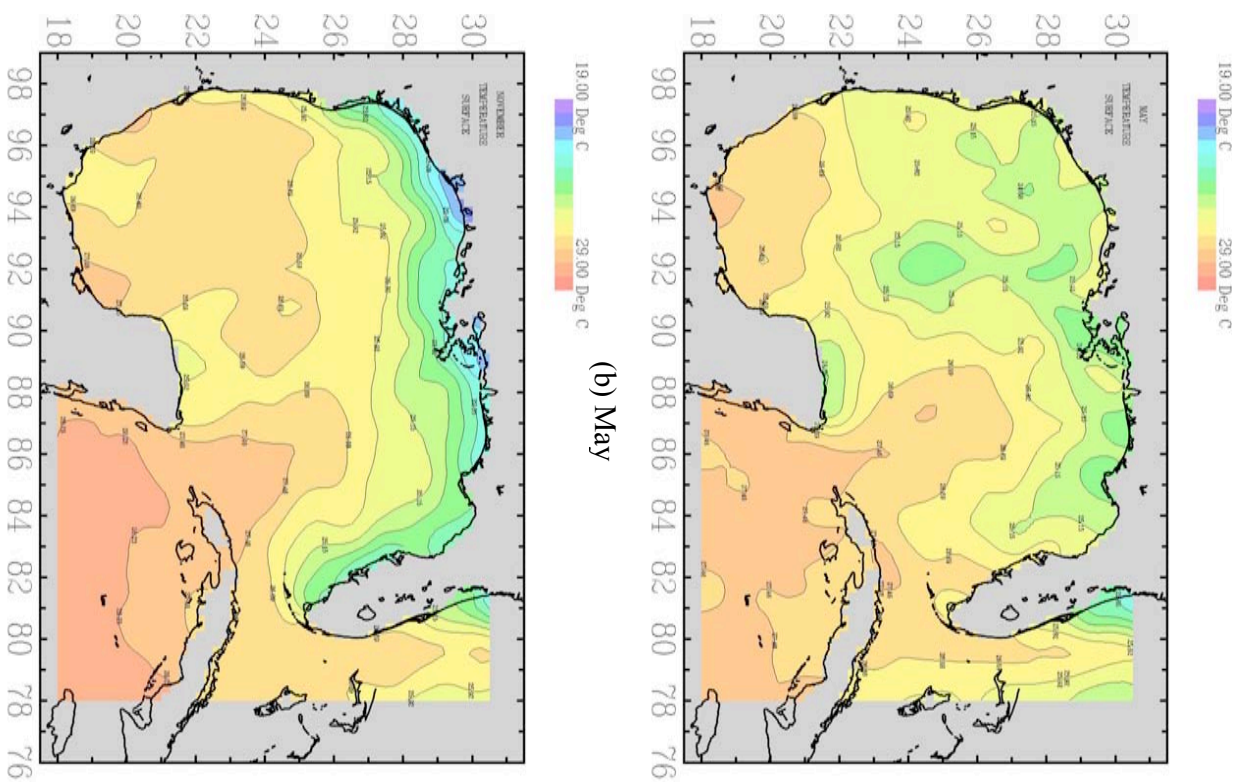
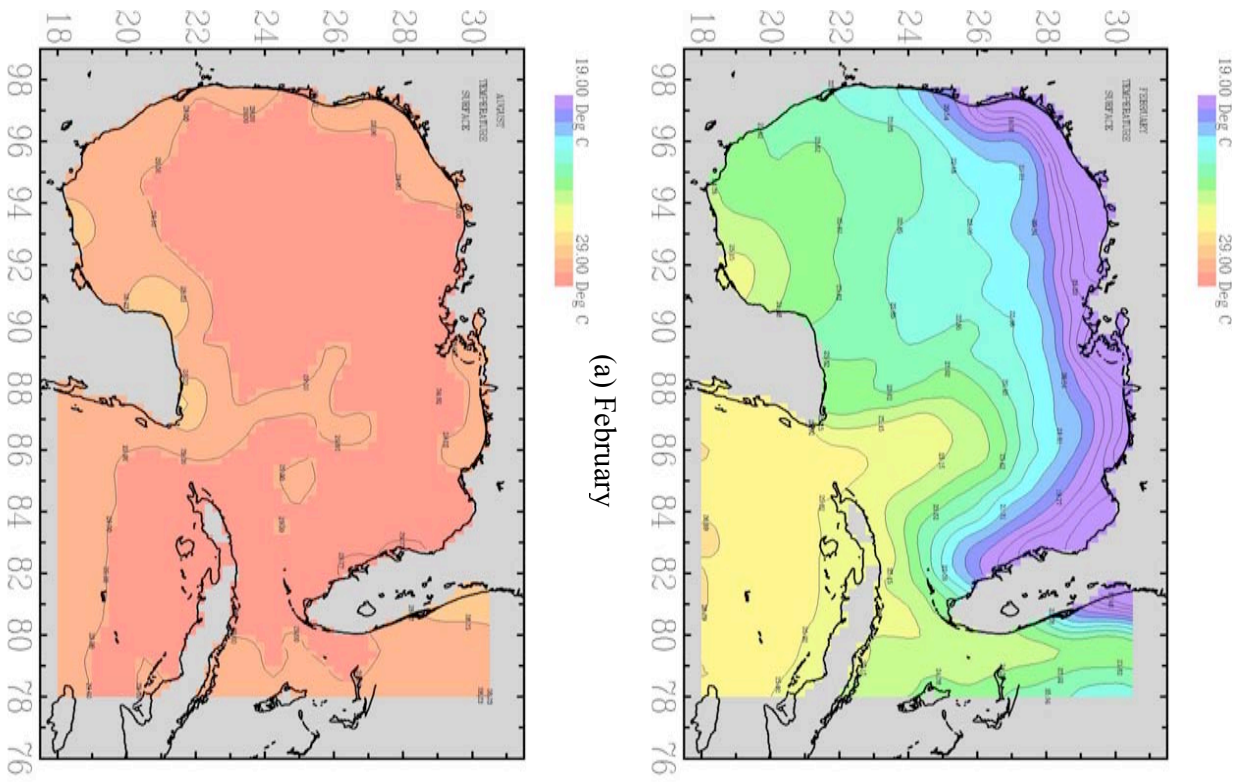
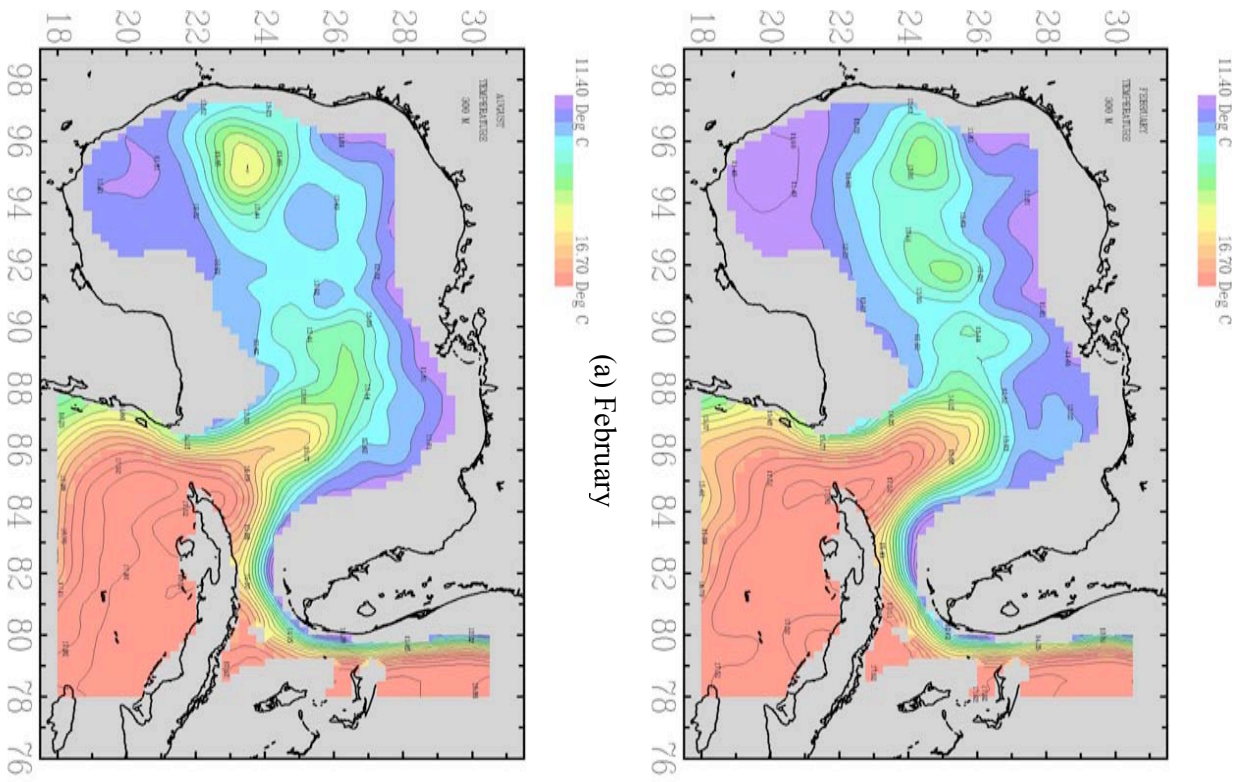
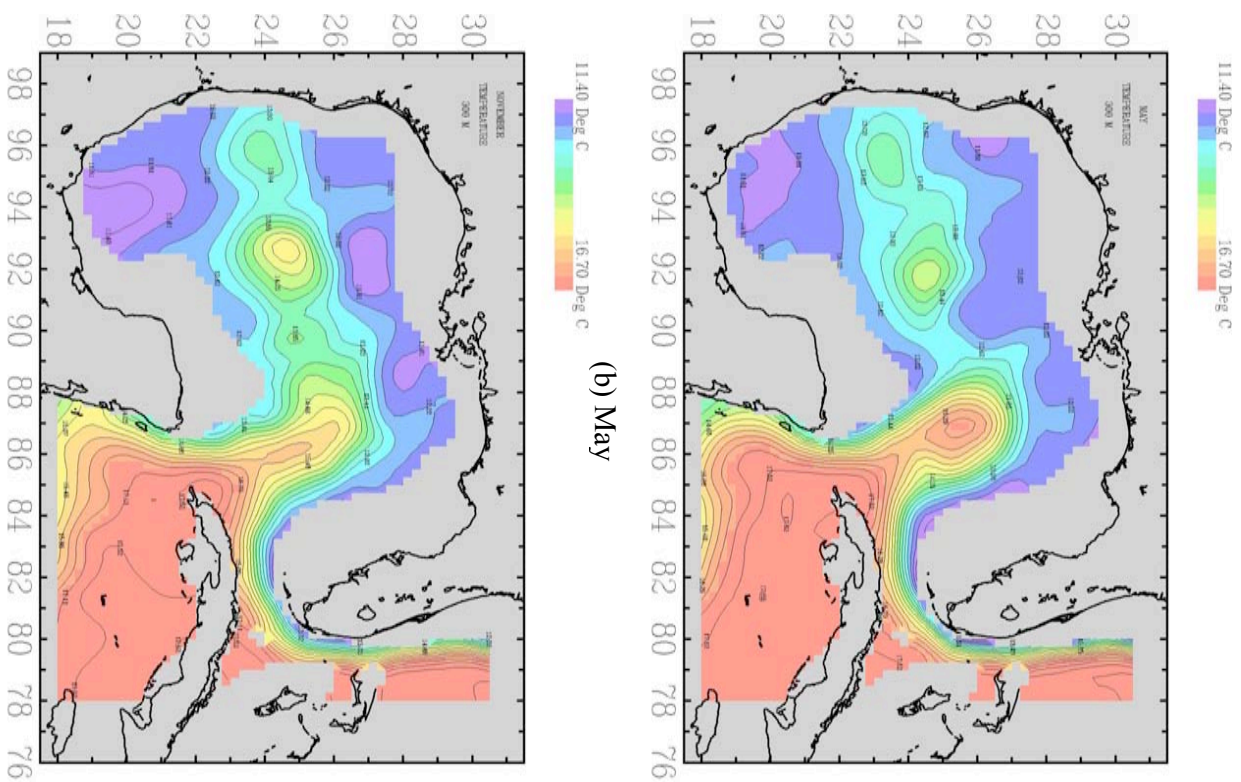


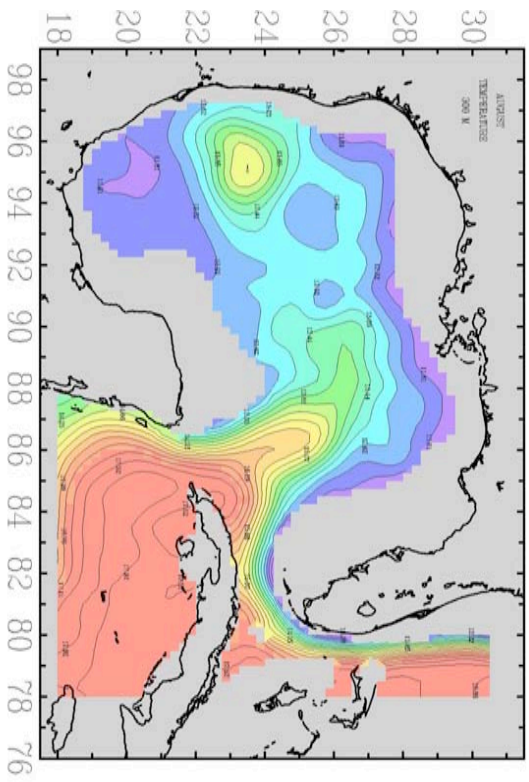
Figure 4.7 NAVOCEANO GDEM climatological surface temperature distributions for representative months during each season.



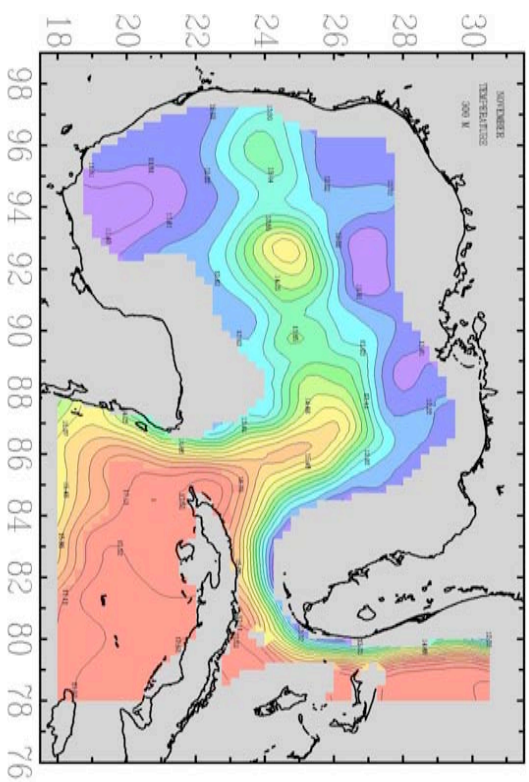
(a) February



(b) May



(c) August



(d) November

Figure 4.8 NAVOCEANO GDEM climatological temperature distributions at 300m for representative months during each season..

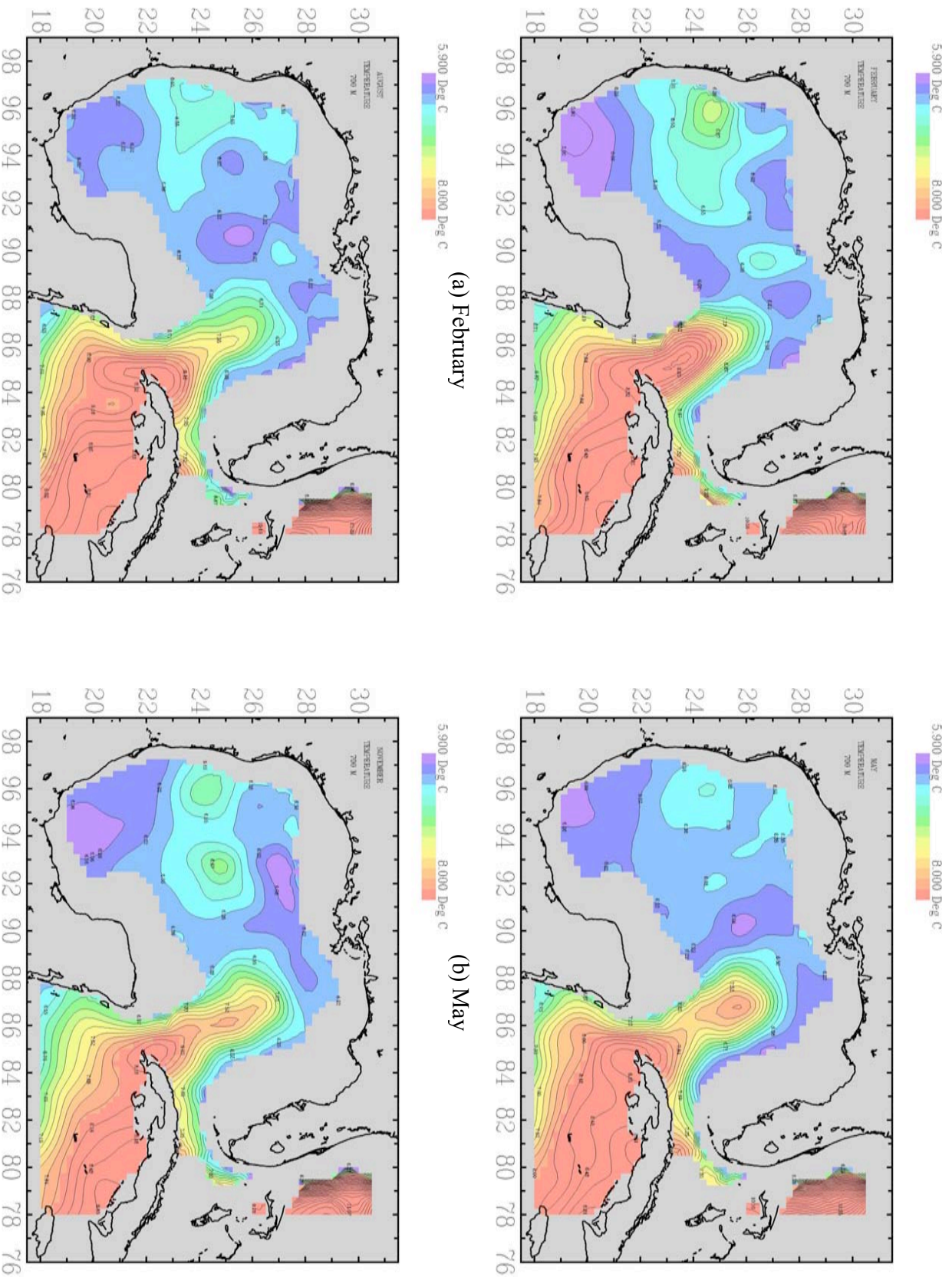


Figure 4.9 NAVOCEANO GDEM climatological temperature distributions at 700m for representative months during each season.

By its very nature a climatological atlas is a statistical construction and, while it can be characterized by its statistical properties such as standard deviation and number of observations, the final form is the result of many arbitrary, but hopefully, informed choices. The objective of these choices is to maximize the robustness of the atlas to forecast future mean conditions based on a limited quantity of historic data. There is no simple set of measurements that can be made to verify an atlas. Having made the choices and developed the fields, only time and much more data will tell how robust the atlas truly is.

4.2 Synoptic Comparison

The ultimate objective of this exercise, as described in Section 3, is to synthesize the time dependent structure of the temperature and salinity fields using sea surface height anomaly data from satellite altimetry. Therefore it is important to examine some direct comparisons between *in situ* hydrographic measurements and synthesized fields. This comparison is constrained the limited quantity of contemporaneous satellite and *in situ* data.

In principle using the method described above it is possible to synthesize the temperature and salinity profiles at the location of any *in situ* measurement in the Gulf of Mexico since 1993, when the TOPEX/Poseidon began transmitting regular sea surface height anomaly data. Daily fields of sea surface height anomaly are available from Robert Leben (2004) at the University of Colorado and as a component of the MODAS data set, Fox, *et al.* (2002). While these fields are extremely useful and a great resource, they are kinematic constructions from the sparse satellite over flight data and introduce their own uncertainty into the comparison.

Fortunately, as a component of the National Ocean Partnership Program study “Gulf of Mexico Ocean Monitoring System,” (Blahe, *et al.*, 1999) a set of *in situ* measurements was made along transects coinciding in time and space with satellite over flights. These data provide a unique opportunity to compare synthesized fields using the measured sea surface height anomaly from the altimeter with hydrographic casts along the same transect.

There are actually two sets of *in situ* data available from this study, both from the period April 19th through May 9th 1998. CTD measurements were made along five transects by Texas A&M (Kelly, *et al.*, 1998), two of which coincide with TOPEX/Poseidon over flights. Then, during nine flights in an Orion P-3, NAVOCEANO personnel (Gilligan, *et al.*, 2002) dropped AXBTs along 22 transects, 9 of which coincided with TOPEX/Poseidon over flights. With these data a direct comparison between the profile synthesis from satellite SSHA data and *in situ* measurements is possible. The satellite track SSHA data, Berwin (2003), were obtained from the Physical Oceanography Distributed Active Archive Center (PO.DAAC) at the NASA Jet Propulsion Laboratory, Pasadena, CA. <http://podaac.jpl.nasa.gov>.

A summary of these two data sets is shown in Figure 4.10. The left two panels show the locations of the casts for each transect. Then, for reference to the conditions in the Gulf, they are plotted on the total surface elevation fields for April 20th and May 3rd, respectively, calculated by superimposing the MODAS sea surface height anomaly field for that day on the annual mean sea surface elevation shown in Figure 3.1.

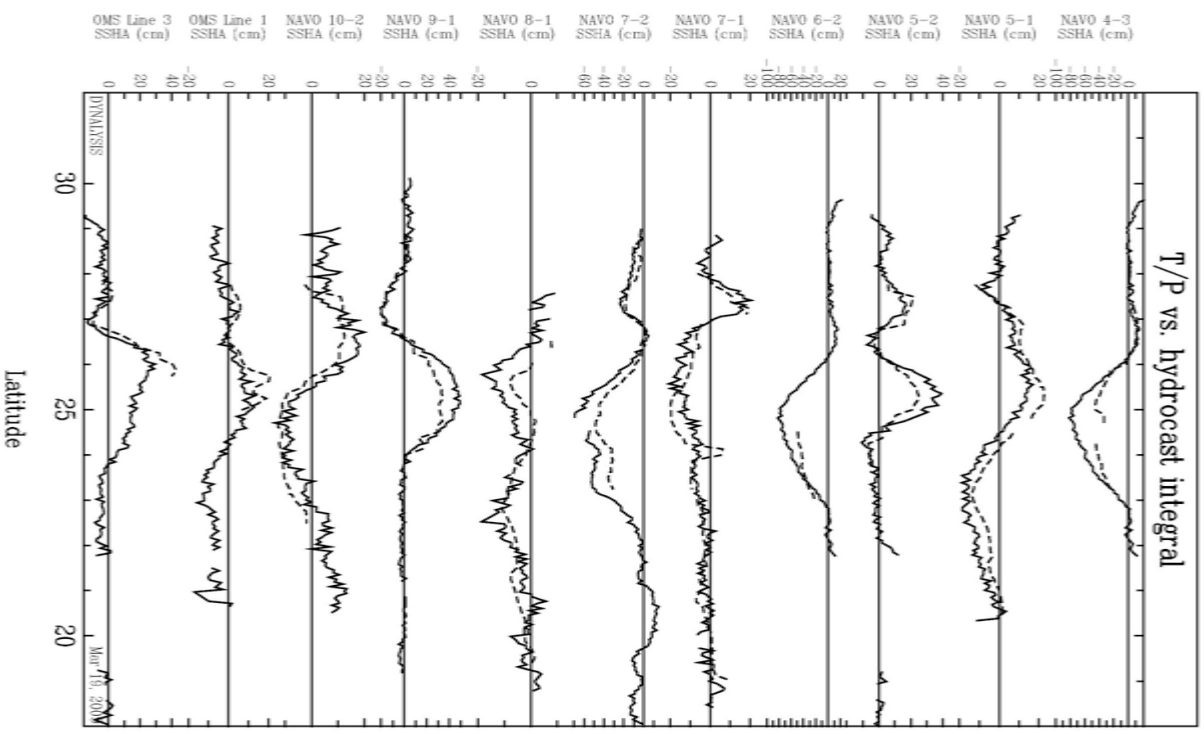
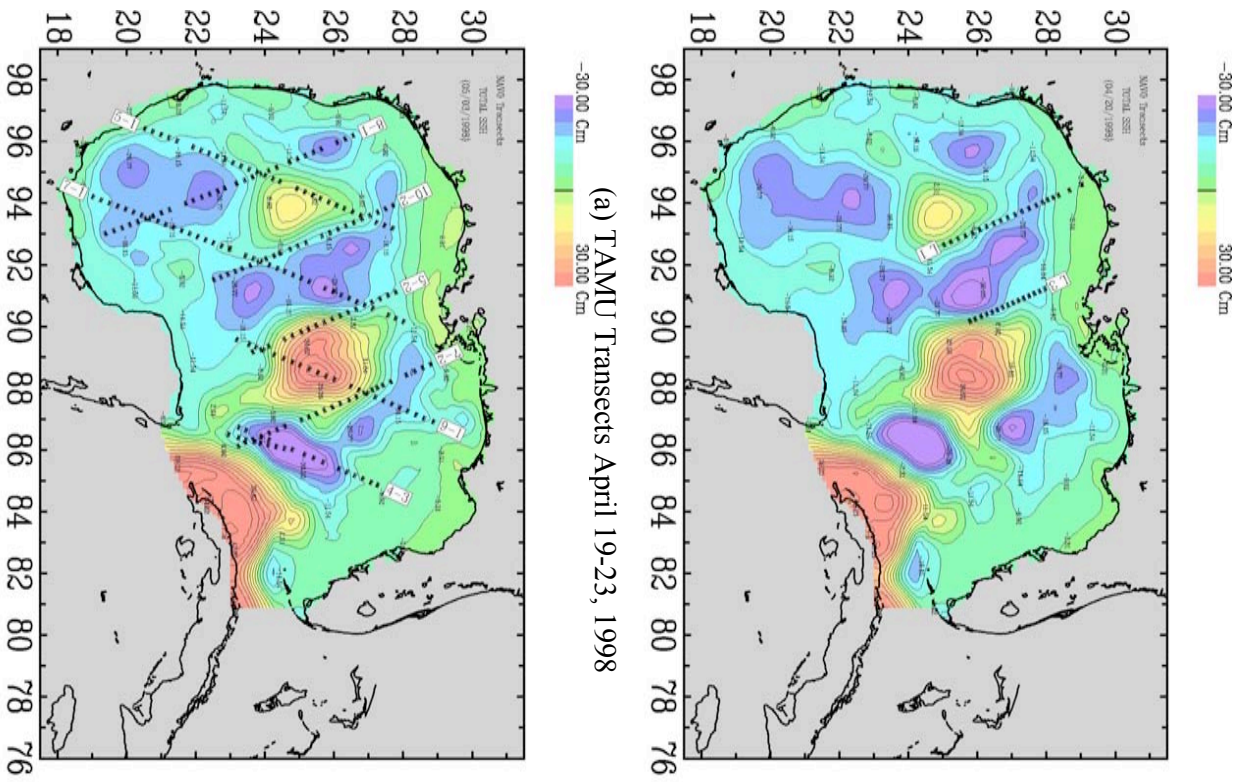
The conditions in the Gulf during late April and early May 1998 were interesting, as is evident from the sea surface elevation maps in Figure 4.10 (a) and (b). A large Eddy had recently separated from the Loop and a strong counter-clockwise gyre formed between them. There is also a weak Eddy in the Western Gulf and a number of smaller counter-clockwise gyres in the central Gulf. As luck would have it, at this particular time many of the satellite paths inexplicably fall between these interesting features. Fortunately, one ascending path passes directly over the large, recently separated Eddy and another passes directly over the strong low between the Eddy and the Loop. These two transects corresponding to NAVO Flight 9-1 and NAVO Flight 4-3 in panel (b) have been selected for comparison here. The results of the comparisons with the other transects are similar so they are not shown here.

The right panel (c) in Figure 4.10 shows, with bold lines, the TOPEX/Poseidon sea surface height anomaly measurements along each transect. For consistency, since the satellite tracks are more nearly in the North-South direction, the horizontal coordinate on all transect plots is the Latitude, which provides a convenient reference on the horizontal maps. Flight 4-3 along Pass 091 occurred on May 1st and corresponds most closely with Cycle 207 on April 30th and Flight 9-1 along Pass 128 occurred on May 8th and corresponds most closely with Cycle 208 on May 7th. As is evident from Figure 4.10 (c), these are interesting transects since the TOPEX/Poseidon measured SSHA low in the Flight 4-3 is -80 cm and the SSHA high in Flight 9-1 is 50 cm.

Before proceeding further, it is noted that the existence of contemporary satellite SSHA and hydrographic transect data sets provides a unique opportunity to examine the correspondence between them. The observed density along the transect can be vertically integrated and, with the local mean sea surface elevation subtracted, the resulting hydrographic sea surface height anomaly may be compared with that of the satellite altimeter. The result is shown with the dashed lines in Figure 4.10(c). Of course, it will be quickly noted that in the case of the AXBT data, there are no corresponding salinity measurements with which to compute the density, so that the only complete data-to-data comparison is with TAMU Lines 1 and 3. Even that, it should be recognized, involves the use of the local mean sea surface elevation from the present climatological data analysis. Nevertheless, this is an instructive comparison, particularly since the satellite SSHA plays such an essential role in both generating and assessing the results.

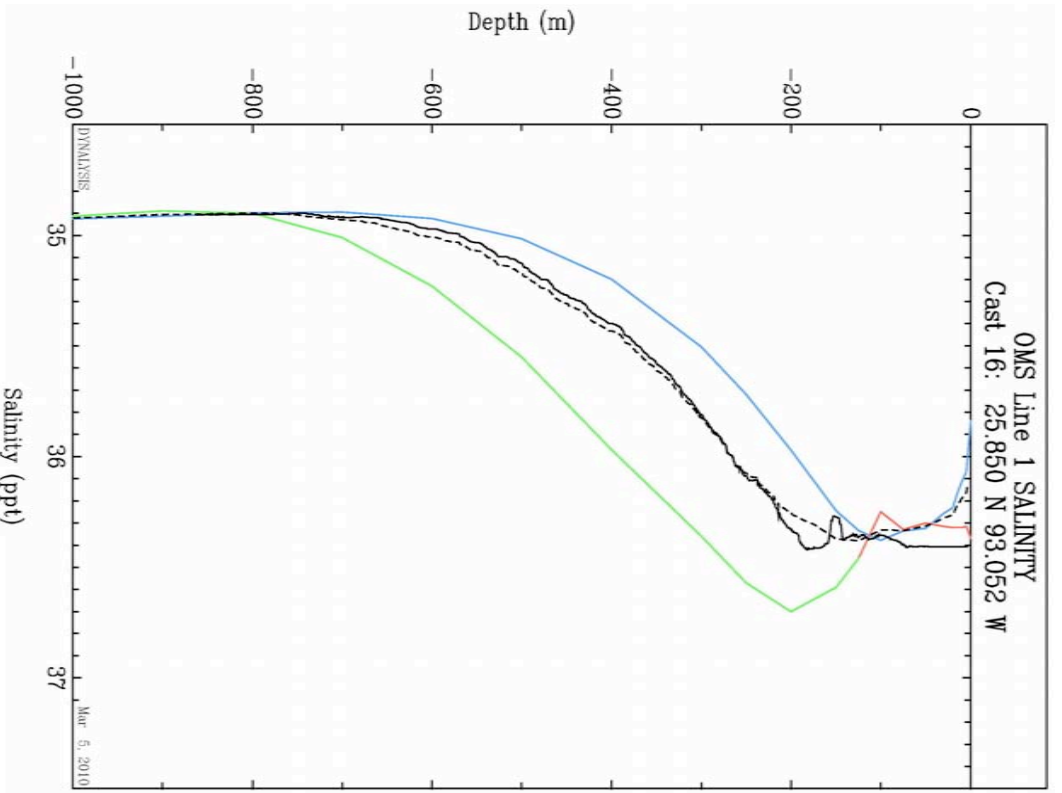
In order to make comparisons using the XBT data, the salinity profiles are synthesized. Using the same climatological data and a slightly more sensitive method it is possible to synthesize the salinity profile that is consistent with a particular given temperature profile. The proportion of LEW is determined for the given temperature profile and then the temperature-salinity relationship that corresponds to that proportion of LEW is used to infer the salinity distribution, directly from the temperature profile. Typical comparisons of synthesized salinity profiles with the salinity data from the TAMU Lines 1 and 3 are shown in Figure 4.11. Incidentally, for those who track these things, none of the data in any of the NAVO and TAMU transect casts was used in the analysis that produced the climatological atlas of hydrographic fields.

The salinity profiles so generated are remarkably accurate in the pycnocline even to the extent of reproducing small ripples in the profile. Above, nearer the surface, the temperature –

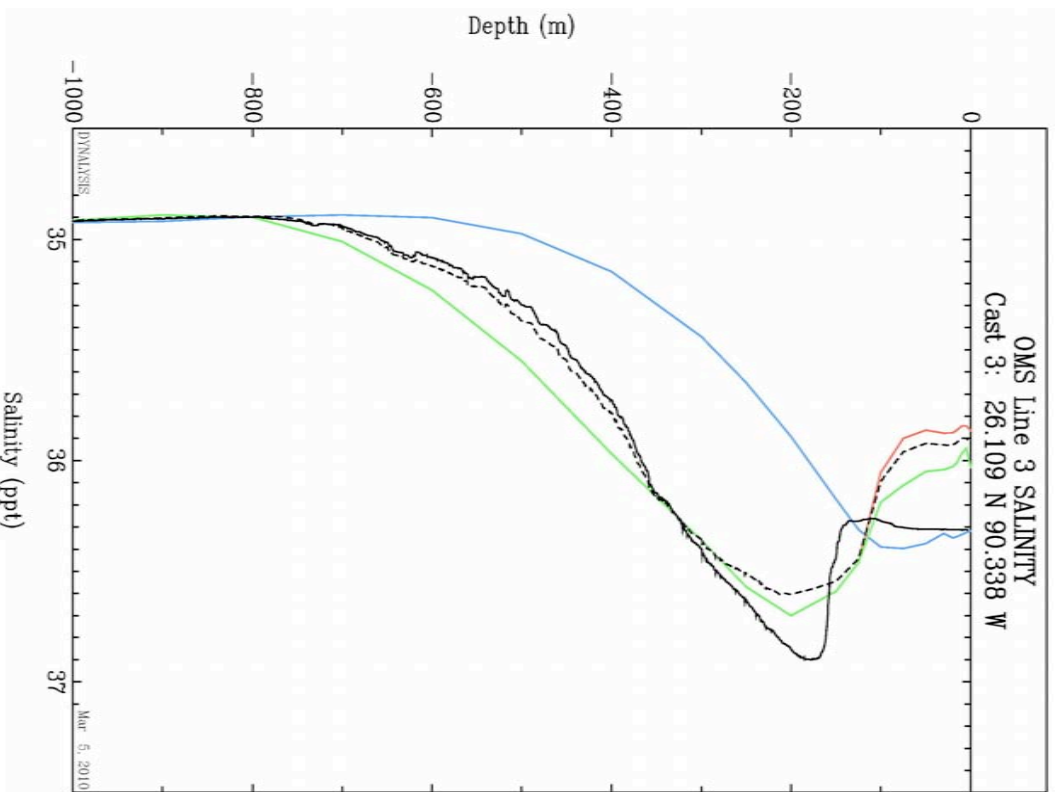


(c) Sea Surface Height Anomaly along Transects

Figure 4.10 Summary of transect data for comparison. TAMU data are CTD measurements and NAVO data are from AXBTs.



(a) Line 1



(b) Line 3

Figure 4.11 Comparison between a profile synthesized from the T-S relationship (dashed line) and a measured salinity profile (solid black line), where the GCW profile (blue), the LEW profile (red) and the normal synthesized profile computed from the proportion of LEW determined from the temperature profile (green) are shown for reference.

salinity relationship breaks down due to non-climatological variations in the surface layer caused by the local surface forcing and the results are clearly not as good. Taking into account the surface forcing might improve the results, but that refinement is beyond the scope of the present effort. Recognizing the strengths and limitations of the profiles produced, examination of the results is still worthwhile. Certainly the surface layer introduces some uncertainty in the density integral, but the large contribution to the density integral is accurate.

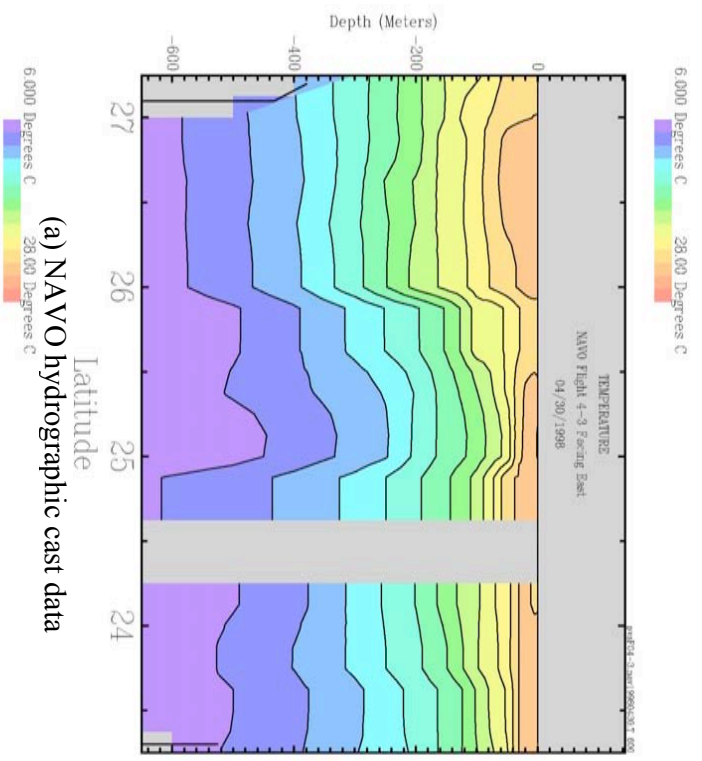
Finally, for completeness, since the NAVO AXBT temperature casts end at about 800m, the temperature profiles are also extended down to the bottom using the proportion of LEW determined in the pycnocline, so that the complete vertical density integral can be evaluated. The dashed lines in the plots of the NAVO AXBT transects of Figure 4.10 (c) are calculated from density profiles determined using temperature and salinity profiles produced in this manner.

The next step is to use TOPEX/Poseidon SSHA to synthesize hydrographic transects according to the method developed in Section 3. The results of the profile synthesis for Flights 4-3 and 9-1 are shown in Figures 4.12 and 4.13, respectively. In each Figure panel (a) shows the vertical section of the temperature field measured by NAVO for comparison with Panel (b), showing the same transect synthesized with the present method based on the satellite SSHA.

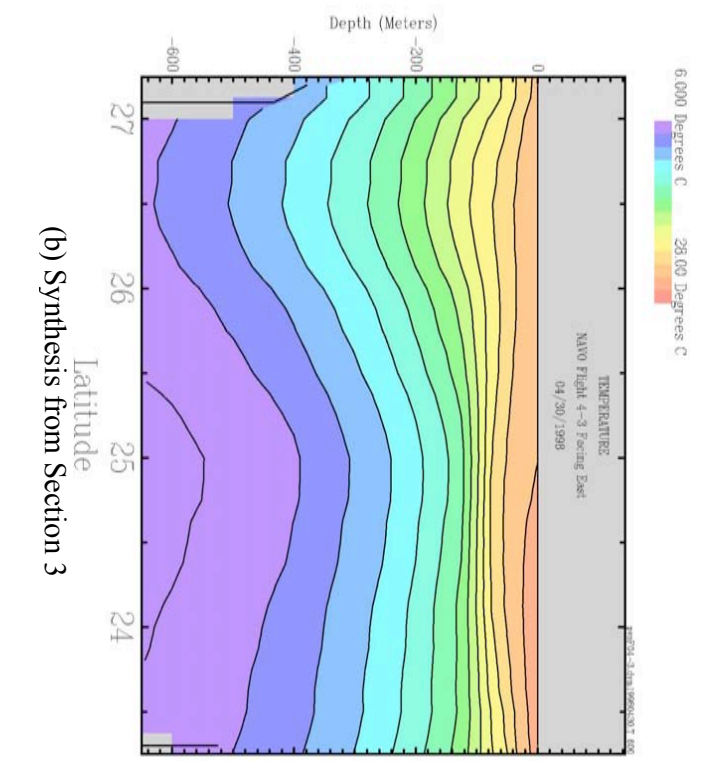
The primary product of the Naval Research Laboratory MODAS data set is a global daily nowcast produced in near-real-time of the temperature and salinity fields driven by the satellite sea surface height anomaly. These fields represent a remarkable achievement, both through their shear volume of data and their timeliness. Panel (c) in Figures 4.12 and 4.13 shows the temperature transect produced by the MODAS analysis for comparison.

The fourth panel, (d), compares the elevations from the different fields. The ordinate in the top two plots is the sea surface height anomaly and the black curves are the TOPEX/Poseidon SSHA and the density integral from Figure 4.10(c), for reference. In the top plot, the red curve is the density integral from the present synthesis. In the second plot, the purple curve is the vertical integral of the MODAS temperature and salinity fields and the turquoise curve is from the MODAS SSHA field that is developed from all satellite SSHA data.

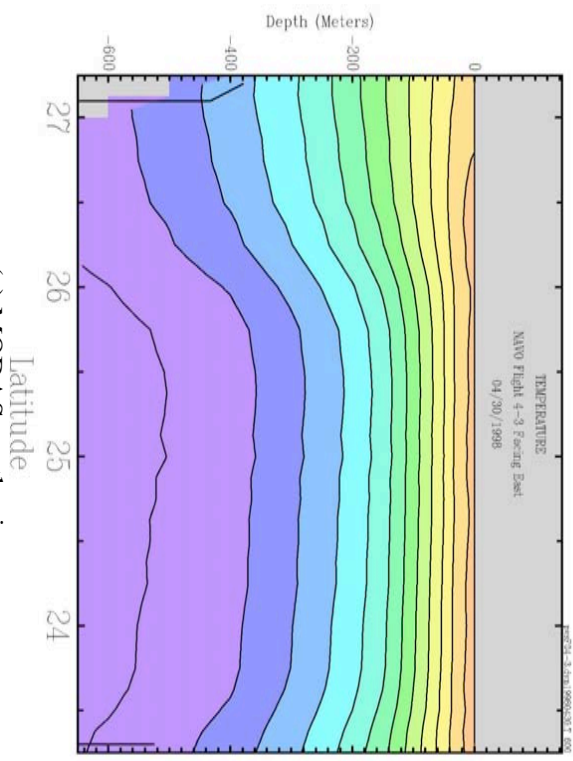
The bottom plot of Figure 4.10(c) is the total surface height along the transect and all of the curves on the plots above are converted to total surface elevation using the climatological mean sea surface height from Figure 3.1. Additional curves for reference, plotted in green, are the height of the GCW (lower dashed line), the LEW (upper dashed line) and the local mean height (solid line). If the surface height anomaly were zero then the total sea surface height would just be the solid green curve. It is evident, then, that when the total height is below the bottom dashed green line, as it is in the cold core Eddy of Flight 4-3, the water column is colder and less saline than normal GCW and must have become so due to upwelling, since there is no other source of colder, less saline water available. Likewise, if the total height is above the upper dashed green line, as it is in the center of the warm core Eddy of Flight 9-1, the water column is warmer and more saline than the LEW profile and this must be due to downwelling of the surface water.



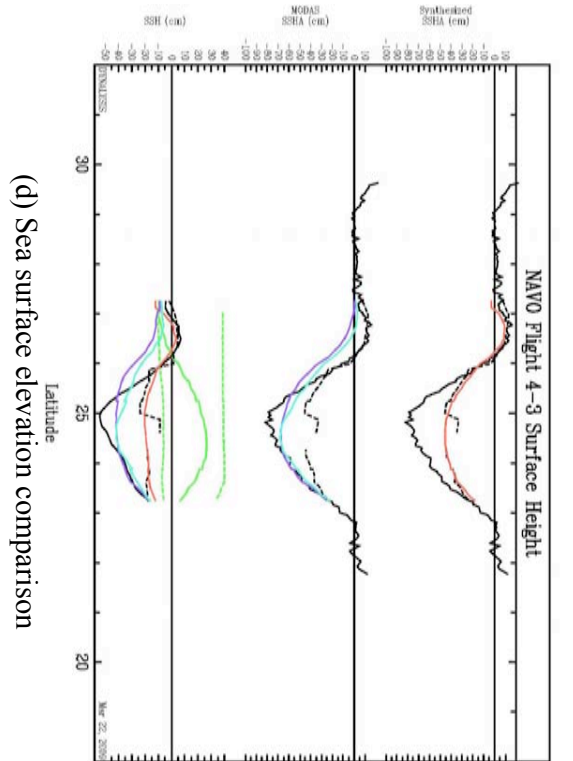
(a) NAVVO hydrographic cast data



(b) Synthesis from Section 3

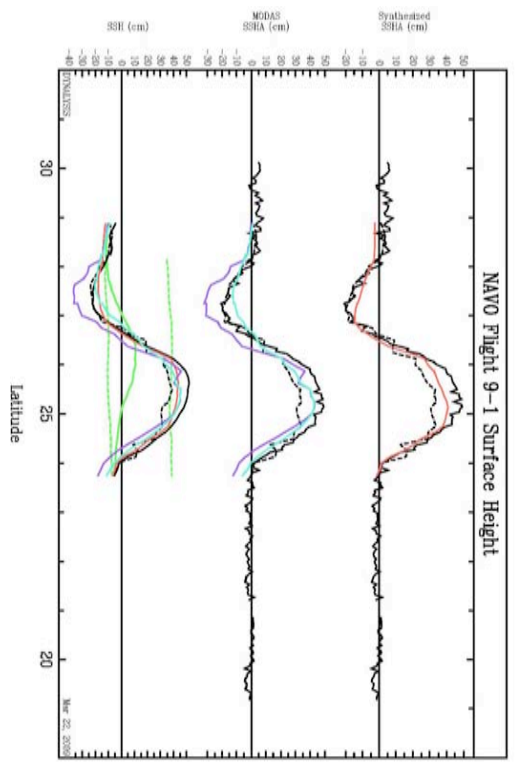
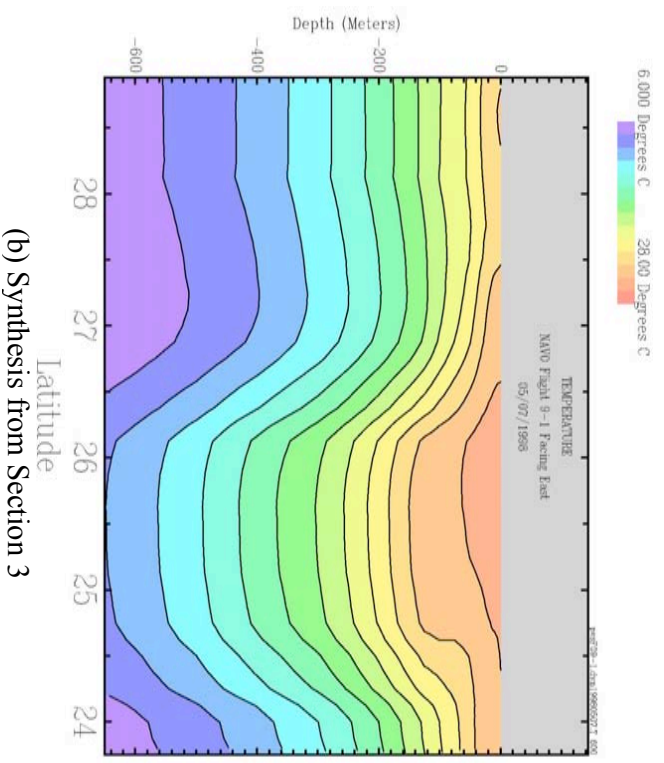
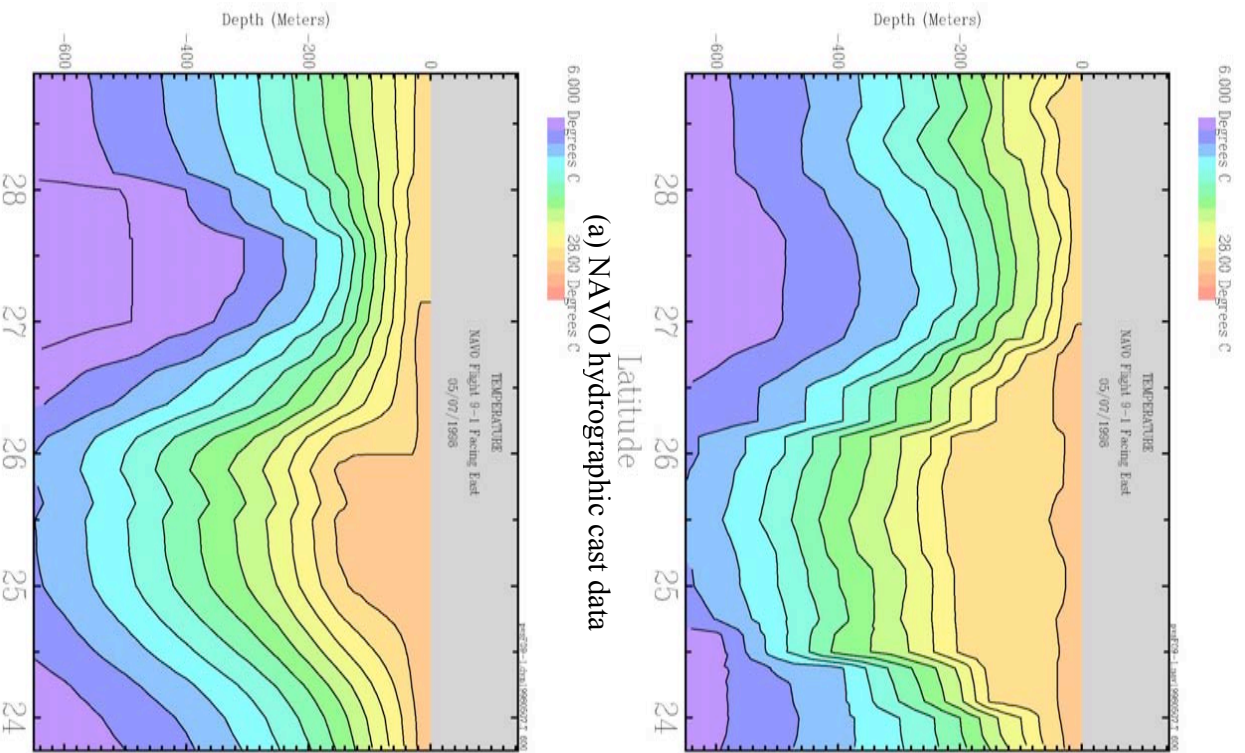


(c) MODAS synthesis



(d) Sea surface elevation comparison

Figure 4.12 Comparison of temperature sections and surface elevations for NAVVO Flight 4-3 through a cold gyre in the eastern Gulf.



(d) Sea surface elevation comparison

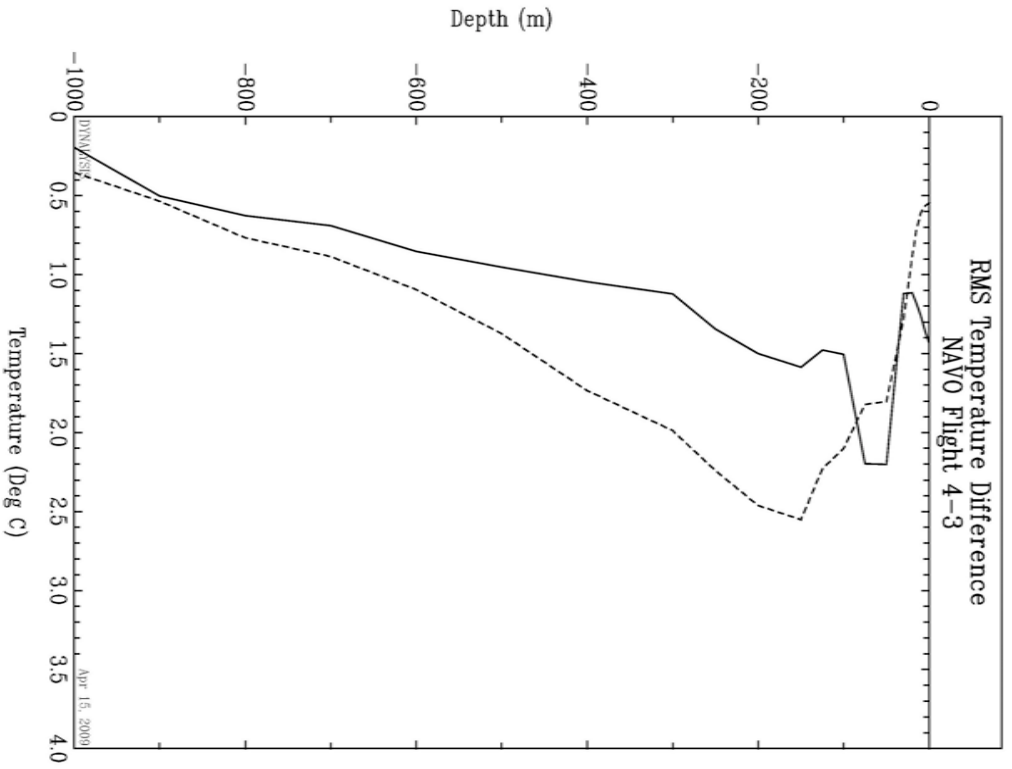
Figure 4.13 Comparison of temperature sections and surface elevations for NAVVO Flight 9-1 through a warm gyre in the central Gulf.

The comparison of the transect temperature distributions are good. The major features are obviously well resolved, which is typical of all of the other transect results. In the case of the Cold Core Eddy, the proposed method produces temperatures a degree or so too cold in the deeper portion of the Eddy. In the Warm Core Eddy the results are remarkably good, within a degree throughout. The density integrals shown in the (c) panels are also very close, as they should be. As a metric of the overall accuracy of the synthesis, the root-mean-squared temperature difference between the synthesized temperature profiles and the observed profiles are shown for the two cases in Figure 4.14. For the Cold Core Eddy the results are less than a degree in the pycnocline and for the Warm Core Eddy they are less than a degree and a half.

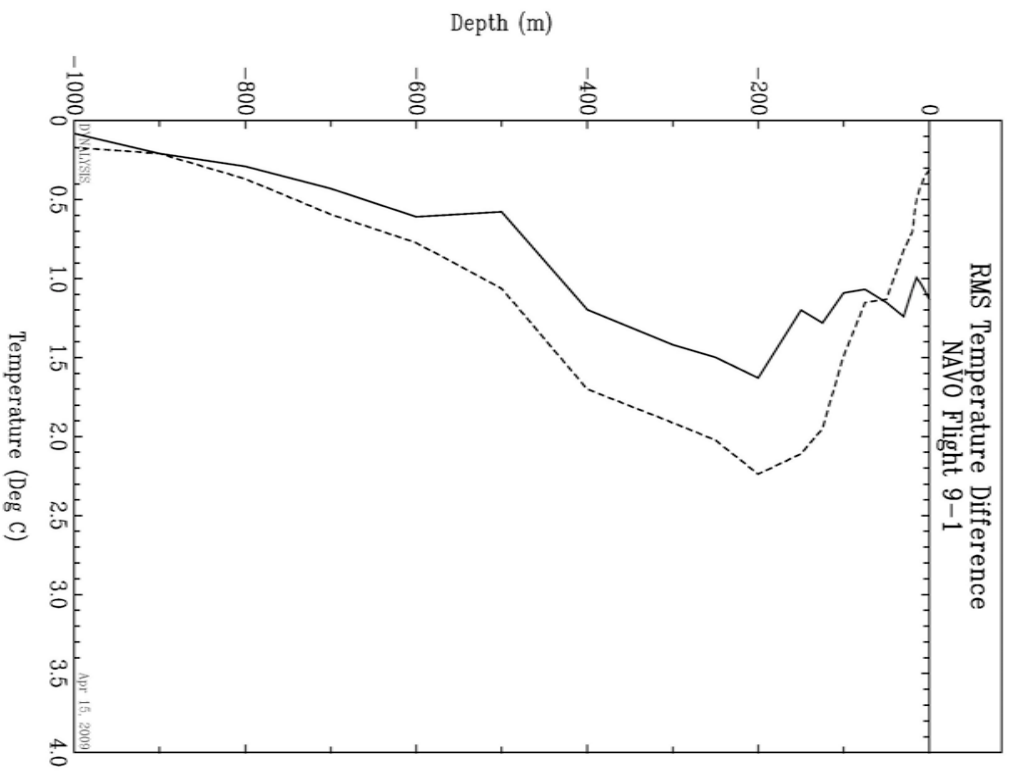
The MODAS results are also good, particularly if they are as good globally. In the Cold Core Eddy most of the water column is more than a degree too cold and the density integral in panel (c) confirms this. For the Warm Core Eddy the temperature distribution and, therefore, the density integral are quite close to those of the measurements.

Having said all of this, regardless of the method of temperature/salinity profile synthesis, there is a considerable difference between the TOPEX/Poseidon SSHA and that of the steric height anomaly from the transect measurements. The density integral height anomaly is most always less and in the most extreme cases it is as much as 40% less. This is too large a discrepancy to be explained by the uncertainty in the integral of the synthesized surface layer. The few cases where the density integral is greater, such as it is at the end of Line 3, may be explained by the motion of a large feature between the time of the satellite over flight and that of the hydrographic survey.

Earlier comparisons, Carnes, *et al.* (1990), also appear to indicate reduced variation of the steric height compared with the SSHA. However, the analysis did not have the benefit of a well established geoid to assess the inconsistencies between variations of the SSHA and steric height anomaly. More recently, the work of Gilson, *et al.*, (1998), McCarthy, *et al.*, (2000), Willis, *et al.*, (2003) and Ivchenko, *et al.*, (2007), all provide further indications of consistent and non negligible differences between the SSHA and the steric height, with the steric height variation always less than that of the SSHA. In evaluating these latter studies one might be inclined to ascribe the reduction in steric height variation to smoothing of the hydrographic data due to the statistical nature of the analysis. However, in view of the direct comparisons between the TOPEX/Poseidon SSHA and the steric heights calculated from the actual observed transects of hydrographic data from the present study, the discrepancy between the SSHA and the steric heights appears to be real. Due to the importance of satellite altimetry in assessing the prevailing ocean conditions, these results suggest that additional data and analysis are desirable to resolve this issue.



(a) NAVO Flight 4-3



(b) NAVO Flight 9-1

Figure 4.14 Comparison of root-mean-square temperature difference between all synthesized temperature profiles and the corresponding measured profiles in the transect shown with a solid line and the same for the MODAS profiles shown with a dashed line.

5. SUMMARY

Using a large quantity of hydrographic data, a climatological atlas of temperature and salinity has been developed that documents the dual water mass description. The distributions and properties of GCW and LEW are determined and the distribution of the proportion of LEW is used to calculate mean climatological fields. The climatological steric height is determined in order to calculate the local total sea surface elevation from satellite sea surface anomaly measurements. Finally a method of constructing the distribution of subsurface temperature and salinity structure using satellite remote-sensing data in conjunction with data from hydrographic climatology has been described and demonstrated.

The basis of the analysis is the dual water mass description of the climatological hydrography. While the concept of the interplay between LEW and GCW masses was well known, the development of an atlas specifying the properties and distribution of each has considerably utility. Although there is inevitably a mixing layer between the two, the integrity of the Eddy properties persist for a remarkably long time as an Eddy moves across the Gulf. From satellite SST images, it is possible to estimate the Eddy boundaries and anticipate the regional conditions with an accuracy not possible using a traditional mean climatological atlas.

The MODAS system does provide profiles reflecting the dual water mass description using empirical profile functions. This description is very compact and efficient, particularly for use throughout the world oceans, but the constraints of the functional formulation are a step removed from the data based fields established here. The present analysis imposes no constraints on the climatological functions, thereby enabling subtle variations in the water mass properties throughout the Gulf to be represented in the profile distribution.

The probability distribution of the presence of LEW is an essential component of the climatology and is required to specify the climatological mean fields. In addition, the probability distribution, based entirely on a century of *in situ* hydrographic observations, provides robust statistical evidence of the actual likelihood of encountering the Loop or an Eddy at any location in the Gulf. It is available for comparison with independent estimates of Loop and Eddy probability from shorter term data sets, such as the satellite SST measurements.

In order to infer the subsurface temperature and salinity from the satellite SSH anomaly, the temporal mean SSH distribution must be established. The primary contribution [Gill and Niiler (1973)] is the temporal mean steric height. Therefore, the relatively high resolution steric height distribution developed here based on the climatological hydrography represents a clear improvement over numerical model SSH distributions frequently employed.

Of course the objective is to determine the subsurface profiles from the satellite SSH anomaly. Although mathematically elegant correlations between the SSH anomaly and the profiles appear to work very well, the method of determining the subsurface profiles from the proportion of LEW utilizes the basic simplicity of the situation and has the advantage of being computationally efficient, operationally robust and physically transparent.

There remains much more work to be done. While the large scale, slowly changing influence of the pycnocline hydrography is the most important for model data assimilation, the specification of the surface layer, which has not been addressed in this study, is very important for other purposes. Local boundary layer calculations based on surface forcing in conjunction with the satellite SST data may be the key here. Furthermore, in attempting to apply this technique to other regions, the simple water mass description employed may not be as clearly defined and work as well in more complex regions where multiple water masses interact.

Even if the basic methodology is viable in the Gulf of Mexico, the results depend heavily on the capability of developing similar water mass climatologies elsewhere. The most far reaching assumption is that the sea surface height anomaly can be attributed to the presence of multiple water masses which can be characterized by profiles below the mixed layer. In the Gulf of Mexico, where the prevailing hydrography can be described by two clearly defined water masses, the assumption is well supported by the hydrographic data, but in a more complex region, this simple approach might not work. Another assumption is that the profiles of both GCW and LEW are seasonally independent, so that variations in the pycnocline are due exclusively to interactions between the water masses, specifically the presence of Eddies. Again, while this is borne out by the data in the Gulf of Mexico, it might not be appropriate in other regions.

Finally, since all available data must be utilized to the fullest extent, Cummings (2005), incorporation of the real-time profiling drifter and glider data, that is becoming increasingly abundant, should be used as an aid in mapping the horizontal structure of the surrounding features as well as providing *in situ* hydrographic measurements.

Acknowledgements: From the outset Richard Patchen provided support and encouragement for this effort. I also thank him for valuable suggestions and insights and for access to oceanographic data for comparison. Over the years my data base has been enriched by the generosity of many investigators who have made their data available to me without reserve. Among these people are Matthew Howard, Norman Guinasso, Frank Kelly, Robert Leben, Van Waddell, Fred Vukovich, William Wiseman, Stephen Murray, Nancy Rabalais, Thomas Curtin, William Teague, Charles Barron, John Blaha and Alexis Lugo-Fernandez. The convenient design and extensive offerings on websites of the National Oceanographic Data Center, the Naval Research Laboratory and the Physical Oceanography Distributed Active Archive Center used during this study were greatly appreciated. Numerous discussions of Gulf oceanography with George Mellor, Peter Niiler, Wilton Sturges and Germana Peggion were very beneficial. I am most grateful for support for this study from the NOAA National Ocean Services Coast Survey Development Laboratory.

REFERENCES

- Barron, Charlie N. and A. Briol Kara, 2006: Satellite-Based Daily SSTs Over the Global Ocean. *Geophys. Res. Lett.*, **33**, L15603, doi:10.1029/2006GL026356.
- Bauer, A. R. and A. D. Stroud, 1985: Final report Master Oceanographic Observation Data Set MOODS4 update. Submitted to Fleet Numerical Oceanography Center, Monterey, CA, by Compass Systems, Inc., San Diego, CA, pp. 25.
- Bauer, Roger, 1985: Functional description Master Oceanographic Observation Data Set (MOODS). Submitted to Fleet Numerical Oceanography Center, Monterey, CA, by Compass Systems, Inc., San Diego, CA, pp 56.
- Bennett, A. F., B.S.Chua, B.L Pflaum, M. Erwig, Z. Fu, R.D. Loft and J.C. Muccino, 2008: The Inverse Ocean Modeling system. I. Implementation, *Journal of Atmospheric and Oceanic Technology*, in press.
- Berwin, R. W., 2003: TOPEX/POSEIDON Sea Surface Height Anomaly Product, User's Reference Manual, Version 2, Physical Oceanography Distributed Active Archive Center (NASA/JPL PO.DAAC).
- Blaha, J., G. H. Born, N. L. Guinasso, Jr., H. J. Herring, G. A. Jacobs, F. J. Kelly, R. R. Leben, R. D. Martin, Jr., G. L. Mellor, P. P. Niiler, M. E. Parke, R. C. Patchen, K. Schaudt, N. W. Scheffer, C. K. Shum, C. Ohlmann, W. Sturges, III, G. L. Weatherly, D Webb and H. J. White, 2000: Gulf of Mexico Ocean Monitoring System, *Oceanography*, **13** (2), 10-17.
- Carnes, M. R., J. L. Mitchell and P. W. deWitt, 1990: Synthetic Temperature Profiles Derived From Geosat Altimetry: Comparison With Air-Dropped Expendable Bathythermograph Profiles, *J. Geophys. Res.*, **95**, C10, pp17,979-17,992.
- Countryman, K. A. and M. J. Carron, 1995: The Navy Ocean-Temperature Temporal-Variability Model, OCEANS apos; 95. MTS/IEEE. Challenges of Our Changing Global Environment. Conference Proceedings. Volume 1, Issue, 9-12 Oct 1995 Page(s):42 - 50 vol.1. doi: 10.1109/OCEANS.1995.526748
- Cummings, J. A., 2005: Operational multivariate ocean data assimilation, *Q. J. R. Meteorol. Soc.*, **131**, pp.3583-3604. doi: 10.1256/qj.05.105
- DiMarco, Steven F., Matthew K. Howard and Ann E. Jochens, 2001: Deepwater Gulf of Mexico Historical Physical Oceanography Data Report, Quality Assurance and Quality Control Procedures and Data Inventory, TAMU Oceanography Technical Report No. 01-01-D, pp 204.

- Donohue, Kathleen, Peter Hamilton, Kevin Leaman, Robert Leben, Mark Prater, Evans Waddell and Randolph Watts, 2006: Exploratory Study of Deepwater Currents in the Gulf of Mexico, Volume II: Technical Report, Science Applications International Corporation, MMS Report No. 2006-074, pp 408.
- Fox, D. N. W. J. Teague, C. N. Barron, M. R. Carnes and C. M. Lee, 2002: The Modular Ocean Data Assimilation System (MODAS), *J. Atmos. Oceanic Technol.*, **19**, 240-252.
- Ghil, M. and P. Malanotte-Rizzoli, 1991: Data assimilation in meteorology and oceanography, *Adv. Geophys.*, **33**, 141-266.
- Gill, A. E. and P. P. Niiler, 1973: The Theory of Seasonal Variability in the Ocean, *Deep Sea Res.*, **20**, 141-177.
- Gilson, J., D. Roemmich, B. Cournuelle and L. L. Fu, 1998: The relationship of TOPEX/POSEIDON altimetric height to the steric height of the sea surface, *J. Geophys. Res.*, **103**, C12, pp 27,947-27865.
- Gilligan, Michael J., John Blaha and Joel Wesson, 2002: Gulf of Mexico Airborne Survey, May 1998: Dynamic Height Determination Using Airborne Expendable Bathythermographs, NAVOCEANO Technical Note TN 01-02, Planning Systems, Inc, pp 21.
- Ivchenko, V. O., S. D. Danilov, D. V. Sidorenko, J. Schröter, M. Wenzel and D. L. Aleynik, 2007: Comparing the Steric Height in the Northern Atlantic with Satellite Altimetry, *Ocean Sci.*, **3**, 485-490.
- Kara, A. B., C. N. Barron, and T. P. Boyer, 2009, Evaluation of SST climatologies in the Tropical Pacific Ocean, *J. Geophys. Res.*, **114**, C02021, doi:10.1029/2008JC004909.
- Kelly, F. N., N. L. Guinasso, Jr., L. Lee, S. DiMarco and A. V. de la Cerda, 1998, Research Vessel Gyre Cruise 98-G-5, Texas A&M University Technical Report 98-112.
- Leben, R. R., 2004: Real-Time Altimetry Project, <http://www-ccar.colorado.edu/~realtime/>.
- Levitus, S., 1994: World Ocean Atlas 1994. CD-ROM Data Set Documentation, National Oceanographic Data Center Informal Report No. 13, NOAA, National Oceanographic Data Center Ocean Climate Laboratory, Washington, D.C., pp. 29.
- McCarthy M., L. Talley, and D. Roemmich, 2000: Seasonal to interannual variability from expendable bathythermograph and TOPEX/POSEIDON altimetric data in the South Pacific subtropical Gyre, *J. Geophys. Res.*, **105**, pp 19,535-19550.
- Mellor, G. L., and D. T. Ezar, 1991: A Gulf Stream model and an altimetry assimilation scheme, *J. Geophys. Res.*, **96**, pp 8779-8795.

- Pazan, S. E., and P. P. Niller, 2004: New Global Drifter Data Set Available, EOS, Vol. 85, No.2.
- Thacker, W. C., 2006: Estimating salinity to complement observer temperature: 1. Gulf of Mexico, *J. Marine Sys.*, **65**, 224-248, doi:10.1016/j.jmarsys.2005.06.008.
- Vukovich, F. M., 1995: An updated evaluation of the Loop Current's eddy-shedding frequency, *J. Geophys. Res.*, **100 (C5)**, 8655-8659.
- Willis, J. K., D. Roemmich and B. Cornuelle, 2003: Combining Altimetric Height with Broadscale Profile Data to Estimate Steric Height, Heat Storage, Subsurface Temperature and Sea-Surface Temperature Variability, *J. Geophys. Res.*, **108 (C9)**, 3292, doi:10.1029/2002JC001755.